AN INVESTIGATION OF THE PHYSICAL AND CHEMICAL CHANGES OCCURRING IN A FISCHER–TROPSCH FIXED BED CATALYST DURING HYDROCARBON SYNTHESIS

Dawid Jakobus Duvenhage

A thesis submitted to the Faculty of Science,
University of the Witwatersrand, Johannesburg,
in partial fulfilment of the requirements for the
degree of Master of Science.

Supervisor : Prof. N.J. Coville
Co–supervisor : Dr. G.A. Foulds

Johannesburg

1990

ABSTRACT

Deactivation studies; making use of fixed bed reactors, wet chemical analysis, surface area, pore volume determinations and X–ray diffraction–, scanning electron microscope– and secondary ion mass spectrometry techniques; were performed on a low temperature iron Fischer–Tropsch catalyst. It was revealed that this catalyst is mainly deactivated by sulphur poisoning, oxidation of the catalytic reactive phases, sintering of the iron crystallites and to a lesser extent deactivation through fouling of the catalytic surface by carbonaceous deposits.

It was found that the top entry section of the catalyst bed deactivated relatively fast, the bottom exit section also deactivated, but not as fast as the top section. The central portion of the catalyst bed was least affected.

Sulphur contaminants in the feed gas, even though present in only minute quantities, results in a loss of catalyst performance of the top section of the catalyst bed, while water, produced as a product from the Fischer–Tropsch reaction, oxidized and sintered the catalyst over the bottom section of the catalyst bed.

OPSOMMING

Deaktiveringstudies is uitgevoer op 'n lae temperatuur yster Fischer–Tropsch katalisator deur gebruik te maak van die volgende tegnieke : vastebedreaktore, natchemiese metodes, oppervlakte area en porievolume bepalings, X–straal diffraksie, skandeer elektron mikroskopie en sekondêre ioon massa spektrometrie. Resultate verkry toon daarop dat hierdie katalisator hoofsaaklik deur swawelvergiftiging, oksidasie van die katalitiese reaktiewe fases en kristallietgroei van die yster kristalliete en tot 'n mindere mate deur belemmering van die katalitiese reaktiewe oppervlakte deur koolstofagtige neerslae gedeaktiveer word.

Dit is interessant om daarop te let dat die boonste ingangsseksie van die katalisator bed relatief vinnig gedeaktiveer word, terwyl die onderste gedeelte stadiger deaktiveer en die middelste gedeelte die minste geaffekteer word.

Die boonste gedeelte van die katalisatorbed word primêr deur swawelonsuiwerhede teenwoordig in die voergas vergiftig, terwyl die onderste segment van die katalisatorbed se deaktivering te wyte is aan water ('n produk van die Fischer–Tropsch reaksie) wat oksidasie en kristallietgroei bevorder.

DECLARATION

I declare that this dissertation is my own, unaided work. It is being submitted for the degree of Master of Science in the University of the Witwatersrand, Johannesburg. It has not been submitted before for any degree or examination at any other university.

L J Louwhagel

(Name of candidate)

5th day of November, 1990

In Memory of my Father

Willem Johannes Paulus Duvenhage

1936 – 1987

LIST OF ABBREVIATIONS

ARGE	Arbeitsgemeinschaft
BET	Brunauer–Emmett–Teller
FTIR	Fourier Transform Infrared
LIA	Link Image Analyzer
MEK	Methyl Ethyl Ketone
MPa	Mega Pascal
RON	Research Octane Number
selec.	selectivity
SEM	Scanning Electron Microscopy
SIMS	Secondary Ion Mass Spectrometry
STP	Standard Temperature and Pressure
tu	time unit
XPS	X–ray Photoelectron Spectroscopy
XRD	X–Ray Diffraction

CONTENTS

		PAGE
	List of Tables	vii
	List of Figures	viii
	Acknowledgements	xv
CHAPTER 1.	INTRODUCTION AND PURPOSE OF STUDY	
1.1.	Introduction	1
1.2.	Purpose of study	4
1.3.	Project scope	5
1.4.	References	5
CHAPTER 2.	LITERATURE STUDY	
2.1.	The Fischer–Tropsch Process	8
2.1.1.	Development and growth	8
2.1.2.	South Africa's commercial Fischer–Tropsch plant	9
2.1.3.	Syngas as a source of hydrocarbons and chemicals	9
2.1.4.	CO hydrogenation (the Sasol process)	11
2.1.5.	The Fischer–Tropsch mechanism	12
2.1.6.	The Fischer–Tropsch product distribution	14
2.1.7.	The Fischer–Tropsch products	17

2.2	Catalysts	18
2.2.1.	Definition of a catalyst	18
2.2.2.	Properties of a catalyst	18
2.2.3.	Fischer–Tropsch catalysts	19
2.2.4.	Effect of process parameters on products	19
2.3.	References	22

CHAPTER 3. CATALYST DEACTIVATION

3.1.	Introduction	26
3.2.	Deactivation by poisoning	27
3.2.1.	Definition of poisoning	27
3.2.2.	Poisoning of catalysts	27
3.2.3.	The poisoning mechanism	32
3.2.4.	Sulphur and the Fischer–Tropsch process	36
3.3.	Deactivation by sintering	45
3.3.1.	Definition of sintering	45
3.3.2.	The sintering of catalysts	46
3.3.3.	The sintering mechanism	50
3.4.	Deactivation by fouling	57
3.4.1.	Definition of fouling	57
3.4.2.	Fouling – an extensive concept	58
3.4.3.	The mechanism of fouling	61

3.4.4.	The nature of carbonaceous deposits	66
3.4.5.	Fouling on iron catalysts	68
3.4.6.	Retardation of fouling	73
3.5.	Other forms of Catalyst Deactivation	74
3.5.1.	Solid State Reactions	75
3.5.2.	Mechanical Failure	75
3.6.	Concluding Remarks	76
3.7.	References	76

CHAPTER 4. EXPERIMENTAL

4.1.	Catalyst characterization	84
4.1.1.	Carbon and sulphur analysis	84
4.1.2.	X–ray diffraction phase analysis	84
4.1.3.	Area and pore volume	85
4.1.4.	SEM and SIMS analysis	85
4.2.	Experimental equipment	86
4.2.1.	Fixed bed reactor	86
4.2.2.	Laboratory micro reactors	88
4.2.3.	Reproducibility of data obtained from the laboratory micro reactors	90
4.3.	References	91

CHAPTER 5. DEACTIVATION OF A LOW TEMPERATURE FISCHER–TROPSCH PRECIPITATED IRON CATALYST IN A FIXED BED REACTOR

5.1.	Introduction	92
5.2.	Fixed bed activity profile	94
5.3.	Physical properties of catalyst samples from different sections of the catalyst bed	100
5.3.1.	Sulphur content	100
5.3.2.	Carbon content	100
5.3.3.	Oxidation and crystallite size	103
5.3.4.	Area and pore volume	103
5.4.	Discussion of results	103
5.4.1.	Catalyst bed deactivation profile : top section	108
5.4.2.	Catalyst bed deactivation profile : middle and bottom sections	110
5.4.3.	Fouling of the iron catalyst	115
5.4.4.	Iron phases present on the different sections of the catalyst bed	117
5.5.	References	119

CHAPTER 6. THE EFFECT OF EMPLOYING A TWO STAGE SYNTHESIS PROCESS

6.1. Introduction 124

6.2. Laboratory tests of the catalysts from the two stage synthesis process 125

6.2.1. Sulphur profiles for the two reactor stages 125

6.2.2. Laboratory micro reactor tests 127

6.2.3. Carbon content 133

6.2.4. Oxidation and crystallite growth 133

6.2.5. Pore volume 136

6.2.6. XRD phase analysis 136

6.3. References 147

CHAPTER 7. SCANNING ELECTRON MICROSCOPY AND SECONDARY ION MASS SPECTROMETRY ANALYSIS

7.1. Introduction 148

7.2. SEM characteristics of an used iron catalyst pellet 149

7.3. Iron crystallite growth 162

7.4. SIMS analysis of an used iron catalyst pellet 168

7.5. References 178

CHAPTER 8. CONCLUSIONS 180

LIST OF TABLES

		PAGE
Table 2.1.	Types of compounds present (Wt. %) in various carbon number products from iron catalysts	20
Table 3.1.	Catalysts arrayed in Periodic Series	29
Table 3.2.	Group Vb and VIb elements	30
Table 3.3.	Influence of electronic configuration on toxicity	31
Table 3.4.	Sulphur distribution in catalyst beds	43
Table 4.1.	Relative activity, calculated as a % of the first reactor tube	91
Table 5.1.	Compounds identified in the carbon residue by means of FTIR	115

LIST OF FIGURES

		PAGE
Figure 1.1.	Catalysts deactivation profile	2
Figure 1.2.	A proposed scheme for the causes of deactivation	3
Figure 2.1.	Lurgi dry coal gasifier	10
Figure 2.2.	Sasol Synthol and ARGE reactors	12
Figure 2.3.	Chain growth and termination probabilities	14
Figure 2.4.	Plots of the selectivities as a function of the probability of chain growth	16
Figure 2.5.	Schultz–Flory plot for a fixed–bed reactor	21
Figure 3.1.	Blocking and electronic effects in poisoning	28
Figure 3.2.	Form of a typical poisoning curve	34
Figure 3.3.	Conversion during hydrogen sulfide exposure during (i) hydrogen rich conditions and (ii) hydrogen lean conditions	38
Figure 3.4.	Conversion and selectivity during hydrogen sulfide exposure under hydrogen rich conditions	39
Figure 3.5.	The variation of catalyst activity from laboratory tests	44
Figure 3.6.	Brunauer–Emmett type II isotherm	49
Figure 3.7.	Schematic of the various stages in the formation and growth of particles from a monomer dispersion	52

Figure 3.8.	Possible routes of carbon formation	60
Figure 3.9.	Reaction pathways for coke formation	62
Figure 3.10.	(i) The relevant steps in the mechanism of carbon formation	
	(ii) Schematic mechanism for carbon formation on a Nickel surface	64
Figure 3.11.	Proposed mechanism for carbon formation on iron	69
Figure 3.12.	Migration of carbon through iron	70

Figure 4.1.	Flow sheet for the first reactor setup	87
Figure 4.2.	Flow sheet for the second reactor setup	89

Figure 5.1.	Deactivation rate of a fixed bed reactor	93
Figure 5.2.	Activity profile through the reactor bed for catalysts for different run lengths	95
Figure 5.3.	Deactivation profile for the discussion of catalyst deactivation	96
Figure 5.4.	Activity of the top and bottom sections of the reactor versus the time the catalyst spent on line	98
Figure 5.5.	Relationship between the temperature and conversion profiles of a fixed bed reactor	99
Figure 5.6.	Sulphur profile for a fixed bed reactor catalyst bed	101
Figure 5.7.	Carbon profile for a fixed bed reactor catalyst bed	102
Figure 5.8.	Mass magnetite through the catalyst bed	104
Figure 5.9.	Crystallite size through the reactor bed	105
Figure 5.10.	Surface area of the catalyst through the reactor bed	106

Figure 5.11.	Pore volume of the catalyst through the reactor bed	107
Figure 5.12.	Effect of sulphur on the activity profile a fixed bed reactor catalyst bed	109
Figure 5.13.	Effect of the amount of magnetite on the activity of a fixed bed reactor catalyst bed	112
Figure 5.14.	Effect of catalyst area on the activity of a fixed bed reactor catalyst bed	114
Figure 5.15.	Effect of carbon on the activity of a fixed bed reactor catalyst bed	116
Figure 5.16.	Typical XRD spectrum for the phases present in the catalyst	118
Figure 5.17.	Gradual phase changes taking place through the catalyst bed	120
Figure 5.18.	The increase in magnetite concentration observed down the reactor	121

Figure 6.1.	Sulphur content through the first and second stage reactor catalyst beds	126
Figure 6.2.	Sulphur content through the catalyst bed for the first and adjusted second stage reactors	128
Figure 6.3.	Activity profiles through the catalyst bed for the first and second stage reactors	129
Figure 6.4.	The effect of the adjusted sulphur content from the second stage reactor catalyst bed on the adjusted activity profile of the catalyst bed	131
Figure 6.5.	Activity profiles through the catalyst bed for the first and adjusted second stage reactors	132

Figure 6.6.	Carbon content for the first and second stage reactor catalyst bed sections	134
Figure 6.7.	Magnetite concentration for the first and second stage reactor catalyst bed sections	135
Figure 6.8.	Magnetite crystallite size for the first and second stage reactor catalyst bed sections	137
Figure 6.9.	B.E.T. surface area for the first and second stage reactor catalyst bed sections	138
Figure 6.10.	Pore volume for the first and second stage reactor catalyst bed sections	139
Figure 6.11.	XRD phase analysis of the top section of the catalyst bed	141
Figure 6.12.	XRD phase analysis of the section $^{2}/_{5}$ from the top of the catalyst bed	142
Figure 6.13.	XRD phase analysis of the section $^{2}/_{5}$ from the middle of the catalyst bed	143
Figure 6.14.	XRD phase analysis of the middle section of the catalyst bed	144
Figure 6.15.	Phase changes through the first stage reactor catalyst bed	145
Figure 6.16.	Change in magnetite concentration through the catalyst bed	146

Figure 7.1.	SEM photo of a reduced unused catalyst	150
Figure 7.2.	SEM photo of an used catalyst from the top section of a fixed bed reactor catalyst bed	150

Figure 7.3.	SEM photo of an used catalyst from one quarter from the top of the catalyst bed	151
Figure 7.4.	SEM photo of an used ARGE catalyst from the middle section of a fixed bed reactor catalyst bed	151
Figure 7.5.	Enlargement of "inkpot", a grey area marked A in Figure 7.2.	152
Figure 7.6.	Enlargement of "tip", a black area marked B in Figure 7.5.	153
Figure 7.7.	SEM–EDAX analysis within the black area as displayed in Figure 7.6.	153
Figure 7.8.	SEM–EDAX analysis within the black area, marked as C, D and E, as displayed in Figure 7.5.	155
Figure 7.9.	SEM photo of an used catalyst from the top section of a fixed bed reactor catalyst bed	157
Figure 7.10.	Enlargement of a porous area, marked A displayed in Figure 7.9.	157
Figure 7.11.	SEM–EDAX analysis within the bright area, marked F in Figure 7.5.	159
Figure 7.12.	Iron rich area analyzed from the bright area, marked G in Figure 7.3.	159
Figure 7.13.	Oxygen and carbon rich area analyzed from the grey area, marked H in Figure 7.3.	160
Figure 7.14.	Granular texture of the interior of a catalyst pellet from two quarter from the top section of the catalyst bed	161
Figure 7.15.	Granular texture of the interior and smooth texture of the outer rim for a catalyst pellet from the middle section of the catalyst bed	162

Figure 7.16.	SEM–EDAX analysis of a bright area (iron rich), marked I in Figure 7.15.	163
Figure 7.17.	SEM photo of a reduced unused catalyst pellet	164
Figure 7.18.	SEM photo of a catalyst pellet, representing the catalysts from the top section of the catalyst bed	164
Figure 7.19.	SEM photo of a catalyst pellet, representing two quarter from the top of the catalyst bed	165
Figure 7.20.	SEM photo of a catalyst pellet, representing the middle section of the catalyst bed	165
Figure 7.21.	SEM photo of a sintered product	167
Figure 7.22.	SEM–EDAX analysis of the grey sintered product (oxygen rich), marked A in Figure 7.21.	167
Figure 7.23.	SEM–EDAX analysis of the bright area (iron rich), marked B in Figure 7.21.	168
Figure 7.24.	Magnification of the bright areas (iron crystallites) representing the top section of the catalyst bed	169
Figure 7.25.	Magnifications of the bright areas (iron crystallites) representing the two quarters from the top section of the catalyst bed	170
Figure 7.26.	Magnifications of the bright areas (iron crystallites) representing the middle section of the catalyst bed	171
Figure 7.27.	Increase in average particle diameter as a function of position in the reactor	172
Figure 7.28.	SIMS photo of the surface of a catalyst pellet representing the top section of the catalyst bed	173

Figure 7.29. SIMS SURFACE MAP of iron oxide present on the surface of a catalyst representing the top section of the catalyst bed 174

Figure 7.30. SIMS SURFACE MAP of sulphur present on the surface of a catalyst representing the top section of the catalyst bed 174

Figure 7.31. SIMS SURFACE MAP of iron carbide (Fe_2C^+) present on the surface of a catalyst representing the top section of the catalyst bed 175

Figure 7.32. Ion Mass Spectra spot analysis within the black rim, within the grey area and within the bright area of a catalyst representing the top section of the catalyst bed 176

Figure 7.33. Negative ion mass spectra of the bright area, marked D in Figure 7.2. 177

ACKNOWLEDGEMENTS

To The Only Living God for entrusting me with the talents to perform this project.

Prof. N.J. Coville (Supervisor) and **Dr. G.A. Foulds** (Co–supervisor) for their continued interest and support throughout this study period.

Sasol for financial support and permission to publish this project.

Last but not least, **my mother, Ute** and **Willem** for putting up with me during the past two years. **Thank you for your patience, participation and love.**

CHAPTER 1
INTRODUCTION AND PURPOSE OF STUDY

1.1. Introduction

The Fischer–Tropsch process[1,2], the reductive polymerization of carbon monoxide[3], has been extensively studied. Most heterogeneous catalysts show a loss of initial activity[4] with time during hydrocarbon synthesis. A faster initial decline in activity is often observed, after which the activity stabilizes and declines more steadily with time (see Figure 1.1.). Region B is of the greatest importance, as far as catalytic activity is concerned, because the catalyst behaviour in this part indicates if it is profitable for industrial purposes.

Loss of catalytic activity makes it necessary to change catalyst reactor loads from time to time. Lywood[5] describes optimum catalyst lifetime as a function of catalyst performance, catalyst manufacturing costs, catalyst reduction costs and catalyst vessel cost.

This study sets out to investigate the reasons for catalyst deactivation in the Fischer–Tropsch reaction. The deactivation of catalysts in general has been the subject of a number of reviews[6-10] in which the reasons for, results of, and operating precautions in connection with deactivation have been investigated.

The nature of catalyst deactivation differs for individual processes, but the following factors play a major role in catalyst deactivation[4] : process conditions, temperature, pressure, feed composition and the type of reaction that is being catalyzed.

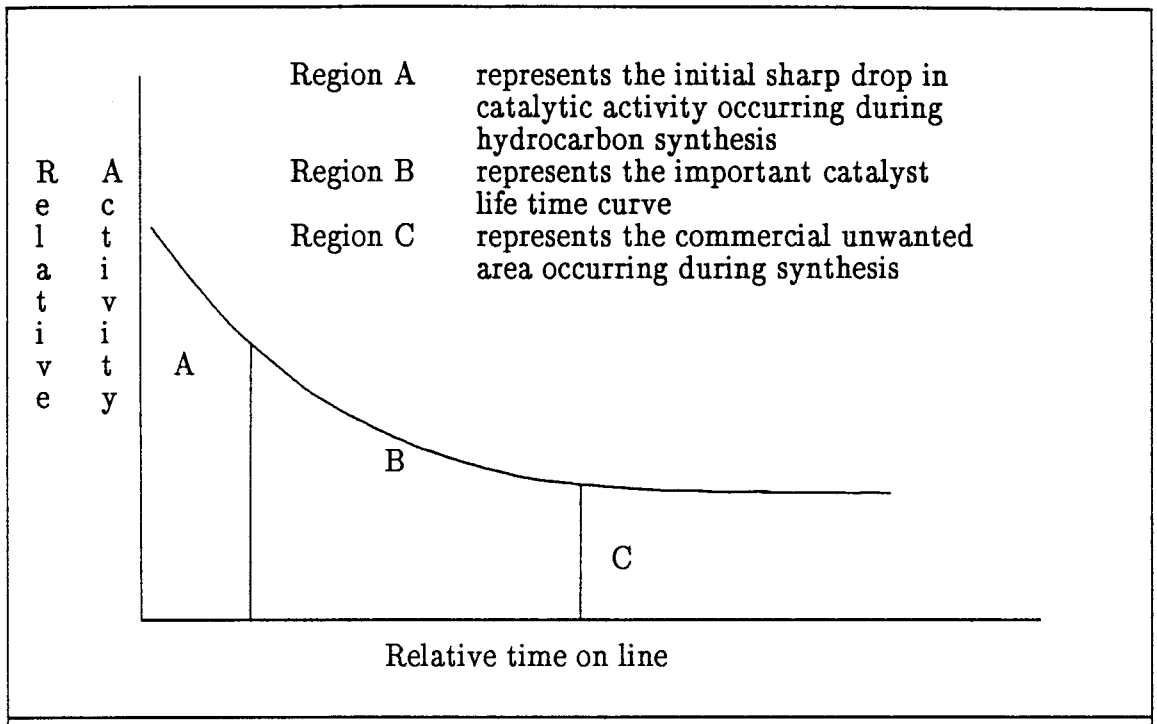

Figure 1.1. Catalyst deactivation profile

The basic causes for deactivation have been classified by Storch et al.[1] as failure of mechanical properties, poisoning (fouling) and sintering of the catalyst.

Trimm[11] gives the fundamental causes for the decline of catalytic activity as the poisoning, coking and sintering of the catalyst, while Forzatti et al.[12] divide the causes for deactivation into four groups, namely poisoning, fouling, sintering and solid state reactions.

Although there is no single cause for the deactivation of catalysts, a scheme is suggested in this study (Figure 1.2.) by which the inter–related causes of catalyst deactivation may be linked.

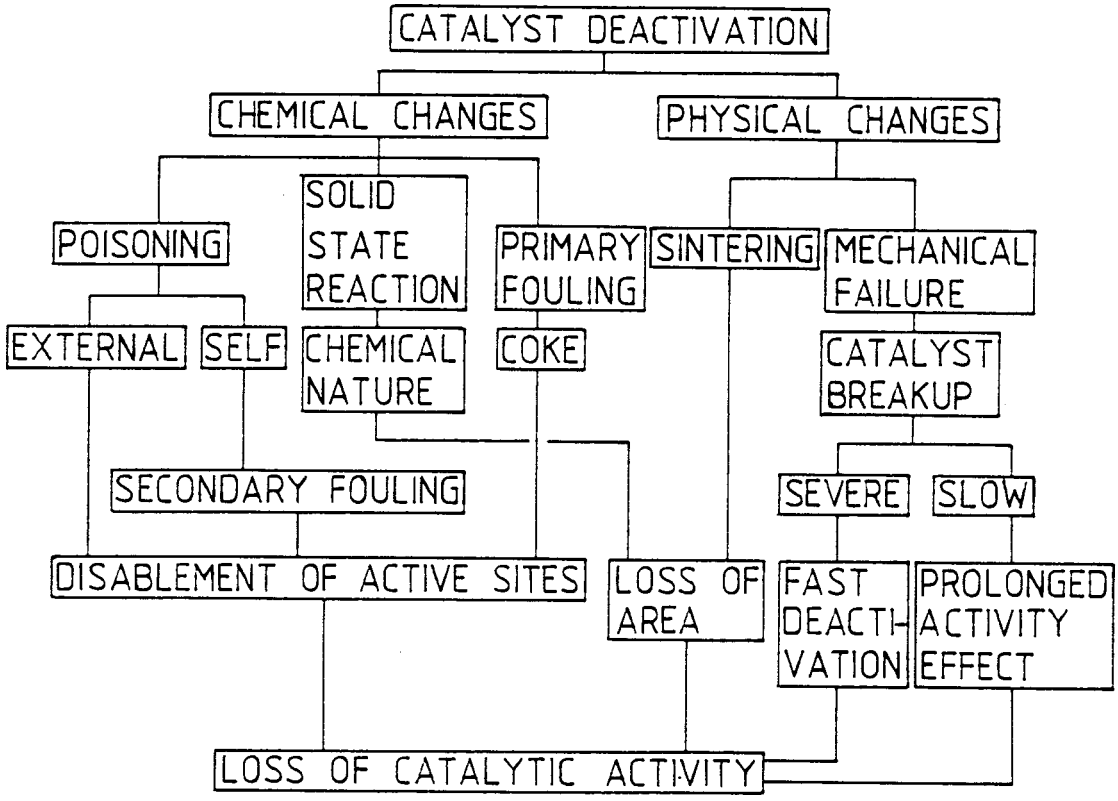

Figure 1.2. A proposed scheme for the causes of deactivation

From Figure 1.2. it can be seen that deactivation normally occurs either from poisoning[13-17], fouling[18-22], sintering[23-27], solid state transformations[2,12,28-30] and mechanical defects[7], or a combination thereof, which leads to either a loss of surface area[11,31-32] , blocking of active sites[13-17] or breakup of the catalysts[7,9].

By determining the chemical and physical changes that occur during the catalyzed reaction, the decline in activity and other parameters occurring with time may be explained.

A literature study on Catalyst Deactivation has been undertaken to place the experimental work in perspective (see Chapter 3). Catalyst deactivation will be grouped under the headings : poisoning, sintering and fouling.

As already stated, these phenomena were identified before 1950[1] as the major causes of catalyst deactivation. Phenomena like mechanical failure and solid state reactions will be discussed under the heading "Other forms of Catalyst Deactivation" (Chapter 3.5.).

1.2. Purpose of study

It is a valid question to ask why catalyst deactivation should be studied. The reasons[4] are that the design and operation of reactors are influenced by the deactivation processes.

Catalyst life time can be defined as the period in which a catalyst produces an expected amount of specified products, and it is of great importance that the catalyst's activity and selectivity remains unchanged during the reaction.

Furthermore, as mentioned in the Introduction, catalytic deactivation has an effect on catalyst performance, manufacturing and reduction costs. It is therefore evident that research into catalytic deactivation may clarify why and how it occurs. Only then can steps be taken to preserve a catalyst to such an extent that maximum life time is obtained.

1.3. Project scope

This dissertation is directed at investigating the basic causes for the deactivation of a fixed bed low temperature Fischer–Tropsch iron catalyst. The study will attempt to show how this catalyst is affected by its immediate surroundings in the reactor bed during hydrocarbon synthesis, and how these surroundings influence the catalyst performance.

1.4. References

1. H.H. Storch, N. Golumbic and R.B. Anderson, *The Fischer–Tropsch and related synthesis*, John Wiley and Sons, Inc., New York, 1951
2. R.B. Anderson, *The Fischer–Tropsch Synthesis*, Academic Press, Inc. Ltd., Florida, 1984
3. C. Masters, *Homogeneous Transition–metal Catalysis*, Chapman and Hall, London, 1981, 228
4. R. Hughes, *Deactivation of Catalysts*, Academic Press, Inc. Ltd., London, 1984, 1
5. W.J. Lywood, *Catalysis Handbook*, (M.V. Twigg, ed.), Wolfe Publishing Ltd., 1989, 96, 101
6. E.B. Maxted, *Adv. Catal.*, *3*, Academic Press Inc. Publishers, New York, 1951, 129
7. B. Dvorák, J. Pasek, P. Pavlas and Z. Hejda, *Catalyst Deactivation* 1987, (B. Delmon and G.F. Froment, eds.), Elsevier Science Publishers B.V., Amsterdam, 1987, 535 – 544

8. P.J. Denny and M.V. Twigg, *Catalyst Deactivation 1980*, (B. Delmon and G.F. Froment, eds.), Elsevier Science Publishers B.V., Amsterdam, 1980, 577 – 598

9. G.F. Froment and K.B. Bischoff, *Chemical Reactor Analysis and Design*, John Wiley and Sons, New York, 1979, 271 – 304

10. S. Berkman, J.C. Morrell and G. Egloff, *Catalysis, Inorganic and Organic*, Reinhold Publishing Corporation, New York, 1940

11. D.L. Trimm, *Progress in Catalyst Deactivation*, (J.L. Figueiredo, ed.), Martinus Nijhoff Publishers, The Hague, 1982

12. P. Forzatti, G. Buzzi–Ferraris, M. Morbidelli and S. Carrá, *Int. Chem. Eng.*, *24*, *1*, 1984, 60

13. L.L. Hegedus and R.W. McCabe, *Catalyst Poisoning*, Marcel Dekker, Inc., New York, 1984

14. A.L. Chaffee, I. Campbell and N. Valentine, *Appl. Catal.*, *47*, 1989, 253

15. J. Oudar, *Catal. Rev. – Sci. Eng.*, *22* , *2*, 1980

16. R.J. Madon and H. Shaw, *Catal. Rev. – Sci. Eng.*, *15* , *1*, 1977, 69

17. P.H. Emmett, *Hydrocarbon Synthesis, Hydrogenation and Cyclization*, Reinhold Publishing Corporation, New York, 1956, 242 – 255

18. J.W. Beeckman, I. Nam and G.F. Froment, *Catalyst Deactivation 1987*, (B. Delmon and G.F. Froment, eds.), Elsevier Science Publishing B.V., Amsterdam, 1987, 365 – 379

19. D. Schanke and A. Holmen, *Catalyst Deactivation 1987*, (B. Delmon and G.F. Froment, eds.), Elsevier Science Publishers B.V., Amsterdam, 1987, 403 – 414

20. E.T.C. Vogt, A.J. van Dillen and J.W. Geus, *Catalyst Deactivation 1987*, (B. Delmon and G.F. Froment, eds.), Elsevier Science Publishers B.V., Amsterdam, 1987, 221 – 233

21. H.P. Bonzel and H.J. Krebs, *Surface Sci.*, *91*, 1980, 499

8. P.J. Denny and M.V. Twigg, *Catalyst Deactivation 1980*, (B. Delmon and G.F. Froment, eds.), Elsevier Science Publishers B.V., Amsterdam, 1980, 577 – 598

9. G.F. Froment and K.B. Bischoff, *Chemical Reactor Analysis and Design*, John Wiley and Sons, New York, 1979, 271 – 304

10. S. Berkman, J.C. Morrell and G. Egloff, *Catalysis, Inorganic and Organic*, Reinhold Publishing Corporation, New York, 1940

11. D.L. Trimm, *Progress in Catalyst Deactivation*, (J.L. Figueiredo, ed.), Martinus Nijhoff Publishers, The Hague, 1982

12. P. Forzatti, G. Buzzi–Ferraris, M. Morbidelli and S. Carrá, *Int. Chem. Eng.*, *24*, *1*, 1984, 60

13. L.L. Hegedus and R.W. McCabe, *Catalyst Poisoning*, Marcel Dekker, Inc., New York, 1984

14. A.L. Chaffee, I. Campbell and N. Valentine, *Appl. Catal.*, *47*, 1989, 253

15. J. Oudar, *Catal. Rev. – Sci. Eng.*, *22* , *2*, 1980

16. R.J. Madon and H. Shaw, *Catal. Rev. – Sci. Eng.*, *15* , *1*, 1977, 69

17. P.H. Emmett, *Hydrocarbon Synthesis, Hydrogenation and Cyclization*, Reinhold Publishing Corporation, New York, 1956, 242 – 255

18. J.W. Beeckman, I. Nam and G.F. Froment, *Catalyst Deactivation 1987*, (B. Delmon and G.F. Froment, eds.), Elsevier Science Publishing B.V., Amsterdam, 1987, 365 – 379

19. D. Schanke and A. Holmen, *Catalyst Deactivation 1987*, (B. Delmon and G.F. Froment, eds.), Elsevier Science Publishers B.V., Amsterdam, 1987, 403 – 414

20. E.T.C. Vogt, A.J. van Dillen and J.W. Geus, *Catalyst Deactivation 1987*, (B. Delmon and G.F. Froment, eds.), Elsevier Science Publishers B.V., Amsterdam, 1987, 221 – 233

21. H.P. Bonzel and H.J. Krebs, *Surface Sci.*, *91*, 1980, 499

22. G.F. Froment, *Catalyst Deactivation 1980*, (B. Delmon and G.F. Froment, eds.), Elsevier Science Publishers B.V., Amsterdam, 1980, 1 – 19

23. P.C. Flynn and S.E. Wanke, *J. Catal.*, *34*, 1974, 300

24. P.C. Flynn and S.E. Wanke, *J. Catal.*, *34*, 1974, 400

25. R.K. Bordia and G.W. Scherer, *Actametall.*, *36*, *9*, 1988, 2393

26. R.K. Bordia and G.W. Scherer, *Actametall.*, *36*, *9*, 1988, 2399

27. R.K. Bordia and G.W. Scherer, *Actametall.*, *36*, *9*, 1988, 2411

28. B. Delmon and P. Grange, *Catalyst Deactivation 1980*, (B. Delmon and G.F. Froment, eds.), Elsevier Science Publishers B.V., Amsterdam, 1980, 507 – 543

29. D.J. Young, P. Udaja and D.L. Trimm, *Catalyst Deactivation 1980*, (B. Delmon and G.F. Froment, eds.), Elsevier Science Publishers B.V., Amsterdam, 1980, 331 – 340

30. N. Burriesci, F. Garbassi, M. Petrera and G. Petrini, *Catalyst Deactivation 1980*, (B. Delmon and G.F. Froment, eds.), Elsevier Science Publishers, Amsterdam, 1980, 115 – 126

31. C.N. Satterfield, *Chemical Engineering Series*, McGraw–Hill Book Company, New York, 1980, 136 – 145

32. R.L. Burwell, jr., *Adv. Catal.*, *26*, 1977, 377

CHAPTER 2

LITERATURE STUDY

2.1. The Fischer–Tropsch process

2.1.1. Development and growth

In 1902 Sabatier and Senderens[1] mentioned a process by which methane could be produced by passing either carbon monoxide or carbon dioxide and hydrogen over a nickel catalyst at atmospheric pressure and 523 K. It was only later, 1923–1925, that liquid hydrocarbons were produced by Fischer and Tropsch[2]; they used a cobalt catalyst with synthesis gas, $H_2 + CO$, at atmospheric pressures and temperatures between 473 K and 523 K. In the next few years Fischer and co–workers[3], especially Pichler, did development work on this process, now known as the Fischer–Tropsch process.

By 1936 the first production plant[3] was established by Ruhrchemie in Germany. This plant used a cobalt catalyst and was run at conditions similar to those mentioned above. In the next few years syngas processes, like the oxo–synthesis[4] and iso–synthesis[5], contributed to the industrial movement towards household products from coal.

In 1955[6] a process using water, oxygen and coal to produce syngas was implemented by Sasol, when the first large scale Fischer–Tropsch plant was built at Sasolburg in the Orange Free State, South Africa. This plant is based on medium pressure synthesis with iron as catalyst in both a fixed bed reactor process (Lurgi–Ruhrchemie) and a fluidised reactor bed process (Kellog)[6].

2.1.2. South Africa's commercial Fischer–Tropsch plant

In 1935 the Anglovaal–group obtained a licence[7] to build a commercial Fischer–Tropsch plant in South Africa. Due to a shortage of money during the second world war and an unsuccessful application for financial help to the World Bank, the project was taken over by the South African government in 1950. By the end of the same year, the South African Coal Oil and Gas Corp., Ltd., better known as Sasol, was registered. In 1952 the construction was started at Sasolburg next to the Vaal River and in 1953 Sasol produced its first products.

With the oil crisis[8] in 1973 the price of oil escalated. In 1974 Sasol management and the government decided to build a second plant to be called Secunda in the Eastern Transvaal Highveld. By the end of 1979 it was decided that a third plant, identical to the second, should also be built. Sasol Two and Three came on line in 1980 and 1982 respectively.

2.1.3. Syngas as a source of hydrocarbons and chemicals

Synthesis gas[9] is a mixture of carbon monoxide and hydrogen. This gas is one of the main reagents used for the synthesis of hydrocarbon products. Natural gas can be produced from any carbon containing source[10] such as coal, biomass, tarsand or heavy oil residues.

Carbon containing sources may be converted to syngas via different processes[11], including pyrolysis, combustion, hydrogenation and indirect hydrogenation (reaction with steam). Another route to synthesis gas is from methane (natural gas) via

steam reforming (shortly to be exploited at Mossel Bay). However, the major route to syngas in South Africa currently remains the gasification of coal. A brief description of this process, as used by Sasol, is described below.

Coal, a complex and heterogeneous matrix of carbon, oxygen, nitrogen, sulphur, etc. is gasified in a Lurgi–gasifier (Figure 2.1.)[13]. The three Sasol plants make use of a low grade coal[14] (that is a coal with up to 40 % ash), oxygen and water in the gasification process[13] to produce raw gas. During the gasification process tars, creosote, pitch, as well as phenol, cresols, H_2S and NH_3 are formed. The effluent is cooled to remove the excess steam (by condensation), tar acids and ammonia in the condensate which are reworked later in the process.

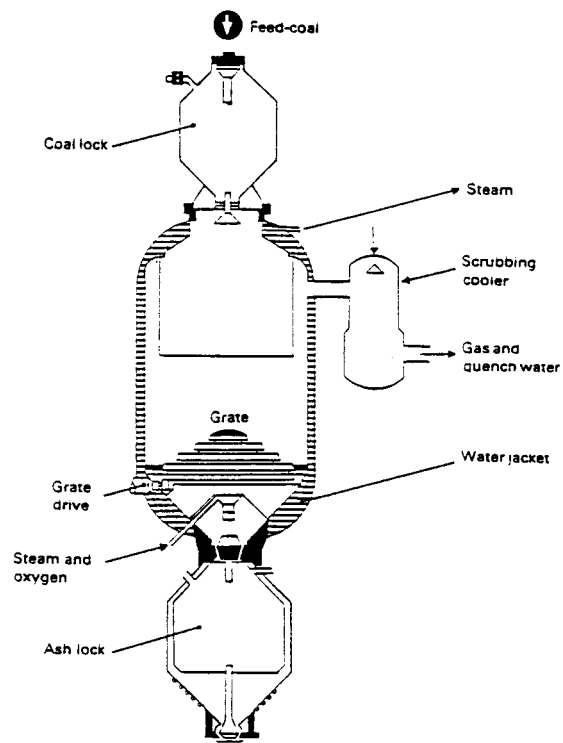

Figure 2.1. Lurgi dry coal gasifier[13]

The molar composition of the raw gas[13] is :

$$9\ \%\ CH_4 : 29\ \%\ CO_2 : 0{,}5\ \%\ H_2S : 1\ \%\ (Ar + N_2) : 60\ \%\ (H_2 + CO)$$

The raw gas is then washed with methanol at –50 °C in the Lurgi–Rectisol process[15,16] to remove CO_2 and H_2S, and this purified syngas[7], which is used in the Fischer–Tropsch process, has the following composition :

$$13\ \%\ CH_4 : 1\ \%\ (Ar + N_2) : 1\ \%\ CO_2 : 85\ \%\ (H_2 + CO)$$

2.1.4. CO hydrogenation (the Sasol process)

The Sasol group makes use of two processes to produce hydrocarbons from syngas : one is a fixed–bed reactor process (ARGE) and the other is a fluidised bed reactor process (Synthol).

The ARGE (Arbeitsgemeinschaft)[17] process makes use of multi–tubular vertical fixed bed reactors (Figure 2.2.). The tube bundles are surrounded by boiling water which controls the temperature of the system. The reaction is exothermic. A high linear gasflow is maintained to ensure isothermal conditions within the reactor.

The second process, the Synthol process[17], makes use of a vertical fluidised reactor (Figure 2.2.) in which a fine particle fused iron catalyst is fed out of a stand pipe by the syngas. A turbulent mixture of syngas and catalyst passes through heat exchangers, whereafter the excess gas and gas–phase hydrocarbon products are removed from the reactor. The boiling range of the liquid product is controlled to

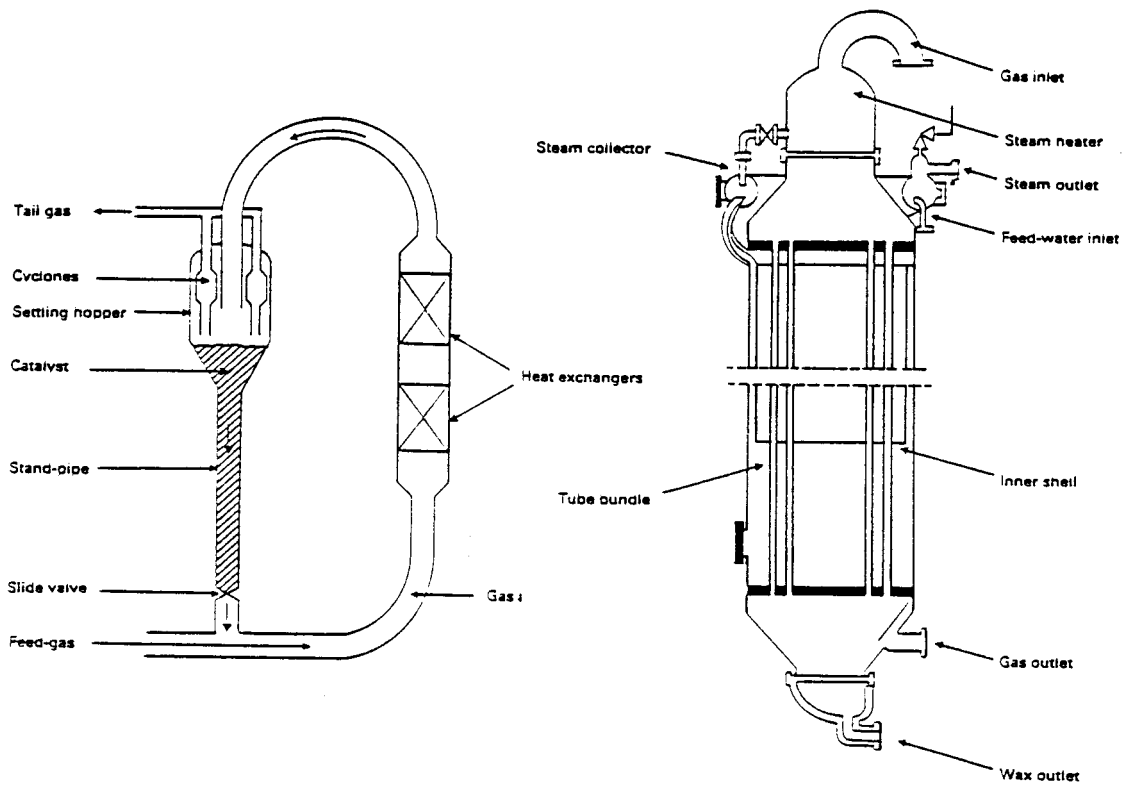

Figure 2.2. Sasol Synthol and ARGE reactors[18]

ensure that no clogging of the catalyst, which might influence the catalyst flow pattern, takes place.

The Synthol reactor produces lighter hydrocarbon products compared to the heavier products produced by the fixed bed system.

2.1.5. The Fischer–Tropsch mechanism

There are many concepts of the Fischer–Tropsch mechanism. The mechanisms

described in the literature[19,20-23] have attempted to explain the reaction route, products formed and the kinetics of the process. No attempt to discuss the various proposals will be given here. One proposal involving a methylene group is however mentioned below.

Masters[24] describes the Fischer–Tropsch process as the reductive polymerization of carbon monoxide while Anderson[8] gives the shortened mechanism as :

$$2H_2 + CO \longrightarrow \underset{\text{methylene}}{(-CH_2-)} + H_2O$$

$$(-CH_2-) + (-CH_2-) \longrightarrow \underset{\text{ethylene}}{(-CH_2-CH_2-)}$$

The methylene group functions as the reaction initiator and building block for the process. Termination of the product polymerization is a result of the desorption of the methylene group as ethylene (C_2H_4) or hydrogenation to ethane (C_2H_6).

The basic Fischer–Tropsch mechanism, which can be summarized from the available literature, involves the following fundamental steps.

1. adsorption of a reactant on the catalyst surface,
2. chain–initiation,
3. chain–growth,
4. chain–termination,
5. desorption of the products,
6. re–adsorption of the chain for further reactions.

2.1.6. The Fischer–Tropsch product distribution

The Fischer–Tropsch process produces a wide spectrum of hydrocarbon products[25], which range from methane to high molecular mass hydrocarbons such as found in hardwax. Although there are several mechanisms (Section 2.1.5.) that can rationalize the production of these products, it is clear that, in all proposals chain–growth involves a stepwise process in which one hydrocarbon unit links to another. This chain–growth procedure, or product forming action, can be controlled by four factors[17] : temperature, pressure, catalysts composition and gas composition

It is commonly found that the hydrocarbon product distribution can be explained by the Schultz–Flory model[26-29]. This distribution was originally developed from kinetic studies of polymers[30] and its extension to the Fischer–Tropsch process is illustrated in Figure 2.3.[26]. This figure incorporates propagation and termination probabilities as factors in the carbon chain building process.

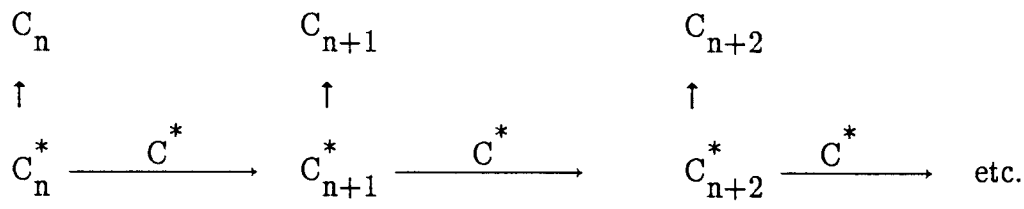

Figure 2.3. Chain growth and termination probabilities[26]

If N_o is the amount of active carbon species (C^*_n), which is initially adsorbed onto the catalyst surface, these species can either form products (C^*_{n+1}) or terminate to form products (C_n), (with n the number of carbon atoms in the chain), then the probability of chain growth, α, for a (C^*_n) species to add to another carbon to form

(C^*_{n+1}) can be given by

$$\alpha = r_p/(r_p + r_t) \qquad 2.1.$$

where r_p = rate of propagation

r_t = rate of termination

The number (N_n) of C_n species formed, is given by

$$N_n = N_0\alpha^{n-1}(1-\alpha) \qquad 2.2.$$

and can be rewritten on a mole fraction base; where the mole fraction (M_n) is defined as

$$M_n = N_n/N_0 = (1-\alpha)\alpha^{n-1} \qquad 2.3.$$

A convenient way of reporting the experimental data is in the logarithmic form :

$$\ln(M_n) = n\ln(\alpha) + \ln(\frac{1-\alpha}{\alpha}) \qquad 2.4.$$

A plot of $\ln(M_n)$ vs. carbon number (n) should be linear, (e.g. Figure 2.5. on page 21 for a precipitated iron catalyst), with the probability of chain growth (α) given by the slope as $\ln(\alpha)$ or by the intercept as $\ln(1-\alpha)$ at $n = 1$. Laboratory data are also normally given as weight fractions and not mole fractions, and this equation can be modified accordingly[31]

$$\log(\frac{W_n}{n}) = n\log\alpha + \log(\frac{1-\alpha}{\alpha})^2 \qquad 2.5.$$

where W_n = weight fraction of carbon number n.

It is evident from the Schultz–Flory distribution[10] that only the light (when $\alpha \to 0$) or heavy (when $\alpha \to \infty$) components can be produced with a high selectivity. All the other products go through a maximum yield, which can be deduced from the above equations (Figure 2.4.)[32]. For instance, it is possible to produce olefins (C_2–C_4) with 56 % selectivity, petrol (C_5–C_{11}) with a 48 % selectivity and ethylene with a 30 % selectivity under suitable conditions, with $\alpha = 0{,}75$.

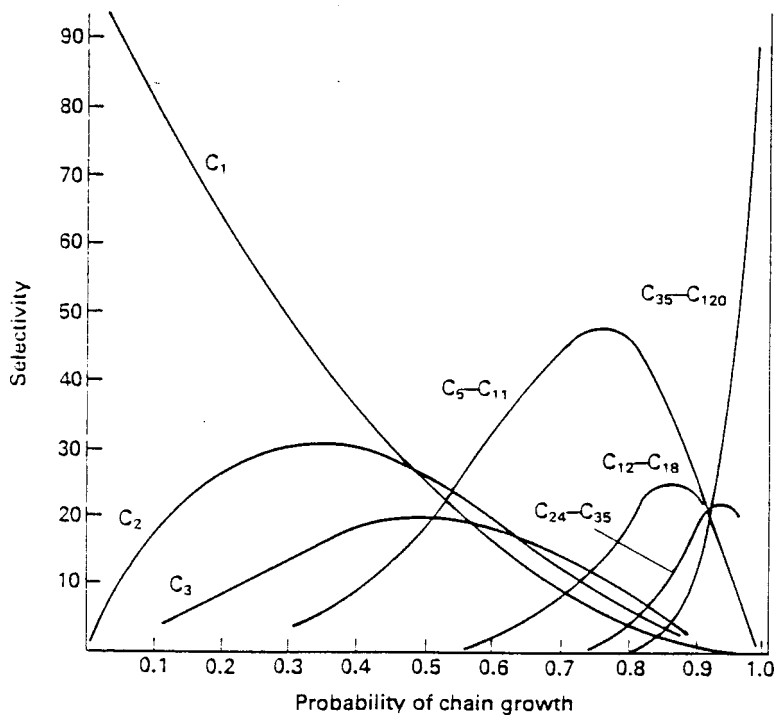

Figure 2.4. Plots of the calculated selectivities as a function of the probability of chain growth[32]

2.1.7. The Fischer–Tropsch products

Amelse[22] divides the product forming reactions for the synthesis of hydrocarbons from carbon monoxide and hydrogen into three groups :

1. Product forming reactions

Methanation :	$3H_2 + CO$	$\rightleftharpoons$	$CH_4 + H_2O$
Paraffins :	$(2n+1)H_2 + nCO$	$\longrightarrow$	$C_nH_{2n+2} + n\,H_2O$
Olefins :	$2nH_2 + nCO$	$\longrightarrow$	$C_nH_{2n} + nH_2O$
Methanol :	$2H_2 + CO$	$\longrightarrow$	CH_3OH
Higher alcohols :	$2nH_2 + nCO$	$\longrightarrow$	$C_nH_{2n+1}OH + (n-1)H_2O$

2. Non–product forming reactions

Boudard disproportionation :

$$2CO \longrightarrow C + CO_2$$

Coke formation :

$$xCO + (x+y/2)H_2 \longrightarrow C_xH_y + xH_2O$$

Carbide formation :

$$xM + 2CO \longrightarrow MxC + CO_2$$

$$xM + CO + H_2 \longrightarrow MxC + H_2O$$

Catalyst oxidation :

$$xM + yH_2O \longrightarrow MxOy + yH_2O$$

Catalyst reduction :

$$MxOy + yCO \rightleftharpoons xM + yCO_2$$

3. Secondary reactions

Water gas shift reaction : $CO + H_2O \rightleftharpoons CO_2 + H_2$

From reaction groups 1 and 2 it is possible to identify three product phases[18] :

1. An aqueous phase, in which low molecular mass products like alcohols, ketones, aldehydes and acids appear,
2. an organic phase consisting of oil and wax (C_5 and heavier) and
3. a gaseous organic phase consisting of hydrocarbons (C_1 to C_4).

2.2. Catalysts

2.2.1. Definition of a catalyst

Glasstone and Lewis[33] define a catalyst as a substance that increases the rate of a chemical reaction, but does not undergo a permanent chemical change in the process. A catalyst may either enhance the rate or decrease the rate of a reaction. In the latter case the catalyst is known as a "negative catalyst"[34].

2.2.2. Properties of a catalyst

Catalysts are broadly grouped[24] as homogeneous or heterogeneous catalysts. Although these catalysts differ greatly in composition, the following basic properties[33] apply to both :

1. The catalyst is chemically unchanged after the reaction is completed.
2. A small amount of catalyst is needed to enhance a reaction.
3. A catalyst does not affect the equilibrium position in a reversible reaction.
4. The catalyst does not initiate the reaction, but only affects the rate of the reaction.
5. During the reaction a catalyst lowers the activation energy[35] of the reaction to such an extent that the reaction goes via an easier or lower energy route[36].

2.2.3. Fischer–Tropsch catalysts

Transition metals have been known to be active in the Fischer–Tropsch reaction[8,19]. Of these metals, Fe, Co, Ru and Ni have been extensively investigated[37,38,39].

2.2.4. Effect of process parameters on the synthesis products

The Fischer–Tropsch process, as already mentioned, is the catalytic hydrogenation of carbon monoxide over a metal catalyst, such as iron, to produce paraffins, olefins and some oxygenated compounds. The product spectrum can be altered[13] by :

1. temperature, which when increased, shifts the product selectivity towards the lighter molecular mass compounds,
2. H_2:CO–ratio of the feedgas; an increase in this ratio shifts the product spectrum towards lighter hydrocarbon products and decreases the amount of olefins produced,

3. reactor pressure; Dry states[13] that most studies indicate a shift towards higher molecular mass product with an increase in oxygenate selectivity as the pressure is increased. The olefin content of the product does not change measurably.

The Fischer–Tropsch product distribution cannot be restricted to one specific product except for the formation of methane in the so called methanation process.

Carbon number	Compound type	Wt.%
6	Straight chain paraffins	45
	Straight chain α–olefins	25
	Straight chain internal olefins	26
	Branched chain paraffins	2.4
	Branched chain olefins	1.5
	Aromatics	0.002
8	Straight chain paraffins	41
	Straight chain α–olefins	35
	Straight chain internal olefins	19
	Branched chain paraffins	1.5
	Branched chain olefins	3.0
	Aromatics	0.17
10	Straight chain paraffins	42
	Straight chain α–olefins	37
	Straight chain internal olefins	15
	Branched chain paraffins	2.0
	Branched chain olefins	3.0

Table 2.1[40] Types of compounds present (Wt. %) in various carbon number products from iron catalysts

The different compounds present in the various carbon number ranges for the process with precipitated iron catalysts in a fixed bed reactor as grouped by Pichler[40] are given in Table 2.1..

The products appear to be mainly straight chain hydrocarbons with a low percentage of branched hydrocarbon chains and aromatics.

These results show that straight chain paraffins and olefins dominate the compound spectrum for both the gasoline and diesel fractions. Small amounts of alcohols, ketones and acids are present and no aromatics were detected.

A typical Schultz–Flory distribution[41] of the above mentioned products is illustrated in Figure 2.5..

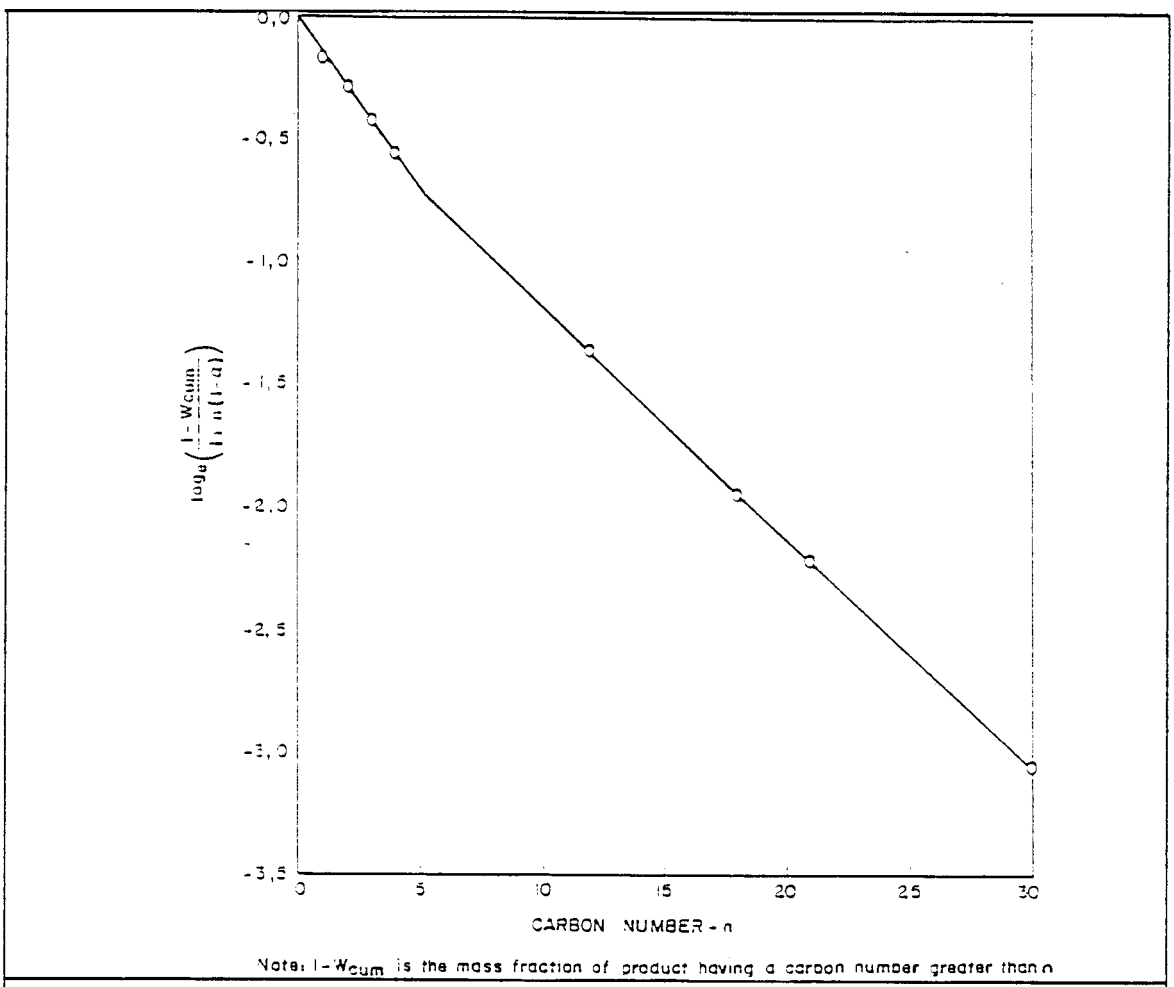

Figure 2.5. Schultz–Flory plot for a fixed bed reactor[41]

The plot of mass fraction product with carbon numbers greater than n vs carbon number n, exhibits two linear regions. In effect this means that two probabilities for growth, α, exist. The reason for this is not clear, but it has been proposed by König and Caube[42] that two active sites, one promoted by potassium and one potassium lean, are responsible for the two different chain growth probabilities within the same product spectrum. However, Dictor and Bell[43] have reported two chain growth probabilities for unpromoted iron catalysts. Donelly et al.[44] have produced a model based on the double probability concept, but results obtained by them and other researchers has placed doubt on the validity of such a model.

2.3. References

1. P. Sabatier and J.B. Senderens, *J. Soc. Chem. Ind.*, *21*, 1902, 504
2. F. Fischer and H. Tropsch, *Brennstoff–Chem.*, *4*, 1923, 276
3. Kirk–Othmer (editor), *Encyclopedia of Chemical Technology*, *4*, John Wiley and Sons, Inc., New York, 1964, 446 – 447
4. Yu–Ren Chin, *SRI International Process Economics Program, Report No. 21C*, 1986
5. E.D. Oliver and R. Hashimoto, *SRI International Process Economics Program, Report No. 91*, 1974
6. J. Meintjies, *SASOL 1950 – 1975*, Tafelberg Uitgewers, Kaapstad, 1975, 33
7. M.E. Dry, *Appl. Ind. Catal.*, *2*, (B.E. Leach, ed.), Academic Press, New York, 1983, 168
8. R.B. Anderson, *The Fischer–Tropsch synthesis*, Academic Press, Inc. Ltd., Florida, 1984, 5

9. B. Cornils, *Chemicals from Coal : New Processes*, John Wiley and Sons, New York, 1987, 3

10. G. van der Lee, *Ph.D–Thesis, Selectivity in Synthesis Gas Reactions*, Rijksuniversiteit, Leiden, Nederland, 1986, 2

11. E.J. Hoffman, *Synfuel Technologies*, The Energon Company, New York, 1982, 155

12. J.A. Linton and G.C. Tisdall, *Coke and Gas*, October, 1957, 402

13. M.E. Dry, *Catalysis – Science and Technology, Vol. 1*, (J.R. Anderson and M. Boudart, eds.), Springer–Verlag, Berlin, 1981

14. C.P. Snyman, M.C.J. van Vuuren and J.M. Barnard, *Chemical and Physical Characteristica of South African Coal and a suggested Classification System*, CSIR, ISBN No. 0798827998, 8

15. J.N. Marriott, *Chemsa*, August, 1986, 174

16. J.A. Linton and G.C. Tisdall, *Coke and Gas*, April, 1958, 148

17. W. Gerhartz, (executive ed.), *Ullmann's Encyclopedia of Industrial Chemistry, A7*, Weinheim, New York, 1986, 206 – 207

18. M.E. Dry, *Chemicals from Coal : New Processes*, John Wiley and Sons, London, 1987, 77, 86 – 92

19. H.H. Storch, N. Golumbic and R.B. Anderson, *The Fischer–Tropsch and related synthesis*, John Wiley and Sons, Inc., New York, 1951, 569 – 593

20. P.J. Denny and D.A. Whan, *Catalysis, 2*, 1978, 53

21. R.J. Kelly, *Ph.D–Thesis, A Study of the Fischer–Tropsch Synthesis at elevated Temperatures in a Shock–tube*, University of Natal, 1973, 4 – 16

22. J.A. Amelse, *Ph.D–Thesis, Silica supported Iron–bimetallic Catalysts for the Fischer–Tropsch Synthesis*, Evanston, Illinois, 1980, 10 – 11

23. R. de Haan, *M.Sc.–Dissertation, Die reaksies van C_2–oksigenate met Fischer–Tropsch katalisatore by 200 – 325 °C*, P.U. for CHE, South Africa, 1972, 2 – 8

24. C. Masters, *Homogeneous Transition–metal Catalysis*, Chapman and Hall, London, 1981, 228

25. M.E. Dry, *Hydrocarbon Processing*, August, 1982, 123

26. C.N. Satterfield, G.A. Huff (jr.) and J.P. Longwell, *Ind. Eng. Chem. Process Dev.*, *21*, *3*, 1982, 466

27. R.J. Madon and W.F. Taylor, *J. Catal.*, *69*, 1981, 41

28. N.O. Egiebor, W.C. Cooper and B.W. Wojciechowski, *Can. J. Chem. Eng.*, *63*, 1985, 826

29. R.A. Dictor and A.T. Bell, *Ind. Eng. Chem. Process Dev.*, *22*, *4*, 1983, 678

30. P.J. Flory, *Principles of Polymer Chemistry*, Carnell University Press, Ithaca, New York, 1953, 317

31. C. O'Young and S.L. Buchwalter, *C_1 Mol. Chem.*, *2*, 1987, 1

32. M.E. Dry, *Industrial Chemicals via C_1 processes*, *2*, 1987, 24 – 28

33. S. Glasstone and D. Lewis, *Elements of Physical Chemistry*, Second Edition, MacMillan Press Limited, 1983, 643 – 645

34. C.N. Satterfield, *Chemical Engineering Series*, McGraw–Hill Book Company, New York, 1980, 136 – 145

35. J.V. Quagliano and L.M. Vallarino, *Chemistry*, Third Edition, Prentice–Hall, Inc., Englewood Cliffs, London, 1969, 593

36. C.R. Dillard and D.E. Goldberg, *Chemistry*, Second Edition, MacMillan Publishing Co., Inc., New York, 1978, 488

37. M. Scurrell, *Scientiae*, *28*, *3*, 1987

38. N.O. Egiebor, *Ph.D–Thesis*, *The Preparation, Characterization and Evaluation of Precipitated Iron Catalysts for the Fischer–Tropsch Synthesis*, Queen's University, Kingston, Canada, 1985

39. C.D. Frohning, H. Kolbel, M. Ralek, W. Rottig, F. Schnur and H. Schulz, *Chemierohstoffe aus Kohle*, (J. Falbe, ed.), G. Thieme–Verlag, Stuttgart, 1977, 247

40. H. Pichler, H. Schulz and D. Kuhne, *Brennstoff Chemie*, *49*, *11*, 1968, 344

41. L. Caldwell, *Selectivity in Fischer–Tropsch synthesis*, CSIR, Pretoria, South–Africa, 1980, 4

42. L. König and J. Gaube, *Chem. Ing. Tech.*, *55*, 1983, 14

43. R.A. Dictor and A.J. Bell, *J. Catal.*, *97*, 1986, 121

44. T.J. Donnelly, I.C. Yates and C.N. Satterfield, *Energy and Fuels*, *2*, *6*, 1988, 734

CHAPTER 3

CATALYST DEACTIVATION

3.1. Introduction

A great number of articles (see sections 3.2., 3.3., 3.4. and 3.5.) have been published on the subject of catalyst deactivation. The aging and deactivation of industrial catalysts[1] may be due to a number of factors including defects in fabrication, the procedure for charging catalyst into the reactor, methods of activation, startup operations, unavoidable aging during a normal synthesis run, mishaps during operation and defects resulting from regeneration procedures.

The main causes for deactivation are normally grouped together and listed as poisoning, sintering and fouling. Although these three are mentioned as the main causes of deactivation, other effects like solid state reactions[2] and mechanical breakup[3] are also mentioned as problems that contribute to deactivation.

This chapter consists of a literature survey in which the reasons for, results of and operating precautions relating to deactivation are discussed. The various aspects of deactivation that will be discussed, are deactivation by poisoning, deactivation by sintering, deactivation by fouling and briefly, the deactivation by phenomena other than these, i.e. mechanical breakup and solid state reactions.

3.2. Deactivation by poisoning

3.2.1. Definition of poisoning

Poisoning may be defined as the reversible or, more often, irreversible chemisorption of an impurity on a catalyst surface, eliminating or altering the active catalytic sites used for synthesis[4,5] to such an extent that the initial activity or product selectivity of the catalytic species is negatively influenced.

3.2.2. Poisoning of catalysts

Catalytic poisoning has been extensively studied and a variety of articles on mono– and multifunctional catalysts[2,6] have been published. It is a problem[7] encountered in many processes such as in steam reforming, CO–shift, polymerization and isomerization reactions, catalytic reforming and cracking and hydrocracking reactions. Early publications on poisoning by Maxted (1951)[8] and Butt[9,10] have provided the framework for all later discussions in this area of catalysis.

In the study which follows, the poisoning of metallic catalysts, in particular the effect which impurities like sulphur have on Fischer–Tropsch iron catalysts and its product behaviour, will provide the basis for an assessment of poisoning studies.

Oudar[11], as well as Hegedus and McCabe[12], distinguish between two main types of poisoning by impurities; competitive reversible adsorption of the impurity, also known as inhibition, and irreversible adsorption of the impurity, leading to permanent poisoning of a catalyst.

Irreversible poisoning may be explained[11] by two different effects :

1. Catalytically active sites blocked by the impurity : The active sites are blocked on a one–to–one basis by the poisoning substance. The catalytic activity decreases linearly as a function of the concentration of the impurity on the surface.
2. Electronic or ligand effects : In this case the reactivity of the catalytically active sites located at varying distances from the site covered by the poison may be influenced negatively through electronic or ligand effects.

Figure 3.1.[11] distinguishes between the different sites that have been deactivated by irreversible poisoning as described above.

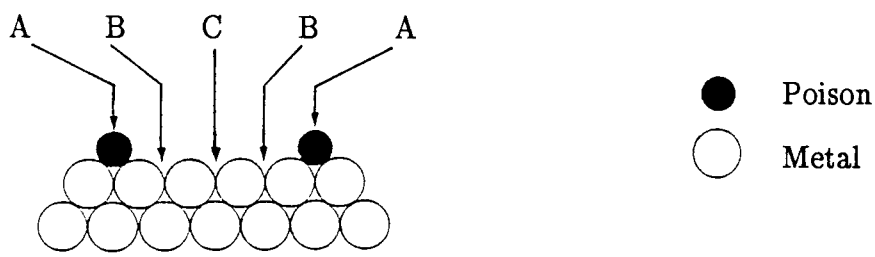

Figure 3.1. Blocking and electronic effects in poisoning[11]. A, blocked site; B, site eventually affected by a short–range electronic effect and by the fact that one of its constitutive atoms is linked directly to the impurity; C, site eventually affected by a long–range electronic effect

Hegedus and McCabe[12] state that poisoning problems are composed mainly of two factors; the nature of the interaction of the poison with the catalyst surface and the

effect of the poison on the catalytic reaction. Four main categories of catalyst poisoning have been mentioned : poison adsorption, poison induction, surface reconstruction and compound formation between the poison and the catalyst.

Earlier work by Maxted[8] and Butt[9,10] indicated that the metals which are most susceptible to poisoning, are predominantly the Group VIII metals. These metals include iron, cobalt, nickel, copper, palladium, silver and gold (see Table 3.1.[8]).

Fe	Co	Ni	Cu
(26)	(27)	(28)	(29)
Ru	Rh	Pd	[Ag]
(44)	(45)	(46)	(47)
Os	Ir	Pt	[Au]
(76)	(77)	(78)	(79)

Table 3.1. Catalysts arrayed in Periodic Series[8]

Three groups of poisons have been identified for these metals, namely molecules containing Group Vb and VIb elements (See Table 3.2.[8]), compounds which consist of toxic metals, and metallic ions and molecules with multiple bonds.

The ability of the group Vb or VIb elements to poison catalysts is related to their valence states (see Table 3.3.[8]). No toxicity is found for the elements which are

coordinately saturated, but those having unshared electron pairs or empty valence orbitals act as active poisons. Thus, whenever chemisorption is possible between the elements with unshared electrons and a specific catalyst, this element may act as a poison preventing the catalyst to perform normally.

Group Vb	Group VIb
N	O
P	S
As	Sc
Sb	Te

Table 3.2. Group Vb and VIb elements[8]

H_2S and volatile S compounds such as CS_2 and mercaptans are generally considered to be poisons[13]. Experimental work by Steinbrecher[14] showed that the poisoning ability of organic sulphur decreases in the order :

$$\text{thiophene} > \text{mercaptans} > CS_2 > COS.$$

Likewise, Maxted and Evans[15] state that the poisoning ability of sulphur compounds increase with an increase in molecular size of the sulphur compounds :

$$\text{cysteine} > CS_2 > H_2S$$

where cysteine is $HSCH_2CH(NH_2)CO_2H$.

Toxic types		Nontoxic types (shielded structure)
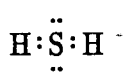	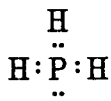	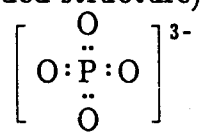
Hydrogen sulphide	Phosphine	Phosphate ion
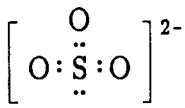		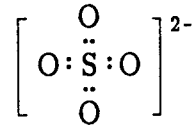
sulfite ion (alo selenite and tellurite)		sulfate ion (also selenate and tellurate)
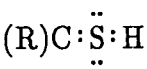		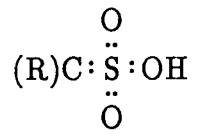
organic thiol		sulfonic acid
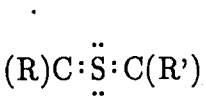		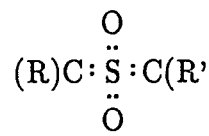
organic sulfide		sulfone

Table 3.3. Influence of electronic configuration on toxicity[8]

It is well known that sulphur compounds, mainly COS and H_2S, are products of the coal gasification process, a process in which the synthesis gas for the Fischer–Tropsch process is produced. Although the gas is purified, very low levels of sulphur may exist in the feed gas, which could poison the catalyst used during hydrocarbon synthesis.

Although sulphur is commonly believed to be a catalyst poison, there are situations in which poisoning is believed to have a positive effect on a process. This occurs when the poison changes the selectivity of the process to a desired product

spectrum. Iron as catalyst is known to be selectively poisoned by phosphorous to give a better yield of C_2–C_4–olefins[16].

Hughes[17] has remarked on three principle ways to minimize the effect that impurities in the feedstock have on the catalysts used in plant operations :

1. Purify the feedstream to such a level that the poisoning effects become unimportant.
2. Make use of guard reactors, to remove the impurity before it reaches the main reactors.
3. Design the reactors to minimize poisoning, i.e. a sufficiently long reactor bed may give adequate catalyst life if the activity profile of the catalyst in the reactor bed is suitable.

3.2.3. The poisoning mechanism

The mechanism by which poisons deactivate a catalyst has been studied from several viewpoints. Many of these studies have dealt with the modification of catalyst surface properties[18]. Equations that relate the position of the poison–front to time[19], kinetic studies using single pellet diffusion reactor techniques[20] and non steady state behaviour studies on the catalyst poisoning process[21] have been used to evaluate the catalyst deactivation reaction.

As it is not the objective of this project to dwell on the mechanistic side of catalytic poisoning, only a basic overview of this very exiting field of study is given.

Poisons may occur in the solid, liquid and gaseous states, but as far as

hydrogenation reactions are concerned, the latter state is most applicable to the Fischer–Tropsch reaction[22].

Several factors are characteristic of the poisoning effect[23]. According to the following equation :

$$K_c = K_o\,(1-\beta\,c) \qquad 3.1.^{23}$$

the poisoning coefficient "β" is the first characteristic factor which describes the susceptibility of a given amount of catalyst to a poison. K_c and K_o are the reaction velocity constants in the presence and absence of the poison, respectively, and c is the concentration of the poison. The second characteristic factor is the absolute amount of poison needed to totally deactivate the catalyst and is a measure of the 'extent' to which a poison acts. The third factor has to do with the tendency with which a poison is retained at the catalyst surface and is also known as the retention factor.

The main effect a poison has, is to slow down a catalytic reaction to such an extent that the process becomes unprofitable for commercial use. Two factors, namely temperature and contact time of the poison with the active surface of the catalyst, play a major role in the effect that the poison has on the catalytic process. Even pressure is known to have an influence on the velocity at which the poison deactivates the reaction. Furthermore, it should be remembered that poisons are very specific for the type of catalyst used and that small quantities of poison may remain inactive up to a point where the concentration is such that the catalyst is negatively affected.

Berkman et al.[23] state that the poisoning of catalysts is primarily a surface effect

where the first stage of the poisoning curve corresponds to that of the adsorption curve. The activity is also a linear function of the poison content as illustrated by Maxted[8] in Figure 3.2..

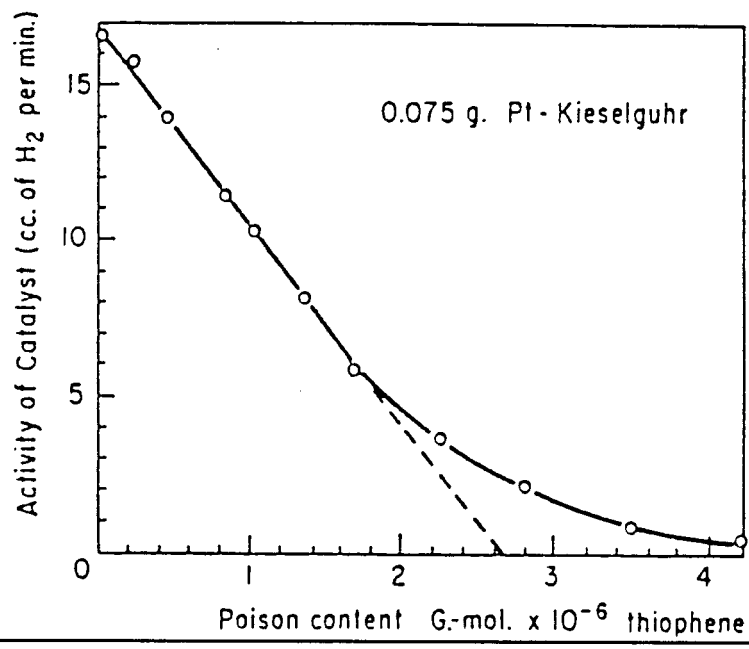

Figure 3.2. Form of a typical poisoning curve[8]

Figure 3.2. shows an approximately linear drop in activity with an increase in catalytic poisoning. The inflection in the graph can be explained by the fact that at some stage during poisoning, the catalyst activity falls far less steeply with an further increase in poison content, as the surface is already saturated with enough poison and therefore any excess increase in the poison level will have little adverse effect on the deactivation profile.

The poisoning coefficient mentioned previously in expression 3.1. can be calculated from the slope of the linear portion of the graph as the expression can be written as :

$$K_c = K_o - K_o \beta c \qquad 3.2.$$

The value for "β" may be useful in comparing the toxicities of different poisons on a specific catalytic surface.

A number of mechanistic considerations have been proposed to explain the poisoning phenomenon. In a review of the literature, Berkman[23] mentions a few of these proposals :

1. The poison adsorbs onto the catalyst surface and acts as a screen, preventing the reactants from coming into contact with the actual catalytic surface.
2. Poisons may adsorb preferentially onto the active centres, preventing the catalytic reaction from taking place.
3. At suitable temperatures the number of catalytic active sites may be reduced by the presence of poisons.
4. In some cases the poison may penetrate into the bulk of the catalyst, while in other cases the poison may only be adsorbed onto the surface of the catalyst.
5. In heterogeneous catalysts, poisoning may result from destruction of the heterogeneity of the catalyst surface as the poison, which comes into contact with the active site, dissolves the active site converting it into a plane crystal phase.
6. With gaseous poisons it is postulated that the poison surrounds the reactant molecules in such a way that it becomes disorientated, so that the reaction with the catalytic surface cannot take place, i.e. the reactive part of the reactant molecule is turned away from the catalyst surface. This therefore implies that only a small quantity of poison is needed to

have a big negative effect on the catalyst reaction.

7. It is also postulated that the mechanism of catalytic poisoning could also be explained by chemical (as well as physical) processes. It is possible that the poison may react with the catalyst surface and thereby change its properties. Hydrogen sulphide is a typical example, reacting with the catalyst surface to form a stable surface compound, which cannot react with the reactants at the specific reaction conditions. However, it should be noted that not all sulphur containing substances act as poisons. Sulphides, for example, inhibit the catalytic hydrogenation reaction, while sodium sulphate does not show this effect.
8. In a paper describing the modeling of poisoning on metals, Oudar[11] has remarked that the presence of sulphur has an influence on certain properties necessary for good catalysis. He postulated that the adsorption rate, binding energy and the adsorption capacity of CO are all decreased in the presence of sulphur. It is also mentioned that the dissociation of a dihydrogen might require two free nearest neighbour sites. Preadsorbed sulphur studies on Pt, Ni, Ru and Fe have revealed that the adsorbed sulphur decreases the initial sticking coefficient for hydrogen as the sulphur blocks the adsorption sites, decreases the adsorption capacity, decreases the binding energy and blocks the sites needed for dihydrogen desorptions. Furthermore, it is concluded that for poisons, which have similar atomic radii, the poisoning effect will increase with increasing electronegativity : Cl > S > P.

3.2.4. Sulphur and the Fischer–Tropsch Process

Although sulphur is known[11,17,24] to deactivate the Fischer–Tropsch catalyst, a

Russian research group[25] claims to have operated a precipitated iron catalyst with sulphur–containing synthesis gas for a period of two months without observing any deactivation. The synthesis gas had a concentration of 50 mg/m^3 H_2S. Similar effects were reported twenty odd years later by a second Russian[26] research group.

There is also evidence that sulphur–containing compounds introduced into synthesis gas have a beneficial effect on both the catalyst activity[27,28] and selectivity[16,28,29] for various products.

On the other hand, Chaffee et al.[30] found that a precipitated iron catalyst system deactivated immediately after introducing H_2S into the feed stream. An immediate drop in CO conversion was observed. This is illustrated in Figure 3.3.[30].

Figure 3.3. shows an essentially linear deactivation rate the moment H_2S is introduced into either a hydrogen rich or hydrogen lean synthesis gas. On introducing 300 ppm H_2S into a similar catalyst system, a drop in CO conversion is observed, while there is an increase in the selectivity of the light hydrocarbons produced. This effect can be seen in Figure 3.4.[30].

XRD[30] analysis on a manganese catalyst showed sulphur to be present in the MnOS phase, while XPS[30] results revealed that the sulphur was trapped mainly in the top part of the reactor with no sulphur present at the bottom part of the reactor. The surface sulphur detected, was present in at least two forms : SO_4^{2-} and S^{2-}. SEM[30] analysis supported the fact that sulphur was found mainly in the top part of the reactor and it became evident that the sulphur was concentrated on the surface of the catalyst and thus had not reacted with the catalyst or migrated to the interior of the catalyst.

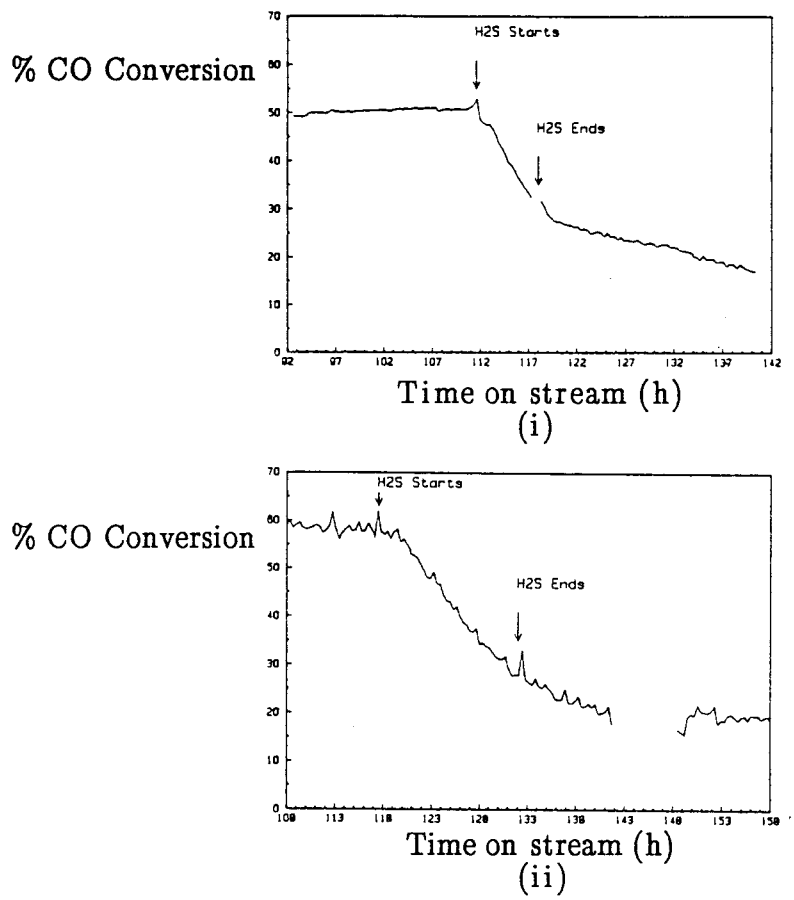

Figure 3.3. Conversion[30] during hydrogen sulfide exposure under (i) hydrogen rich conditions and (ii) hydrogen lean conditions

These results show that a manganese Fischer–Tropsch catalyst may act as a very effective sulphur removing agent. Thus, if a guard reactor with the same catalyst that is used for synthesis purposes is employed, the actual synthesis reactor might receive a sulphur free feed, or at least a feed containing such a low sulphur level that the catalyst activity of the synthesis reactor is not influenced drastically. This corresponds with the suggestion by Hughes[17] that one of the three principal ways to minimize harmful impurities, in this case sulphur in the feed gas, would be to purify

the feed gas by making use of a guard reactor, to remove the poison before it reaches the synthesis reactor.

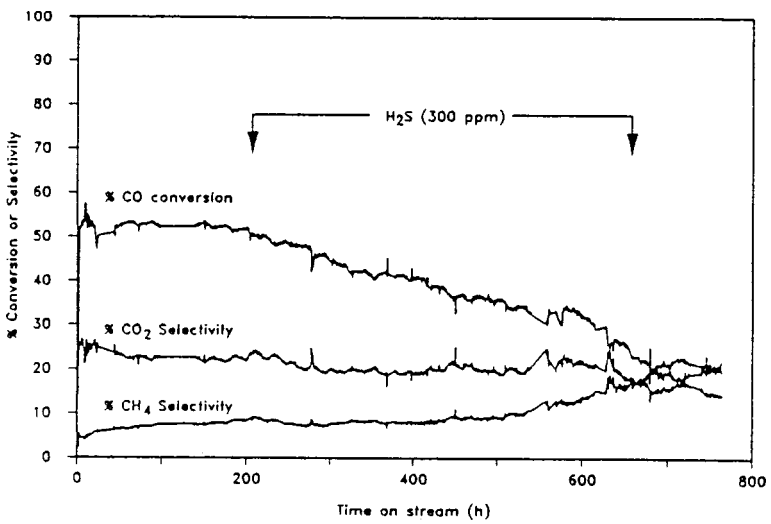

Figure 3.4. Conversion and selectivity[30] during hydrogen sulphide exposure under hydrogen rich conditions

In a review on catalyst poisoning covering the literature prior to 1970, Madon and Shaw[13] documented some interesting findings. A short overview of relevant information as published by these authors follows.

A patent by the I.G. Farbenindustrie Aktiengesellschaft[31] claims, that small quantities of sulphur, with the necessary alkali promoters, extends the life of the group VIII metals as catalysts. The production of higher hydrocarbon products was reduced while the olefin content of the lower hydrocarbon products was increased.

Similar results were reported by Fujimura and co–workers[32], who exposed a Ni–Mn catalyst, promoted with Fullers earth, to CS_2 and H_2S, and found a small improvement in the activity and selectivity of this catalyst. An enhancement of the olefin production was also reported by Myddelton[33] for a cobalt Fischer–Tropsch catalyst poisoned by organic sulphur and hydrogen sulphide.

By adding small quantities of sulphur (0,8 % by weight) to a cobalt catalyst, Herington and Woodward[34] found that the yield of liquid hydrocarbons increased, while the amount of gaseous hydrocarbons decreased. They also observed an increase in the molecular weight of the liquid hydrocarbons for reactions performed at 300 °C. Larger quantities of sulphur were, however, found to totally deactivate the catalyst.

Experiments performed by Fischer and Meyer[35], and also King[36], on nickel and cobalt catalysts poisoned by CS_2, showed similar results to those reported by Herrington and Woodward.

When sulphur–containing gases were passed over a fused Fe catalyst, Layng[37] observed a reduction in CO_2 production and an improvement in the yield of liquid hydrocarbon products and olefin selectivity. Sebastian[38] found a MoS_2 catalyst, which had methanation activity, to be resistant to sulphur poisoning, while Wencke[39] demonstrated that activity loss due to sulphiding on a Mo–Al_2O_3 catalyst could be compensated for by increasing the reaction temperature. They also showed that H_2S poisoning was temporary and reversible with this catalyst. Similarly Steward[40] reported studies on a sulphur resistant molybdenum–based catalyst.

Shultz et al.[41] have proposed that sulphur located in the bulk of a molybdenum–based catalyst does not affect activity, whereas it is sulphur on the catalyst surface

that causes deactivation. Increased oil yields were reported by Mulford and Russell[42] for a cobalt based catalyst 'poisoned' by sodium sulphide. An iron based catalyst, which was treated with halogen compounds and tested by Davis et al.[43], yielded more C_2–C_{10}–olefins than the untreated catalyst. Treatment of the catalyst with 0,02 % to 0,5 % (by weight) of a sulphur containing compound, increased the olefin yield even further.

Kingdom[44] showed that when H_2S was introduced to a mill scale catalyst, methane production was favoured and that an increase in the sulphur level produced more alcohols and less olefins. Furthermore, Rapopart and Muzovskaya[25] demonstrated that a precipitated Fe–Cu catalyst system, promoted with an alkali and reduced in an H_2 atmosphere at a low temperature, was resistant to high concentrations of organic sulphur, COS and CS_2.

Madon and Shaw[13] concluded their review by giving a summary of possible mechanisms which they thought contributed to the observed effect of sulphur on the catalytic processes. In the summary it was suggested that reduction of the catalytic activity by sulphur takes place to such an extent that the reactions would be kinetically rather than diffusion controlled. As far as the authors were concerned, hot spots in the reactor would be eliminated and beneficial changes in the selectivity could occur. They postulated that if the catalytic surface is composed of active sites with surface atoms having different coordination numbers, then sulphur can react with certain sites and inhibit reactions which normally occur on those sites. New catalytically active sites may be formed by reaction of sulphur with the active material. The activity of the reaction may be enhanced by this action and a change in selectivity may be observed.

Considering the above arguments, two main conclusions may be made :

1. When low loadings of sulphur (0,05 % – 0,8 % by weight) are introduced into a catalytic system, the catalyst activity may be slightly increased and olefin selectivity of the lower hydrocarbon products may be enhanced. It appears to be that these very low levels of sulphur may improve the actual life time of the catalyst.
2. Whenever higher loadings of sulphur (> 1 % by weight) are introduced into the catalytic system, the catalyst activity declines, more methane is produced and the selectivity to higher hydrocarbons is unlikely.

In a more recent publication on the effect of sulphur poisoning on cobalt and iron Fischer–Tropsch catalysts, Bartholomew and Bowman[45] state that monolayer surface sulphides are formed on iron catalysts. The iron catalysts were poisoned by low concentrations of H_2S (2 ppm) at 500 K. At higher sulphur concentrations bulk sulphides were formed. They also state that a greater loss of activity is observed whenever in situ poisoning, instead of presulphiding, is performed. It is also interesting to note that they observed an increase in the average molecular weight of hydrocarbon produced by cobalt during in situ exposure to H_2S, but not for the iron catalysts.

H_2S sulphiding[46] of a cobalt catalyst in a fixed bed reactor at 180 °C, atmospheric pressure and a H_2:CO–ratio of 2:1 with 250 ppm H_2S, gave the results shown in Table 3.4.. In all cases the catalyst nearest to the inlet of the reactor, i.e. first 20 % of the catalyst bed, contained most of the sulphur. The amount of sulphur decreased very rapidly further down the reactor bed to a nominal sulphur content < 0,01 % S by weight. These findings confirm the results given on page 37 for XRD, XPS and SEM analysis on a Fischer–Tropsch manganese catalyst.

Section	Reactor 1	Reactor 2	Reactor 3	Reactor 4
1	4,96	5,36	7,66	7,57
2	1,32	2,07	2,53	2,17
3	1,02	0,81	1,38	0,74
4	0,06	0,09	0,05	0,05
5	0,05	0,04	0,08	0,06
6	0,03	0,46	0,01	0,02
7	0,03	0,16	0,04	0,05
8	0,01	0,13	0,03	0,02
9	0,02	0,08	0,04	0,03
10	0,03	0,07	0,04	0,05
11	0,01	0,10	0,05	0,01
12	0,02	0,09	0,02	0,02
13	0,01	0,08	0,02	0,05
14	0,01	0,10	0,03	0,03
15	0,01	0,03	0,02	0,01
16	0,01	0,08	0,01	0,02
17	0,01	0,04	0,02	0,06

Table 3.4. Sulphur distribution (weight %) in catalyst beds[46]

Sulphur poisoning studies of Ni, Co, Fe and Ru catalysts in the CO hydrogenation reaction referred by Agrawal et al.[47], has shown that the presence of even 13 ppb H_2S in the gas phase reduces the methanation activity of these catalysts about tenfold and indications are that the surface sulphides are much more stable than the bulk sulphides. They postulate that sulphur adsorption is the primary reason for deactivation and that this is caused by geometric blockage of the active sites. Any electronic effects arising from the sulphur poisoning are believed to have only a secondary effect.

Denny and Twigg[3] plotted a graph of activity, crystallite size and poison level for different sections of a copper–based low temperature–shift catalyst unloaded, section by section, from a plant scale reactor. They found sulphur to be the main

contributor to loss in activity in the top part of a reactor. This effect is illustrated in Figure 3.5. These results again confirm results as discussed previously.

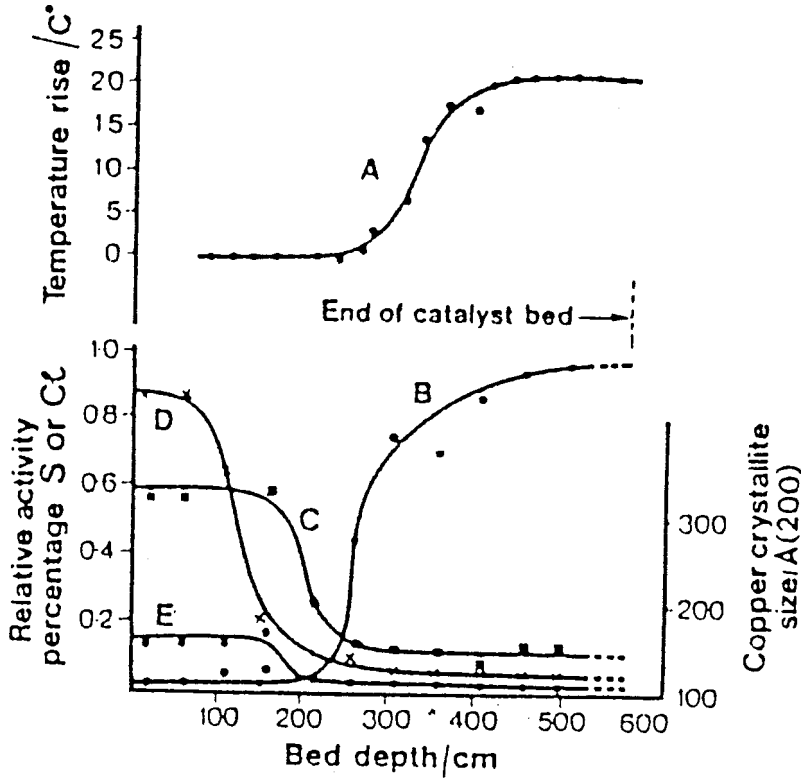

Figure 3.5. The variation of catalyst activity[3] (from laboratory tests), copper crystallite size and poison levels (Cl and S) with reactor depth for an old charge of low temperature shift catalyst in a commercial reactor.
A : temperature profile immediately before discharge;
B : relative activity; C : copper crystallite size;
D : sulphur content; E : chloride content

When using sulphur to perform poisoning studies, it should be noted that sulphur tends to deposit even on stainless steel surfaces[48]. Sulphur deposits in the experimental equipment can jeopardize further experimental results obtained for experiments performed in 'sulphur free' systems.

Finally, it is appropriate to conclude this section with the following remarks.

1. Sulphur containing compounds, like H_2S, originating from coal gasification, are definitely a threat to a precipitated iron catalyst, and will deactivate this catalyst when coming into contact with it.
2. It has been clearly shown that sulphur is normally trapped in the top section of a fixed bed reactor with very low concentrations appearing in the middle and bottom sections of the reactor bed. Therefore it seems to be appropriate to use a guard reactor to purify the feed gas before it enters the synthesis reactor.
3. As low concentrations of sulphur, i.e. 13 ppb – 300 ppm H_2S, are known to deactivate Fischer–Tropsch catalysts, it appears that the poisoning effect may be mainly due to the adsorption (chemisorption) of the poisonous substance onto the catalyst surface, screening the catalytic active sites from taking part in the reaction.
4. It is also evident that surface techniques like XRD, XPS and SEM may be put to good use in verifying the above mentioned factors.

3.3 Deactivation by sintering

3.3.1. Definition of sintering

Sintering may be defined as an irreversible[49] physical process, causing a loss in catalytic activity due to a loss of active surface area[2]. This loss of active surface area is caused by the growth of metal crystallites[49] on a support, decreasing the surface area of the catalyst.

3.3.2. The sintering of catalysts

Sintering of catalysts is of importance in most catalytic systems, especially in high temperature catalytic processes. This topic has been dealt with extensively in several publications[2,11,49,50,51].

The sintering process is a very complex one and several factors should be taken into account when trying to explain it. Cusumano et al.[51] has summarized these factors as being the structure and stability of the metal surface, the equilibrium shape or configuration of the metal particles, the stability of metal particles with respect to dissociation as a function of particle size and shape, the mobility of metal atoms over the metal surface, the interaction of metal particles and individual atoms from these particles with the support surface, the mobility of metal particles and atoms over the support surface, and the support morphology.

The activation energy of sintering is generally high and therefore an increase in temperature results in an increase in the sintering rate. The rate of sintering is also faster in an oxygen–containing atmosphere than in a hydrogen–containing atmosphere[11,50]. Furthermore, sintering increases with time and therefore is typical of the catalyst aging process.

Other factors influencing the ability of a catalyst to sinter, are the nature of the support[50] and the degree of metal loading.

In a comprehensive, well structured look at sintering, Hughes[17] describes sintering as follows :

"From a structural viewpoint, loss of area in catalysts compacts is caused by crystal growth through smaller crystals growing into larger crystals with reduction in

surface free energy. Metals and metal oxides sinter readily if they are present in the system as very small crystals (< 50 nm)."

Supported metal catalysts are thermally more stable[51] towards sintering than unsupported metal catalysts, and therefore the presence of a support produces a more stable[2] catalyst. The function of the support is to act primarily as a spacer[11], preventing or minimizing the growth of and movement by metal crystallites to form clusters.

In his discussion, Hughes[17] also shows that a metal with a low melting point will sinter more rapidly than one with a higher melting point. This means that the lower the melting point of the metal, the larger the portion of refracting material needed to act as a spacer between the metal particles.

Finally, Hughes remarks that most spacer materials, such as aluminas and silicas, can be manufactured in a high surface area form, making them suitable support materials for catalysts, and many are known to have a beneficial effect on the activity of the catalyst.

Another factor that needs to be investigated when considering sintering, is the morphology of the support. The surface morphology[11] has two main effects on the sintering process, one being the effect on pore structure of the support and the other being irregularities of the surface structure itself. These effects cause energetically stable and metastable positions for the crystallite on the surface. As a result, metal particles present in a pore of the support are not able to migrate and stabilization of the catalyst surface in the presence of the support is observed. It is also suggested that particle growth can occur via atomic migration or vapour transport mechanisms.

Furthermore, Dowden[52] describes the effect of polar molecules on metals and concludes that water as well as a large number of other polar impurities, accelerates the sintering of catalysts, even when present in small concentrations. He mentions five adsorption types through which an oxygen–containing polar molecule like water can adsorb onto oxides :

(i) strong dissociative chemisorption

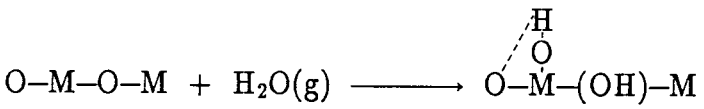

(ii) associative chemisorption

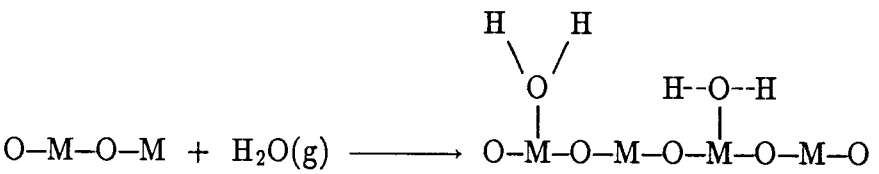

(iii) physisorption, hydrogen bonded second layer

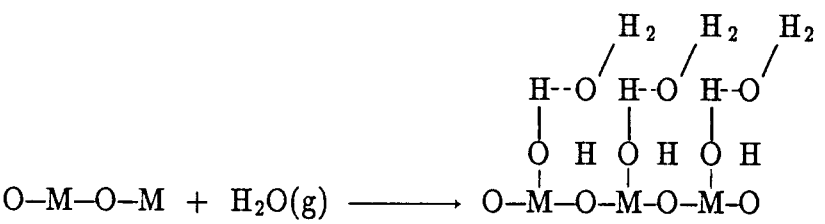

(iv) physisorbed multilayers

(v) capillary condensed adsorbtion

Using a type II Brunauer–Emmett isotherm (Figure 3.6.), with p the partial pressure watervapour and p_0 the saturated vapour pressure of water, Dowden proposed that an increase in water vapour partial pressure would have an effect on the growing of crystallites through stages (i) to (v), as given above.

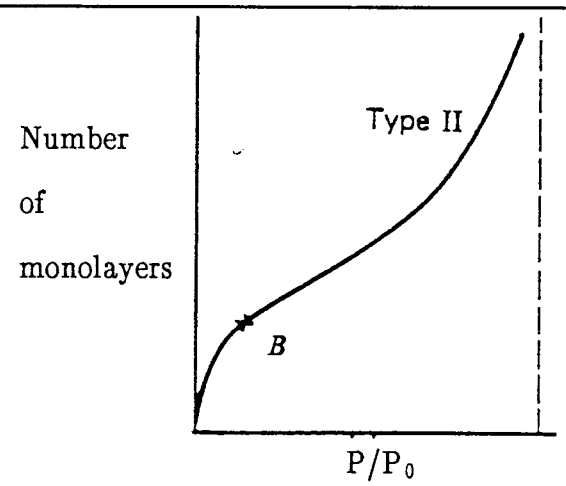

Figure 3.6. Brunauer–Emmett type II isotherm[52]

It is mentioned that all classes of solid, i.e. metals, semiconductors and insulators, when wetted by water, will take up water in the states through (i) to (v), with the result that the polar molecules can affect the rate of leptan (atom, ion, molecule, etc.) transport during sintering in at least five ways. Complexes of greater volatility than the isolated solid are formed (e.g. hydroxides), or condensed liquid phase, in which leptans are soluble, may be formed. Multilayers of adsorbed molecules, which dissolve leptans, can also form. Furthermore, the molecules could chemisorb forming states which increase the rate of surface diffusion. Finally, molecules may dissolve in the volume to form defects or compounds which increase rates of volume diffusion.

The stability of a metal towards sintering[49] can be obtained by using lower metal particle densities and also metals with lower values of surface diffusion. It is also suggested that a catalyst with a broad pore–size distribution will sinter more rapidly than one with a narrow pore–size distribution.

Satterfield[49] also states that alloying of a metal with a second metal of higher melting point, should also increase the stability towards sintering, but that this might have an effect on the catalytic properties of the catalyst. It is also evident from the literature review[49] that, where possible, lower temperatures and lower water vapour pressures should be employed in the catalytic process used.

3.3.3. The sintering mechanism

Active studies on the mechanism of sintering and models of these mechanisms date back to the early 1970's, when Flynn and Wanke[53,54] and Ruckenstein and Pulvermacher[55], published work on the modeling of supported metal catalyst sintering and the growth kinetics and size distributions of supported metal crystallites, respectively. In the late 1970's, Ruckenstein and Dadyburjor[56] published mechanistic work on the aging of supported metal catalysts. More recent publications by Bordia and Scherer[57,58,59] include a constitutive model and a comparison of constitutive models and rigid inclusions on constrained sintering. In addition, Bellare et al.[60] have published work on the modeling of the bimodal distribution of particle sizes, shapes and relative positions of supported metal catalysts.

Basically two types of sintering models have been proposed[61] :

1. Single species or atoms migrating from one particle to another.
2. The particles themselves move over the substrate and coalescence with other particles[55].

These two models are extreme cases of a more general model[56], which takes into account the fact that a wide range of particle sizes, ranging from adatoms to large particles exist, and that all these particles move over the substrate. This movement is related to diffusional parameters which are size dependant.

This study is not concerned with the detailed mechanism of sintering. However, a basic overview on the mechanism of sintering of a catalyst follows.

In a short review on the sintering and mobility of metal particles, Satterfield[49] has explained the various stages of sintering making use of Figure 3.7. :

(a) It is stated that a metal present in the form of separate atoms, as a monomer dispersion, will strive to obtain a more stable two dimensional cluster, one atom thick. This two dimensional raft of atoms will form through surface–diffusion of the atoms. These larger two dimensional clusters are more stable since the atoms on the edge of the raft have higher energies than those in the interior, thus preventing these atoms from diffusing away from the raft.

(b) It is also suggested that a two dimensional cluster can rearrange into a more stable form in which the metal–metal bond energies will exceed that of the metal–support energies. These larger three dimensional crystallites are much more stable than the smaller crystallites.

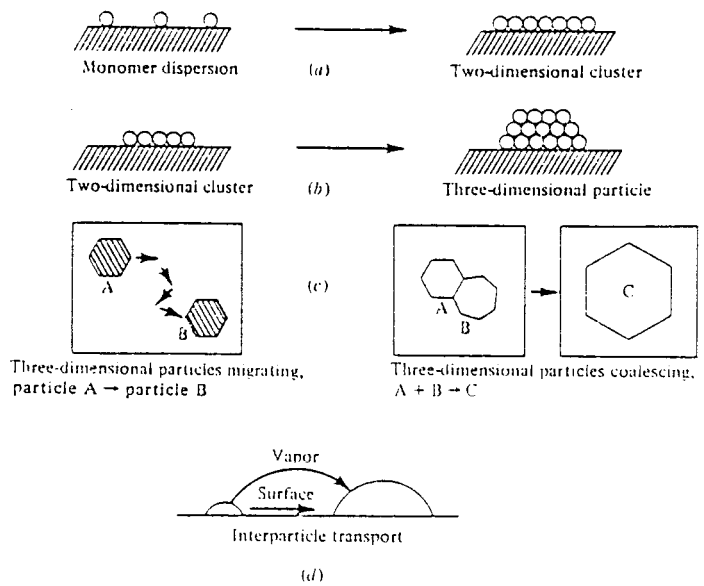

Figure 3.7. Schematic of the various stages in the formation and growth of particles from a monomer dispersion[49]

(c) Further crystalline growth of a stable three dimensional clusters may occur via two mechanisms :

1. Ostwald ripening, in which atoms of particle A detach and move to particle B.
2. In the second mechanism individual crystallites move along the surface to cause growth through coalescence similar to Brownian movement. The three dimensional particles will coalesce through a neck between two particles to take on the shape of the lowest energy configuration.

The rates of these different processes are determined either by the metal–metal bond energies relative to the bond strength between the metal and the support, the size of the growing particles (the bigger the less mobile) or the geometry of the surface (diffusion more rapid on smooth surfaces).

As already stated, two main mechanisms exist for the growth of metal particles on a surface; Ostwald ripening and coalescence through Brownian motion. These two proposed mechanisms[50] are the same as the atomic migration model and crystallite migration models proposed and developed by Ruckenstein and Pulvermacher[55] and Flynn and Wanke[53,54], respectively.

A short summary of these two models follows :

1. Crystallite Migration Model[50]

   It is postulated that surface diffusion causes Brownian type motion of the metal particles to occur on the support. Brownian movement is the continuous agitation of particles in a colloidal solution. The surrounding medium causes an unbalanced impact with the observed molecules.

   In the case of metal and support, metal crystallites migrate along the surface of the support. As these crystallites migrate, atoms may diffuse from the surface of the metal crystallite, thus causing the metal atoms to accumulate on one side of the crystallite. This process takes place at a fast rate, resulting in Brownian movement of the particles on the support.

   The crystallite migration model has been used to determine the rate of surface diffusion for two cases. Both these cases are surface diffusion

controlled in which the rate of migration of crystallites is the rate determining step, or sintering controlled, in which the merging of two metal crystallites coming in contact by collision is the rate determining step.

2. Atomic Migration Model[50]

This model considers sintering to be a three–step–process; first metal atoms escape from the metal crystallite to the support surface, after which these atoms migrate along the support surface, and finally stationary metal crystallites capture the migrating atoms upon colliding with them.

Although the experimental identification of a correct sintering mechanism is difficult, some useful comments have been made by Wanke and Flynn[50] on discriminating between the above mentioned models.

In a comprehensive investigation on the role of interactions and surface phenomena in sintering and re–dispersion (the formation of more metal crystallites through crystallite breakup) of supported metal catalysts, Ruckenstein[62] explained how crystallite growth (through the above mentioned mechanisms) is possible by making use of the wetting and spreading abilities of metal crystallites and a substrate. He states that the spreading behaviour of a metal crystallite is a function of the ability of the crystallite to wet the surface of a substrate, the substrate being the type of support used.

The interfacial free energies of the substrate–gas (δ_{sg}), crystallite–gas (δ_{cg}) and the crystallite–substrate (δ_{cs}) determine the capability of a metal crystallite to wet the substrate and consequently spread over the substrate, by the following equation :

$$\delta_{\infty} = \delta_{cg} + \delta_{cs} - \delta_{sg} \qquad 3.3.$$

in which δ_{∞} is the specific free energy for crystallite formation. It should be remembered that sintering or crystallite growth through crystallite migration, occurs so as to decrease the free energy of the whole system. See Figure 3.7. and the accompanying explanation in the relevant section described earlier.

Whenever $\delta_{\infty} < 0$, spreading (migration) of a crystallite over the substrate is likely to occur, as a decrease in free energy is expected and therefore wetting of the substrate is possible. If however $\delta_{\infty} > 0$, no wetting of the substrate by the crystallites is possible and single islands of crystallites are formed through coalescence of particles on the substrate in an effort to reduce the free energy of the system.

Crystallite islands of a wide variety and distribution of sizes may be formed and it is believed that the angle (θ) between the coalesced islands and the substrate is given by the Young equation :

$$\delta_{cg} \text{Cos } \theta = \delta_{sg} - \delta_{cs} \qquad 3.4.$$

Metals tested in vacuum and inert atmospheres showed θ values greater than 90°, as high interfacial free energy values for δ_{cg} and δ_{cs} are obtained. Equation 3.4. can be rearranged to :

$$\delta_{sg} = \delta_{cg} \text{Cos } \theta + \delta_{cs} \qquad 3.5.$$

and then substituted into equation 3.3. :

$$\delta_{\infty} = \delta_{cg} + \delta_{cs} - (\delta_{cg} \text{Cos } \theta + \delta_{cs}) \qquad 3.6.$$

which then can be simplified to :

$$\delta_{\infty} = \delta_{cg}(1 - \text{Cos } \theta) \qquad 3.7.$$

Therefore, if $\theta > 90^{\circ}$, as mentioned above, then $\delta_{\infty} > 0$ and this in effect means that no wetting of the substrate will take place and therefore no migration of the crystallites is expected.

If however, these tests are performed in an oxidizing atmosphere, the contact angle is decreased and the opposite result is obtained.

Furthermore, it should be noted that an oxide crystallite will wet a metal substrate better than a metal crystallite an oxide substrate. Also impurities, like catalyst promoters, in metal crystallites can decrease the wetting angle of a particular system, therefore making it more mobile.

From the above, it can be seen that both the nature of the substrate and the metal play a major role in the sintering process.

Substrates should be chosen so as to ensure that maximum dispersion of the crystallite phase is obtained on the substrate surface. From their respective surface free energies it is believed that structural promoters have a stability to sintering in the following order :

$$TiC > TaC > WC > ZrO_2 > MgO > Al_2O_3 > SiO_2 > TiO_2 > Ta_2O_5 > V_2O_5$$

It is also observed that metals which readily form oxides, especially Fe and Ni, will react more strongly with the exposed oxygen ions of the substrate, especially SiO_2, and therefore give a smaller wetting angle. This will induce spreading of the metal crystallites over the substrate.

Furthermore, the atoms within the crystallites also effect the sintering process as the metal atom bond strengths have an effect on the likelihood of atoms being emitted from the crystallites. If the metal atom bond strength can be used as a criteria to distinguish between the sintering stabilities of metals, the order can be given as :

$$Re > Os > Ir > Ru > Rh > Pt > Co > Ni > Fe > Pd > Au > Cu > Ag$$

Finally it should be noted, that sintering either by migration or coalescence or by both mechanisms is possible only if the substrate–crystallite interactions are sufficiently small.

3.4. Deactivation by fouling

3.4.1. Definition of fouling

Fouling may be defined as the loss of catalytic activity by either physical or chemical occurrences[17], originating from surface reactions[2] whereby carbonaceous deposits[4] or other impurities adsorb strongly onto the surface of the catalyst, physically blocking[49] the active sites through which the principal reaction takes place.

3.4.2. Fouling – an extensive concept

Foulants, which lead to the disablement of catalyst active sites and subsequently a loss in activity and possible blockage of the reactor through catalyst disintegration[63,64], may be divided into two main categories :

1. Carbonaceous deposits, commonly perceived[17] as the primary cause of fouling.
2. Impurity foulants[17], which originate from impurities in the feed, and act very much like poisons (Section 3.2), adsorb onto the catalyst surface, thus screening the active sites from the reactants.

The following discussion on fouling will concentrate on the deposition of carbonaceous species on the catalyst surface.

Kissinger and Khang[65] have divided deactivation by carbonaceous deposits into three groups. Inactive fouling involves the physical deposition of a foulant on the catalyst and has an effect on the catalyst performance. Active fouling involves the creation of new active sites during the deposition of the foulant on the catalyst surface. Finally, hardshell fouling is an active form of fouling whereby the reaction is limited to the surface of the foulant specimen.

These results were based on the fact that a porous catalyst has a complex maze of micropores (pore diameter < 20 A); mesopores, which have a relative large area and are the important pore type for the catalytic reaction, and macropores (pore diameter = several hundreds of armstrongs), which provide the main channels by which reactants and products flow. Micropores, which are easily clogged up, are believed to have an effect on the initial activity and selectivity of a catalyst. This

explains the initial sharp drop in activity obtained for most catalysts. Meso– and macropores are also believed to play a major role in the life time of a catalyst. Galiasso[66], like Kissinger and Khang[65], based his studies on pore plugging by coke in the various pores mentioned above.

The most common form of carbonaceous deposit is coke. Catalyst coking is a well–known phenomenon[67] and reports on studies range from coke properties[68,69,70], its effect on catalyst activity[71], the mechanisms by which it is deposited[72] to the modeling of its behaviour[73]. Lately the coking of bifunctional catalysts[74] and more significant contributions to improved quantitive[75] approaches of catalyst coking have been published. Coke, a product of most petroleum refining and petrochemical processes[72], may be formed via the cracking of aromatic or olefinic compounds[4,76] which then form macromolecular carbon deposits[5] by means of a polymerization reaction. These coke residues contain an average molecular mass in the range of 900 to 10 000. The deposits are not necessarily distributed evenly through the reactor bed or the catalyst pellet, and coke deposits on metal surfaces contain little or no hydrogen[49].

Coke, which may contain[70,77] graphite, ordered and disordered carbon and soot (a product resulting from gaseous hydrocarbon dissociation[78]), may form via several different[75] routes, as shown in Figure 3.8.. Coking[4] can be formed from the reactants, or products formed during the reaction, or the product intermediates that are formed in the reaction.

The amount of coke deposited may be controlled by the composition of the feed[4,2,79], the temperature[4,79], the catalyst activity[4,79], the conversion level[80], the type of catalyst used[2], the type of reaction that is being catalysed[2], as well as the type of catalyst support[2] used and the time the catalyst is on line[2].

The above mentioned variables also determine the chemical state of the foulant. It is further known that the contaminants, coke or other carbonaceous deposits, are mainly formed on the catalyst surface and not in the gas phase[5], although this latter possibility cannot be excluded.

The reactions by which the coke deposits are formed are well known[49]. These are :

1. the decomposition of carbon monoxide,

   $2CO \longrightarrow C + CO_2$

2. the decomposition of methane, and

   $CH_4 \longrightarrow C + 2H_2$

3. other gaseous reactions.

   $2H_2 + CO_2 \longrightarrow C + 2H_2O$

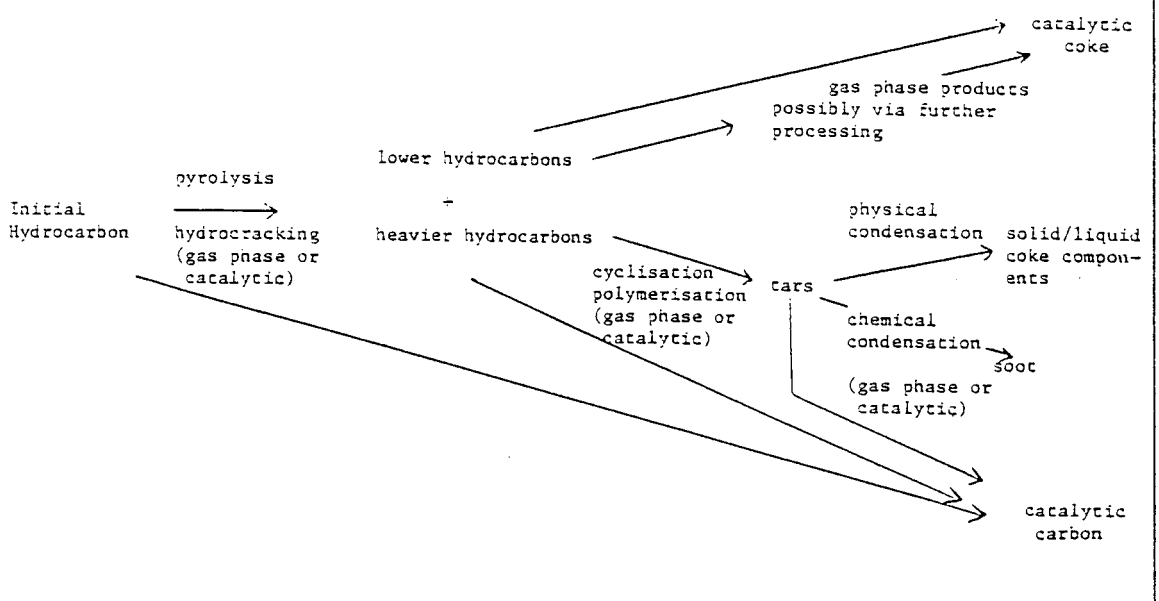

Figure 3.8. Possible routes of carbon formation[75]

It is also believed[2] that coke formation occurs, not so much through the disproportionation of the CO molecules, but through the polymerization–dehydrogenation of the intermediates. Further, it should be noted, that coke can be formed from both saturated and unsaturated hydrocarbons[70] and that the coke formed on the catalyst surface may be gasified[81] by steam, hydrogen and carbon dioxide present in the system.

$$C + O_2 \longrightarrow CO_2$$
$$C + H_2O \longrightarrow CO + H_2$$
$$C + CO_2 \longrightarrow 2CO$$
$$C + 2H_2 \longrightarrow CH_4$$

However, although a catalyst decreases the temperature at which coke gasification takes place, it seems that the lowest possible gasification temperature for coke is in the order of 400 $^{\circ}C$[82].

Work done on nickel catalysts showed that the coke forming tendency decreases in the order :

acetylenes > olefins > paraffins.

Coking of the catalysts surface may also alter the selectivity for a specific product and a drop in conversion[5] may occur during synthesis.

3.4.3. The mechanism of fouling

As mentioned in Section 3.4.2., coke formation originates from reactions between

the reactants, the products and the product intermediates, or a combination thereof. Reaction conditions have an influence on coke deposition and an effect on the mechanism. A wide variety of literature reports[4,17] concerning the coke forming mechanism is available. It is generally agreed that there are two types of coke forming reaction pathways. The one reaction is parallel to the main reaction while the other is consecutive or serial to the main reaction (see Figure 3.9.). Both these reactions may take place at the same time, at different active centres, on the same catalyst surface.

Froment and Bischoff[83] state that large coke deposits are obtained for parallel fouling if the concentration of the reactant A is high. The reactant is the coke precursor in this reaction and the greatest deposition of coke is expected at the reactor inlet. In the case of serial fouling, the product R or the product intermediates formed, are the coke precursors. Therefore the deposition of coke will increase through the reactor bed, downwards, as the precursor concentration is increasing.

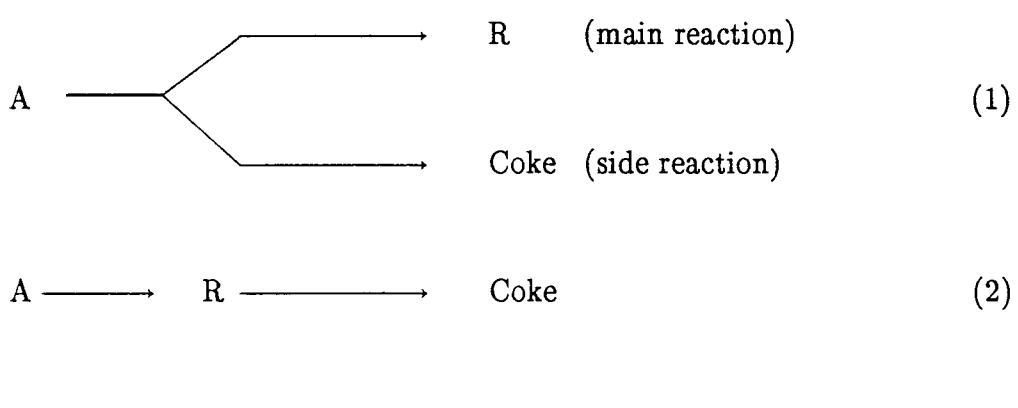

Figure 3.9. Reaction pathways for coke formation[17]

Hughes[17] views coking as being highly dependant on the order of the main reaction with respect to the formation of the products. It is also believed that carbon forming reactions take place faster than carbon removal reactions[49]. Hughes mentions that in high temperature processes, coke may be formed as a result of gas phase cracking, while coke is formed at the catalyst surface by surface reactions during low temperature processes.

Working on nickel catalysts, Lobo[84] proposed the following general mechanism for carbonaceous formation on a catalyst surface – see Figure 3.10.. The gas (feed) adsorbs on the metal surface, whereafter the surface reactions produces carbon atoms, which then chemisorb onto the surface. The carbon atoms then dissolve into and diffuse through the metal, lifting the metal crystallites up from the catalyst surface. Encapsulation through surface nucleation may also occur during this process.

Quantification of coke deposition is possible by simple concentration–time functions[67]. The basis of this and other ideas on the quantification of coke deposition is not dealt with in this literature study.

It has been reported[85] that an increase in temperature results in an increase in coke deposition during carbon monoxide hydrogenation over an alumina–supported cobalt catalyst. It is stated that the surface carbon appears to be transformed morphologically into polymeric and graphitic carbon, which decreases the activation energy of the main reaction. This may be due to the blocking of active sites by the various carbonaceous deposits. These site blockages decrease the activity of the catalyst and only slightly effect the hydrocarbon product distribution, but shift the reaction products from paraffinic to more olefinic content.

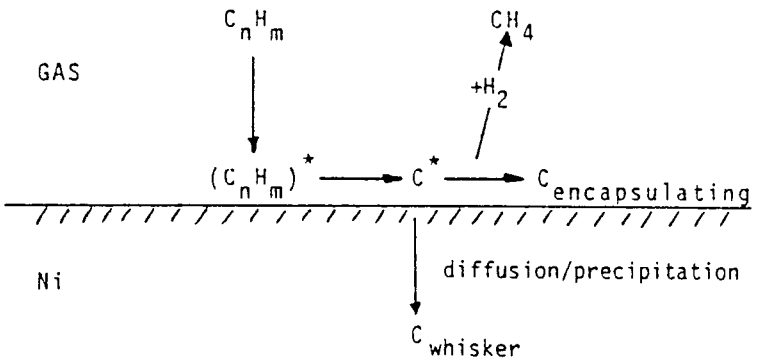

(i)

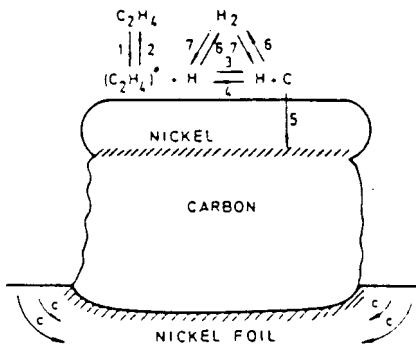

(ii)

Figure 3.10.[84] (i) The relevant steps in the mechanism of carbon formation
(ii) Schematic mechanism for carbon formation on a nickel surface

Trimm[70] also states that coke formation at low temperatures, ca < 500 °C, on a nickel catalyst showed an increase in the rate of carbon deposition with an increase

in temperature. He found coke formation from paraffins negligible below 500 °C in a hydrogen lean atmosphere and that, although carbon deposition was obtained at 400 °C in an atmosphere of 5 volume % hydrogen, the rate of coking, as to be expected, did not increase for higher volumes of hydrogen present.

Experimentation with a BASF supported copper catalyst[5], showed exactly the opposite trend to that found by Don–Keun Lee and co–workers[85] working with cobalt catalysts. A 25 % decrease in the average amount of carbon formed in the catalyst bed was observed at temperatures between 160 °C to 300 °C. This could be explained by the fact that the product, formed through the main reaction and the carbon depositing reaction, proceeded via a common precursor, P, in two parallel reactions which have different activation energies.

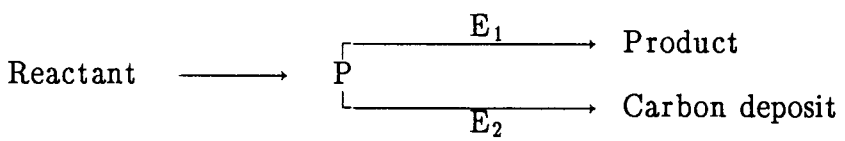

If the activation energy $E_1 > E_2$, an increase in temperature will favour the main reaction instead of the formation of carbon. However, Dvorák et al.[5] did mention that the copper catalyst sintered on increasing the temperature to sufficiently high levels.

An increase in the H_2:CO–ratio of the feed reduces the formation of carbonaceous products during synthesis[86]. This can be explained by one of two mechanisms. Firstly, it may be possible that the hydrocarbon products and carbonaceous products compete for the same supply of carbide, which is believed to be the active phase during synthesis. The higher hydrogen partial pressure, with higher H_2:CO–ratios in the feed, will increase the rate of hydrocarbon synthesis, thus eliminating the formation of carbonaceous products to some extent. This, however,

assumes that a bulk carbide is the necessary intermediate in the Fischer–Tropsch synthesis, which has been proved incorrect by Emmett et al.[87].

The second and more likely mechanism is based on the rate of carbidic carbon diffusion into the catalyst lattice. It is proposed that carbon–carbon bonding in the catalyst lattice is necessary to obtain elemental carbon from metal carbide. If the diffusion of carbidic carbon towards the potential carbon–carbon formation positions is retarded by the penetration of hydrogen, the rate at which unreactive coke forms will be slowed down.

The idea of diffusion into the metal lattice bears similarities to the idea of Lobo[84] in that he also proposed the diffusion of carbon atoms into and through the metal catalyst.

3.4.4. The nature of carbonaceous deposits

Carbonaceous deposits may be formed from aromatics, olefins and their derivatives. Trimm[81] states that coke formed on a catalyst surface may contain soot (which is a gas phase product[88]) or ordered and disordered carbon. These carbons either form on an inert surface, known as surface carbon, or on a surface which may catalyze the formation of carbon, known as catalytic carbon.

Coke formation[89], resulting from gas phase reactions, is a very complex topic and involves free radicals, and is beyond the scope of this work. Of more importance, as far as this project is concerned, is the surface on which the coking takes place. This plays a major role in the coke deposition process. Surfaces may either be

1. non–catalytic, acting to collect condensed tars and soot, thereby affecting the heat and mass distributions in the reaction system, or concentrate tars and soot whereby further non–catalytic reactions may occur, or
2. catalytic, which promote the formation of carbon and alter the nature of the gases present in the reactor, thus altering the nature and amount of carbon formed in the gas phase or on a down stream surface.

In practice, carbon monoxide hydrogenation under Fischer–Tropsch conditions over a 9,5 % Fe/Al_2O_3 catalyst[90] yields several types of carbon which form during synthesis.

Analysis of these catalysts reveal the following :

1. a reactive carbon,
2. a less reactive surface carbon,
3. a bulk iron carbide,
4. graphite,
5. a carbon containing species which forms independently on the Al_2O_3 surface.

The coke formed during synthesis normally has a carbon structure with little hydrogen present[49], e.g. CH_1 and $CH_{0,5}$.

Carbonaceous deposits on a Fe(110) surface studied, using AES and XPS[79], showed similar results to these obtained for the above mentioned Fe/Al_2O_3 catalyst. Present were well characterized carbidic forms of carbon, graphitic carbon, carbon

monoxide and C_2H_2 as identified by their respective carbon Auger peak fine structures and C_1 binding energies.

Electron microscopy studies[91], on various metals, have revealed a variety of carbon products of which filamentous and lamellar products were the most common ones. Carbon black is the most important example[2] of a carbonaceous deposit and exists in a number of forms like wiskers, lamellar graphite, amorphous masses and carbide compounds. It is also believed[49] that a more active form, Dent carbon, is produced at temperatures below 700 °C. Baired et al.[92] found that the nature of the carbon deposit is a function of the rate of deposition and is not necessarily related to the type of hydrocarbon from which the deposit originated. He also states that unsaturated hydrocarbons give a faster deposition rate and more discreet carbons than those formed from the corresponding saturated gases.

3.4.5. Fouling on iron catalysts

Carbonaceous deposits, like coke, are formed more readily on iron than on nickel[49,93]. This is because of iron's high reactivity[94,95] towards the dissociation of carbon monoxide[96,97-99].

$$2CO + 2Fe \longrightarrow Fe_2C + CO_2 \qquad \Delta Hr = -152{,}7 \text{ kJ/mol}$$

$$2CO + 3Ni \longrightarrow Ni_3C + CO_2 \qquad \Delta Hr = -126{,}0 \text{ kJ/mol}$$

$$2CO \longrightarrow C + CO_2 \qquad \Delta Hr = -172{,}4 \text{ kJ/mol}$$

Graphite may also result from the metal carbides :

$$Fe_2C \longrightarrow 2Fe + C$$

$$Ni_3C \longrightarrow 3Ni + C$$

The mechanism of carbon formation on iron is similar to that for carbon on nickel[84]. At temperatures lower than 600 °C, the formation of carbon appears to be diffusion controlled[100], i.e. is the diffusion of carbon into the iron lattice. At higher temperatures, above 600 °C, the deposition of carbon is due to the surface decomposition of the feed gas. Using the same scheme as mentioned in Section 3.4.3. for the general mechanism of carbon formation as deduced from work done on nickel based catalysts, as well as the fact that iron surfaces have a greater affinity than nickel surfaces to form coke, and the fact that Lobo foresees many similarities in the mechanisms of these two metals, the mechanism for carbon formation on iron surfaces can be explained as follows (see Figure 3.11.).

The gas is adsorbed onto the metal surface, in this case iron, whereafter mono carbon fragments[101] are produced which can either dissolve into the iron surface or encapsulate the iron phase.

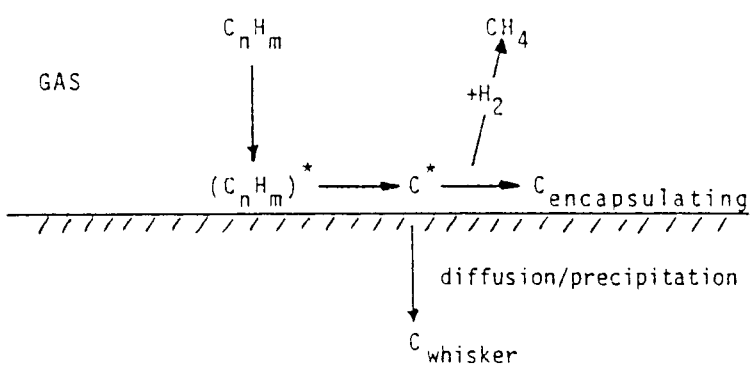

Figure 3.11. Proposed mechanism for carbon formation on iron[84]

The dissolution/migration process into the iron, as shown in Figure 3.11., may be described by Figure 3.12., in which the migration of carbon from iron carbide through the iron metal is shown. Trimm[100] states that this could well be the rate determining step for the carbon formation process on a fresh iron surface at low temperatures. Later on, as the carbon deposits build up on the catalyst surface, the decomposition of hydrocarbons, catalyzed by the iron carbide phase formed, takes over as the rate determining step. It is also suggested that the role encapsulation plays, increases with increasing carbon build up.

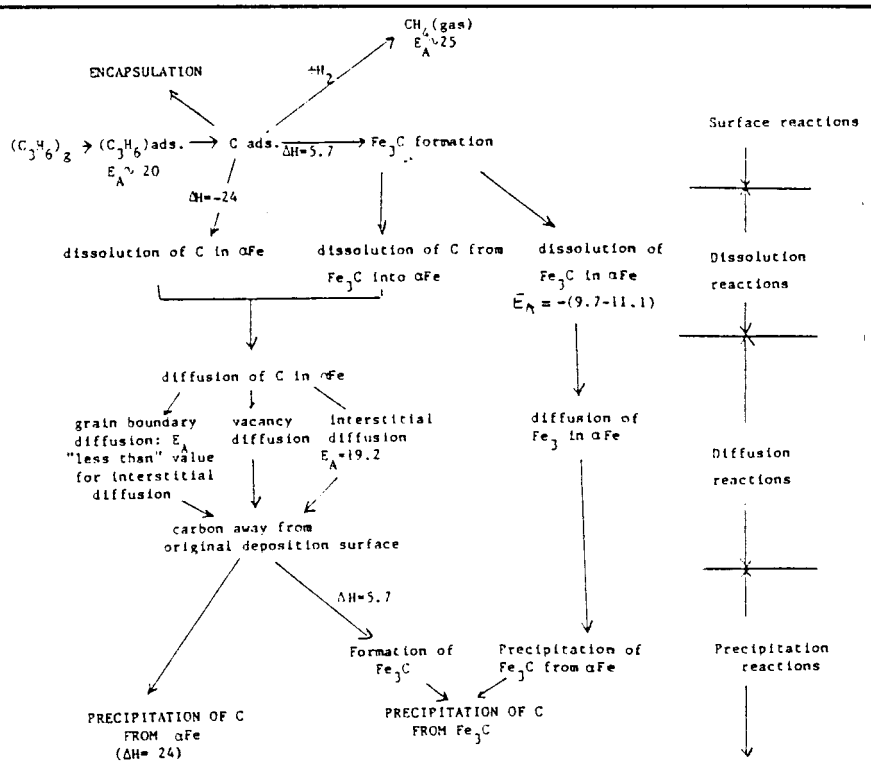

Figure 3.12. Migration of carbon through iron[100]

As mentioned previously, the deposited carbon may take on various forms. This is also true for carbon formed on iron catalysts.

Ruston et al.[102] observed carbonaceous filaments formed on an iron surface in contact with CO at 550 °C. They stated that the decomposition reaction of CO came to a halt when the content of iron in the deposited carbon layer was lower than 3 Wt. %. No carbides are detected for iron at temperatures lower than 350 °C[91,93]. Carbon foulants detected at 350 °C were very amorphous and by increasing the temperature to 500 °C, gave an increased crystallinity. When the carbon formation temperature was between 500 °C and 700 °C, graphitic carbon formed. Bonzel and Krebs[79] observed that the graphitic form of carbon, on a Fe(110) surface layer, was very stable towards hydrogen treatment at 1 bar and elevated temperatures.

Storch[86] mentions the fact that carbon deposits could not be detected on iron and iron–copper catalysts that did not contain a certain level of iron or copper. This indicates that the coke deposit was either in the crystal lattice of the catalyst, and thus like Trimm[100] proposes, migration of coke into the lattice of the metal, or that the coke was formed from an iron carbide intermediate.

Tests[86] done at the Kaiser Wilhelm Institute fur Kohlenforschung on Fischer–Tropsch catalysts showed that precipitated iron catalysts responded with a slow increase in Fe_2C content after 120 hours on line at 235 °C and 18 atm. The ratio of Fe_2C : Fe_3O_4 was 3:10. It is stated that the activity of the catalyst during synthesis increased to a maximum during this period, which indicates that the major reactions of the process were already in action.

It is believed that iron carbide is the active metal state of the Fischer–Tropsch process[86]. This belief has been adapted by various researchers during their studies on the mechanism of the Fischer–Tropsch process, see Chapter 2.

Bonzel and Krebs[79] also mention a heavily hydrogenated carbidic carbon phase, existing as a CH_x phase, which consisted mainly of CH species, which is unstable and can easily be removed from the catalyst surface by hydrogenation, and that this CH_x phase can be formed from carbidic carbon and hydrogen without the presence of carbon monoxide.

Another interesting phenomenon mentioned in the literature[49,91] is that filamentous carbon, which exists as hollow tubes of carbon, contains a metal particle at the growing tip of the filament. If the metal particle should disintegrate, it may leave finely divided carbon, full of tiny metal pieces, thus increasing the number of available active sites on the catalyst surface. With time, the fibrous carbon structure may sinter, becoming less reactive, and in some cases, where possible, had to be removed by steam.

Thus far, fouling has been classified mainly as coke formed in the higher temperature ranges, ca. > 300 °C. So, where does low temperature Fischer–Tropsch catalysis fit in as far as coke formation is concerned ? Dry[24] suggests that fouling from deposition of inactive coke on the catalyst surface, prohibiting the main reaction from taking place, is unlikely to occur at the lower temperature ranges used for the fixed bed catalytic processes. Dry proposes that, since the Fischer–Tropsch process produces a wide range of hydrocarbon products (methane to high molecular mass waxes), it is possible that the wax producing conditions may have a diffusion limitation effect on the ingoing reactants and outcoming products in the catalytic pores. This idea contributes to the suggestion, that different types of pores have an effect on the catalytic process, as proposed by Kissinger and Khang[65] in Section 3.4.2.. Solvent treatment of iron and cobalt catalysts (research done in Germany[103]) proved that diffusion plays a major role in decreasing the activity of these catalysts with time.

From this literature study the following conclusions for the formation of carbonaceous foulants can be drawn :

1. Surface and pore blockages by high molecular mass hydrocarbon products may lead to product/reactant diffusional limitations. Thus waxes may form a heavy carbonaceous "liquid", which might retard the reaction by increased diffusion resistance.
2. It cannot be excluded that high temperature zones may be present in the pores of the catalyst and thus lead to the formation of coke based products which screen active sites from the main reaction, resulting in a loss of catalytic activity.

3.4.6. Retardation of fouling

Fouling is a problem in reforming, cracking and hydrogenation processes[63]. It is necessary to obtain maximum life time, activity and selectivity from the catalysts used in these processes, as the production costs of these catalysts are never low. Coke formation may be reduced by :

1. using a support with non–acid characteristics[2,93,104],
2. minimizing the contribution due to thermal cracking by using optimum temperature conditions[2,104],
3. increasing the H_2:CO–ratio[80] and
4. by controlling the level of conversion[80].

Furthermore, the following operational conditions[105] should be taken into consideration when operating on a plant scale :

1. use small amounts of catalyst,
2. operate at low temperatures,
3. operate at low residence times,
4. operate at a single pressure,
5. operate under a constant gas composition, and
6. remove all impurities from the feed stream.

Thus far precautions, rather than real time actions for preventing fouling, have been mentioned. A more severe form of treatment, after fouling takes place, is to regenerate[13,18,106] the catalyst under reaction conditions without unloading it from the reactor. In this case the coke is gasified at controlled temperatures with either oxygen, steam, carbon dioxide or hydrogen.

$$C + O_2 \longrightarrow CO_2$$
$$C + H_2O \longrightarrow CO + H_2$$
$$C + CO_2 \longrightarrow 2CO$$
$$C + 2H_2 \longrightarrow CH_4$$

A discussion on catalytic regeneration, a field of study in itself, will not be included in this literature study.

3.5 Other forms of Catalyst Deactivation

As stated earlier and shown in Figure 1.2. on page 3, solid state reactions and mechanical failure of catalysts can also have contributions to the loss observed in catalytic activity during commercial processes. These two phenomena are briefly discussed in this section.

3.5.1. Solid State Reactions

Changes in the chemical nature of the compounds within the catalyst matrix, which may lead to a loss in catalyst activity, are known as solid state reactions[2]. This is still a recent research field[107], in which high temperatures (ca. > 500 °C) and oxidizing atmospheres permits reactions between the constituents of the catalyst, which results in a loss of total and active metal surface area[108] and therefore a subsequent loss of activity[109]. Mechanical failure is also known to occur as a result of modification through solid state reactions[2] and subsequently leads to a increased pressure drop over the catalyst bed[109].

3.5.2. Mechanical Failure

Dvorák et al.[5] mentions that an important criterion for the choice of a commercial catalyst is the mechanical strength of its pellets. Mechanical failure is a common problem in which a catalyst pellet looses its structural stability, and is mentioned by many researchers[2,3,4,5] as a major problem in the loss of catalyst performance.

Catalyst pellets are known to gradually loose[5] their mechanical strength, crumble and break up, subsequently increasing the pressure drop over the catalyst bed[3]. Actual blocking of a catalyst bed is then possible. It is also known[5] that a slow disintegration process of the catalyst pellets may prolong the catalyst life as new catalytic active sites become available to the reaction.

Finally, mechanical failure is known to occur as a consequence of severe catalyst fouling and extreme reactor operating conditions[17], and is therefore mainly a result of the deactivation phenomena already discussed in sections 3.2., 3.3., 3.4. and 3.5.,

and will therefore require no further discussion.

3.6. Concluding Remarks

In the above chapter no attempt has been made to give a comprehensive survey of catalyst deactivation – the wealth of data reported on this area of catalysis is voluminous – but rather the emphasis has been on the role of catalyst deactivation as applied to the Fischer–Tropsch reaction. This has necessitated making general statements, eg. deactivation definitions, mechanisms, etc., but as far as possible these have been related to the thesis topic. Causes of catalyst deactivation have been identified (poisoning, sintering, fouling, mechanical failure and solid state reactions) and the various reports on these phenomena have been described in the review. Where possible an assessment of the information has been made.

As can be seen from the review of the literature, little has been reported on catalyst deactivation as it applies to the Fischer–Tropsch reaction. It is thus apparent that a study on the role of deactivation of these catalysts could have important consequences on the operating conditions required for the synthesis of fuels and chemicals from CO and H_2. The chapter that follows describes an experimental approach to evaluate the causes of catalyst deactivation in the Fischer–Tropsch reaction.

3.7. References

1. B. Delmon and P. Grange, *Progress in Catalyst Deactivation*, (J.L. Figueiredo, ed.), Martinus Nijhoff Publishers, The Hague, 1982, 231 – 236

2. P. Forzatti, G. Buzzi–Ferraris, M. Morbidelli and S. Carrá, *Int. Chem. Eng.*, *24*, *1*, 1984, 60

3. P.J. Denny and M.V. Twigg, *Catalyst Deactivation 1980*, (B. Delmon and G.F. Froment, eds.), Elsevier Science Publishers B.V., Amsterdam, 1980, 580

4. G.F. Froment and K.B. Bischoff, *Chemical Reactor Analysis and Design*, John Wiley and Sons, New York, 1979, 271 – 272

5. B. Dvorák, J. Pasek, P. Pavlas and Z. Hejda, *Catalyst Deactivation 1980*, (B. Delmon and G.F. Froment, eds.), Elsevier Science Publishers B.V., Amsterdam, 1980, 539

6. L.L. Hegedus and R.W. McCabe, *Catalyst Deactivation 1980*, (B. Delmon and G.F. Froment, eds.), Elsevier Science Publishers B.V., Amsterdam, 1980, 471 – 502

7. S.T. Sie, *Catalyst Deactivation 1980*, (B. Delmon and G.F. Froment, eds.), Elsevier Science Publishers B.V., Amsterdam, 1980, 545

8. E.B. Maxted, *Adv. Catal.*, *3*, 1951, 129

9. J.B. Butt, *Adv. in Chem.*, *109*, 1972, 259

10. J.B. Butt and R.M. Billimoria, *Am. Chem. Soc. Symp. Ser. 72*, 1978, 288

11. J. Oudar, *Chem. Ind.*, *20*, 1985, 62

12. L.L. Hegedus and R.W. McCabe, *Catalyst Poisoning*, Marcel Dekker, Inc., New York, 1984, 5 – 6

13. R.J. Madon and H. Shaw, *Catal. Rev. – Sci. Eng.*, *15*, *1*, 1977, 70

14. Steinbrecher and Weingaertner, *FIAT Reel K25, Frames 003*, 1938, 782 – 803, 796 (as reported by R.J. Madon and H. Shaw, *Catal. Rev. – Sci. Eng.*, *15*, *1*, 1977)

15. E.B. Maxted and H.C. Evans, *J. Chem. Soc.*, 1937, 603

16. C.B. Murchison, *US Patent Nr. 4 539 334*, 1985

17. R. Hughes, *Deactivation of Catalysts*, Academic Press, Inc. Ltd., London, 1984, 1 – 143, 212 – 242

18. J. Oudar, *Catal. Rev. – Sci. Eng.*, *22*, *2*, 1980, 172

19. D.R. Ardiles and A.A. Castro, *Chem. Eng. Comm.*, *52*, 1987, 301

20. L.L. Hegedus and E.E. Petersen, *Cat. Rev. – Sci. Eng.*, *9*, *2*, 1974, 245

21. J.B. Butt, *Catalyst Deactivation 1980*, (B. Delmon and G.F. Froment, eds.), Elsevier Science Publishers B.V., Amsterdam, 1980, 21

22. J.P. Boitiaux, J.C. Cosyns and F. Verna, *Catalyst Deactivation 1987*, (B. Delmon and G.F. Froment, eds.), Elsevier Science Publishers B.V., Amsterdam, 1987, 118 – 122

23. S. Berkman, J.C. Morrell and G. Egloff, *Catalysis, Inorganic and Organic*, Reinhold Publishing Corporation, New York, 1940, 372

24. M.E. Dry, *Catalysis – Science and Technology, Vol. 1*, (J.R. Anderson and M. Boudard, eds.), Springer Verlag, Berlin, 1981, 169

25. I.B. Rapoport and O.A. Muzovskaya, *Khim. Tekhnol. Topl. Masel*, *2*, 1957, 18

26. A.K. Golovko, A.V. Kravstov, Yu.V. Maksimov, S.I. Smal'yaninov and N.V. Lavrov, *Khim. Tverd. Topl.*, *13*, 1979, 381

27. H. Adkins, D.S. Fae, J.W. Davis, G.F. Hager and K.J. Hoyle, *J. Am. Chem. Soc.*, *70*, 1948, 381

28. H. Adkins and H.R. Billica, *J. Am. Chem. Soc.*, *70*, 1948, 3118

29. J.T. Richardson, *J. Catal.*, *21*, 1971, 122

30. A.L. Chaffee, I. Campbell and N. Valentine, *Appl. Catal.*, *47*, 1989, 253

31. I.G. Farbenindustrie Aktiengesellschaft, *British Patent Nr. 322 284*, 1929

32. K. Fujimura, S. Tsuneoka and K. Kawamichi, *J. Soc. Chem. Ind. Japn.*, *37*, 1934, 395

33. W.W. Myddleton, *British Patent Nr. 509 325*, 1939

34. E.F.G. Herington and L.A. Woodward, *Trans. Faraday Soc.*, *35*, 1939, 958

35. F. Fischer and K. Meyer, *Gest. Abh. Kennt. Kohle*, *11*, 1934, 497

36. J.G. King, *J. Inst. Fuel*, *11*, 1938, 484

37. E.T. Layng, *U.S.Patent Nr. 2 446 426*, 1948

38. J.J.S. Sebastian, *Carnegie Inst. Technol., Coal Res. Lab., 35*, 1936, 1

39. K. Wencke, *Freiberg Forschungsk., A, 151*, 1960

40. S.G. Stewart, *U.S. Patent Nr. 2 490 488*, 1949

41. J.F. Shultz, F.S. Karn and R.B. Anderson, *U.S. Bur. Mines, Rep. Invest., 6974*, 1967 (as reported by R.J. Madon and H. Shaw, *Catal. Rev. – Sci. Eng., 15, 1*, 1977)

42. R.N.R. Mulford and W.W. Russell, *J. Am. Chem. Soc., 74*, 1952, 1969

43. H.G. Davies, T.P. Wilson and A.N. Kurtz, *British Patent Nr. 727 833*, 1955

44. *Great Britain Fuel Research Board Report*, 1955, 20, 1956, 22

45. C.H. Bartholomew and R.M. Bowman, *Appl. Catal., 15*, 1985, 59

46. R.J. Madon and W.F. Taylor, *Hydrocarbon Synthesis*, 1979, 98

47. P.K. Agrawal, W.D. Fitzharris and J.R. Katzer, *Catalyst Deactivation 1980*, (B. Delmon and G.F. Froment, eds.), Elsevier Science Publishers B.V., Amsterdam, 1980, 179

48. Kirk–Othmer, *Encyclopedia of Chemical Technology, 22*, John Wiley and Sons, Inc., New York, 1983, 119

49. C.N. Satterfield, *Heterogeneous Catalysis in Practice*, McGraw–Hill Book Company, New York, 1980, 14, 136 – 141

50. S.E. Wanke, and P.C. Flynn, *Catal. Rev. – Sci. Eng., 12, 1*, 1975, 93

51. J.A. Cusumano, R.A. Dalla Betta and R.B. Levy, *Catalysis in Coal Conversion*, Academic Press, New York, 1978, 130 – 134

52. D.A. Dowden, *Progress in Catalyst Deactivation*, (J.L. Figueiredo, ed.), Martinus Nijhoff Publishers, The Hague, 1982, 283, 298 – 305

53. P.C. Flynn and S.E. Wanke, *J. Catal., 34*, 1974, 390

54. P.C. Flynn and S.E. Wanke, *J. Catal., 34*, 1974, 400

55. E. Ruckenstein and B. Pulvermacher, *J. Catal., 29*, 1973, 224

56. E. Ruckenstein and D.B. Dadyburjor, *J. Catal., 48*, 1977, 73

57. R.K. Bordia and G.W. Scherer, *Acta Metall.*, *36*, *9*, 1988, 2393

58. R.K. Bordia and G.W. Scherer, *Acta Metall.*, *36*, *9*, 1988, 2399

59. R.K. Bordia and G.W. Scherer, *Acta Metall.*, *36*, *9*, 1988, 2411

60. A. Bellare, D.B. Dadyburjor and M.J. Kelley, *J. Catal.*, *117*, 1989, 78

61. D.B. Dadyburjor, *Catalyst Deactivation 1987*, (B. Delmon and G.F. Froment, eds.), Elsevier Science Publishers B.V., Amsterdam, 1987, 21

62. E. Ruckenstein, *Metal–support interactions in Catalysis, Sintering and Redispersion*, Van Nostrand Reinhold Company, New York, 1987, 230 – 236, 239 – 241, 271, 287, 291 – 294, 296

63. C.H. Bartholomew, *Catal. Rev. – Sci. Eng.*, *24*, *1*, 1982, 68

64. G.A. Mills and F.W. Steffgen, *Catal. Reviews*, *8*, *2*, 1973, 164, 196

65. S.L. Kissinger and S. Khang, *Chem. Eng. Sci.*, *44*, *2*, 1989, 418

66. R. Galiasso, R. Blanco, C. Gonzalez and N. Quinteros, *Fuel*, *62*, *7*, 1983, 817

67. A. Voorhies, Jr., *Inst. Eng. Chem.*, *37*, *4*, 1945, 318

68. J.G. McCarty and H. Wise, *J. Catal.*, *57*, 1979, 406

69. J. Rostrup–Nielsen and D.L. Trimm, *J. Catal.*, *48*, 1977, 157

70. D.L. Trimm, *Catal. Rev. – Sci. Eng.*, *16*, *2*, 1977, 155

71. G.F. Froment, *Proceedings of the sixth International Congress on Catalysis*, (G.C. Bond, P.B. Wells and F.C. Tompkins, eds.), 1977, 10 – 31

72. H. Beuther, O.A. Larson and A.J. Perrotta, *Catalyst Deactivation 1980*, (B. Delmon and G.F. Froment, eds.), Elsevier Science Publishers B.V., Amsterdam, 1980, 271 – 282

73. M.A. Pacheco and E.E. Petersen, *J. Catal.*, *88*, 1984, 400

74. J.M. Parera, R.J. Verderone and C.A. Querini, *Catalyst Deactivation 1987*, (B. Delmon and G.F. Froment, eds.), Elsevier Science Publishers B.V., Amsterdam, 1987, 135 – 145

75. G.F. Froment, *Catalyst Deactivation 1980*, (B. Delmon and G.F. Froment, eds.), Elsevier Science Publishers B.V., Amsterdam, 1980, 1 – 19

76. B.M. Des Rochettes, C. Marcilly, C. Gueguen and J. Bousquet, *Catalyst Deactivation 1987*, (B. Delmon and G.F. Froment, eds.), Elsevier Science Publishers B.V., Amsterdam, 1987, 589

77. M. Masai, S. Shimadzu, T. Sashiwa, S. Sawa and M. Mimura, *Catalyst Deactivation 1980*, (B. Delmon and G.F. Froment, eds.), Elsevier Science Publishers B.V., Amsterdam, 1980, 265 – 266

78. P.A. Tesner, *Farad. Symp.*, *7*, 1973, 104

79. H.P. Bonzel and H.J. Krebs, *Surface Sci.*, *91*, 1980, 501

80. J.W. Gosselink, W.H.J. Stork, A.F. de Vries and C.H. Smit, *Catalyst Deactivation 1987*, (B. Delmon and G.F. Froment, eds.), Elsevier Science Publishers B.V., Amsterdam, 1987, 286

81. D.L. Trimm, *Progress in Catalyst Deactivation*, (J.L. Figueiredo, ed.), Martinus Nijhoff Publishers, The Hague, 1982, 17

82. C.A. Bernado and D.L. Trimm, *Carbon*, *17*, 1979, 115

83. G.F. Froment and K.B. Bischoff, *Chem. Eng. Sci.*, *17*, 1962, 106

84. L.S. Lobo, D.L. Trimm and J.L. Figueiredo, *Proc. 5th Intr. Congr. Catal.*, *2*, 1973, 1125

85. D. Lee, J. Lee and S. Ihm, *Appl. Catal.*, *36*, 1988, 207

86. H.H. Storch and W.G. Franckenberg, *Adv. Catal.*, *1*, (E.K. Rideal and V.I. Komarewsky, eds.), 1948, 138 – 140

87. J.T. Kummer, T.W. De Witt and P.H. Emmett, *Am. Chem. Soc. Meeting*, New York, 1947

88. H.B. Palmer and C.F. Cullis, *Chemistry and Physics of Carbon*, *1*, 1965, 288

89. D.L. Trimm, *Progress in Catalyst Deactivation*, (J.L. Figueiredo, ed.), Martinus Nijhoff Publishers, The Hague, 1982, 31 – 43

90. D. Schanke and A. Holmen, *Catalyst Deactivation 1987*, (B. Delmon and G.F. Froment, eds.), Elsevier Science Publishers B.V., Amsterdam, 1987, 413 – 414

91. T. Baird, *Catalysis, 5*, (G.C. Bond and G. Webb, eds.), 1981, 213

92. T. Baird, J.R. Fryer and B. Grant, *Carbon, 12*, 1974, 591

93. E.T.C. Vogt, A.J. van Dillen and J.W. Geus, *Catalyst Deactivation 1987*, (B. Delmon and G.F. Froment, eds.), Elsevier Science Publishers B.V., Amsterdam, 1987, 223

94. D.J. Dwyer and G.A. Somorjai, *J. Catal., 52*, 1978, 291

95. H.J. Krebs, H.P. Bonzel and G. Gafner, *Surface Sci., 88*, 1979, 269

96. K. Kishi and M.W. Roberts, *J. Chem. Soc., Faraday Trans. 1, 71*, 1975, 1715

97. C.R. Bundle, *I.B.M. J. Res. Develop., 11*, 1978, 235

98. G. Boden, G. Gafner and H.P. Bonzel, *Appl. Phys., 13*, 1977, 333

99. T.N. Rhodin and C.F. Brucker, *Solid State Commun., 23*, 1977, 275

100. D.L. Trimm, *Progress in Catalyst Deactivation*, (J.L. Figueiredo, ed.), Martinus Nijhoff Publishers, The Hague, 1982, 69

101. B.J. Cooper and D.L. Trimm, *J. Catal., 62*, 1980, 35

102. W.R. Ruston, M. Warzee, J. Hennaut and J. Waty, *Carbon, 7*, 1969, 47

103. R.G. Anderson, *Catalysis, 4*, (P.H. Emmett, ed.), Reinhold, New York, 1956

104. S.P.S. Andrew, *I & EC Product Research and Development, 8, 3*, 1969, 322

105. D.L.Trimm, *Progress in Catalyst Deactivation*, (J.L. Figueiredo, ed.), Martinus Nijhoff Publishers, The Hague, 1982, 24 – 25

106. J.L. Figueiredo, *Progress in Catalyst Deactivation*, (J.L. Figueiredo, ed.), Martinus Nijhoff Publishers, The Hague, 1982, 57, 59, 62

107. B. Delmon and P. Grange, *Catalyst Deactivation 1980*, (B. Delmon and G.F. Froment, eds.), Elsevier Science Publishers B.V., Amsterdam, 1980, 521 – 523, 536

108. D.J. Young, P. Udaja and D.L. Trimm, *Catalyst Deactivation 1980*, (B. Delmon and G.F. Froment, eds.), Elsevier Science Publishers B.V., Amsterdam, 1980, 338

109. N. Burriesci, F. Garbassi, M. Petrera, G. Petrini and N. Pernicone, *Catalyst Deactivation 1980*, (B. Delmon and G.F. Froment, eds.), Elsevier Science Publishers B.V., Amsterdam, 1980, 115, 120 – 125

CHAPTER 4

EXPERIMENTAL

4.1. Catalyst characterization

4.1.1. Carbon and sulphur analysis

The used catalysts, as obtained from the fixed bed pilot plant reactors, is extracted with M.E.K. to remove the synthesis wax produced during hydrocarbon synthesis.

After the extraction of wax, the used catalysts from the pilot plant reactors are analyzed for sulphur and carbon to obtain the profiles of these elements throughout the catalyst bed. The carbonaceous residue was analyzed for carbon and hydrogen by FTIR to obtain information of the nature of the carbonaceous compounds.

All abovementioned analysis were done with Sasol One Laboratory Analysis Methods[1].

4.1.2. X–ray diffraction phase analysis[2]

X–ray diffraction patterns were recorded on either a Phillips (equipped with a PV 1130 X–ray generator and a PV 1050 vertical gionometer) or a Siemens D 500 diffractometer. Only the Phillips apparatus was available when the first pilot plant reactor system (see Section 4.2.) catalyst beds were unloaded and the X–ray pattern output, traced by a simple pen recorder, which is very unclear when reproduced, had to be redrawn by hand for a clearer presentation. A typical X–ray pattern for one

of the catalysts, with the new instrument, is however included (see Figure 5.16. on page 117).

Phase analysis scanning in the 4 two–theta to 94 two–theta degrees scanning area was carried out in each case. Relative quantitative analysis making use of peak areas is given and crystallite sizes of the magnetite peak are also reported. Where necessary, the scanning area was reduced to show more pronounced effects between two specific two–theta degree areas.

4.1.3. Area and Pore Volume

Area and micro–pore volume analysis were performed with the micromeretices ASAP 2000 system. B.E.T. surface area, nitrogen micro–pore volume and total pore area for the catalysts unloaded from the pilot plant reactors are reported.

4.1.4. Scanning Electron Microscopy[2] and Secondary Ion Mass Spectrometry[2]

Studies, making use of Scanning Electron Microscopy (SEM) and Secondary Ion Mass Spectrometry (SIMS) techniques, to confirm the presence of sulphur contaminants[3] and other chemical phases on the catalyst surface and also to show the growth of small iron crystallites into bigger iron crystallites (sintering[4]), within the catalyst pellets, taken from different sections in a fixed bed reactor, has been performed. A Cambridge Instruments Stereoscan 360 SEM fitted with a tungsten hair pin filament, Energy Dispersive Analysis unit (EDAX) and Link Image Analyzer (LIA), was used. The SIMS analysis was done on a ESCALAB MK II equipped with a gallium gun.

Three catalyst samples representing the top, middle and bottom sections of a fixed bed reactor were analyzed.

During these analysis, SEM photographs, representing typical catalyst surfaces from each of the mentioned sections, were taken. SEM–EDAX spot analysis was performed on the different phases observed to obtain information of the composition of these phases. Similarly, ion mass spectra and elemental surface mapping of the iron catalyst surface were obtained by SIMS to gain more information on the catalyst surface composition.

Finally, making use of SEM's particle counting abilities (LIA), the amount and average size (through particle distribution) of the iron crystallites was determined.

4.2. Experimental Equipment

4.2.1. Fixed bed reactor

Two fixed bed reactor systems were used during the experiments.

For the first fixed bed reactor system (see Figure 4.1.) a reactor tube with gas recycle was used. Catalyst beds of different run lengths, i.e. 1, 50, 270 and 1000 time units (tu) were unloaded section by section and stored separately in sample holders under a nitrogen blanket to prevent oxidation of the unloaded used catalyst in air.

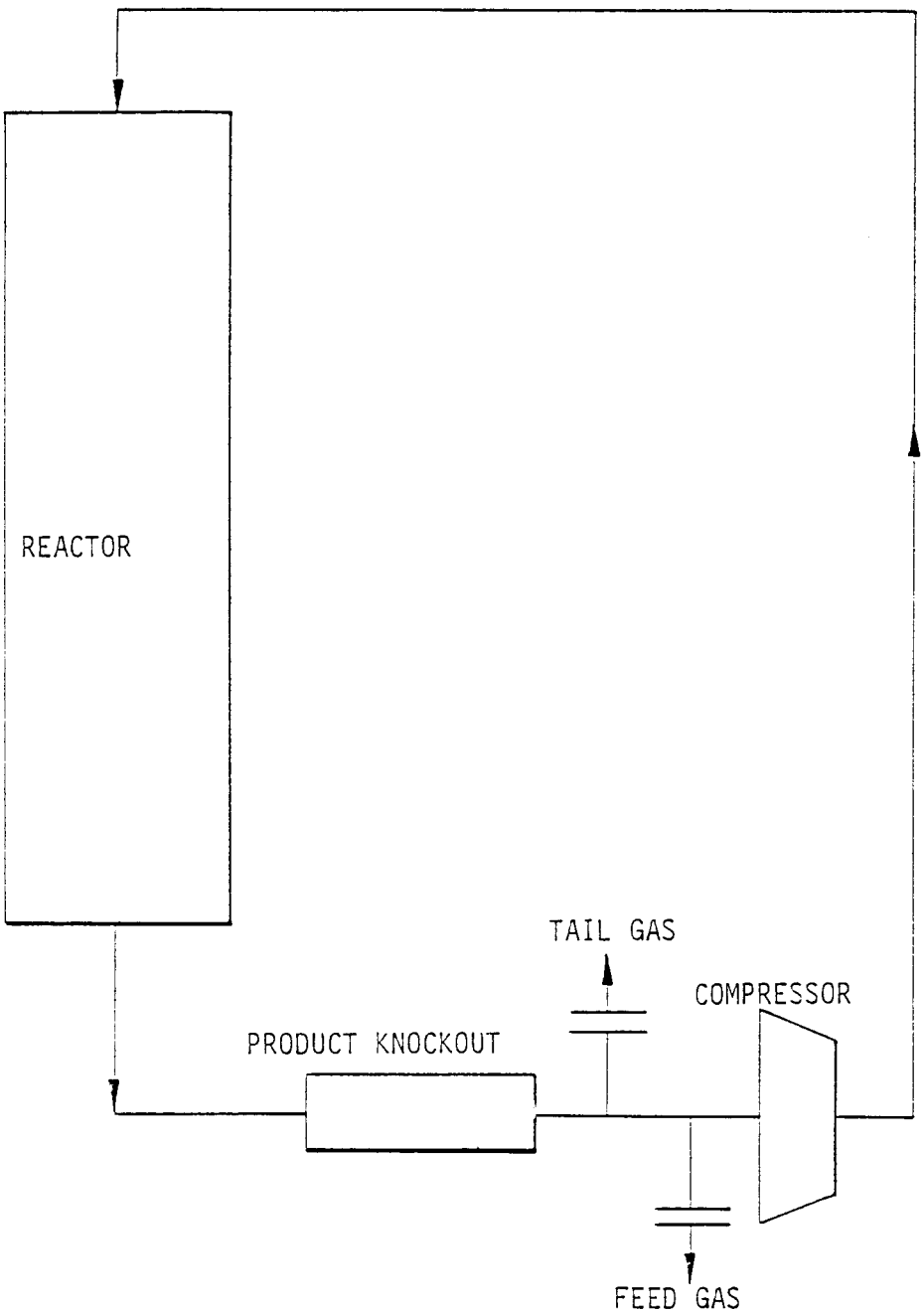

Figure 4.1. Flow sheet for the first reactor setup

The catalyst samples were then subjected to various experimental analyses to determine the effect of the synthesis conditions on the catalysts chemical and physical properties. The tests included laboratory micro reactor runs, and the characterization tests mentioned in Sections 4.1.1. to 4.1.3..

In the second fixed bed reactor system, see Figure 4.2., two reactor tubes in series were used. In this two stage reactor setup, the tail gas of the first reactor is directly introduced as feed gas for the second fixed bed reactor. The tail gas of the second reactor was recycled and mixed with the feed of the first reactor. All condensable products produced by the first of the two reactors was knocked out before it reached the second reactor. To simplify terminology, these two reactors will from now on be referred to as the first and second stage reactors.

As only the top half of the catalyst bed is of importance during these experiments, the top half of both the reactors are loaded with the iron catalyst, while the bottom half of the both reactors are loaded with inactive ceramic spheres. This was done to ensure that a direct comparison could be made with the earlier study (see Chapter 5). The two catalyst beds were run in series for 375 time units (tu), the runs were terminated, and the catalyst unloaded in similar fashion as was mentioned above. The catalysts were then subjected to the same analytical procedures as already described.

4.2.2. Laboratory micro reactors

The catalysts unloaded from the fixed bed reactors were tested in laboratory micro reactors to obtain the total activity profile for each of the 20 samples in the fixed bed reactor catalyst bed. The laboratory micro reactor system consists of four

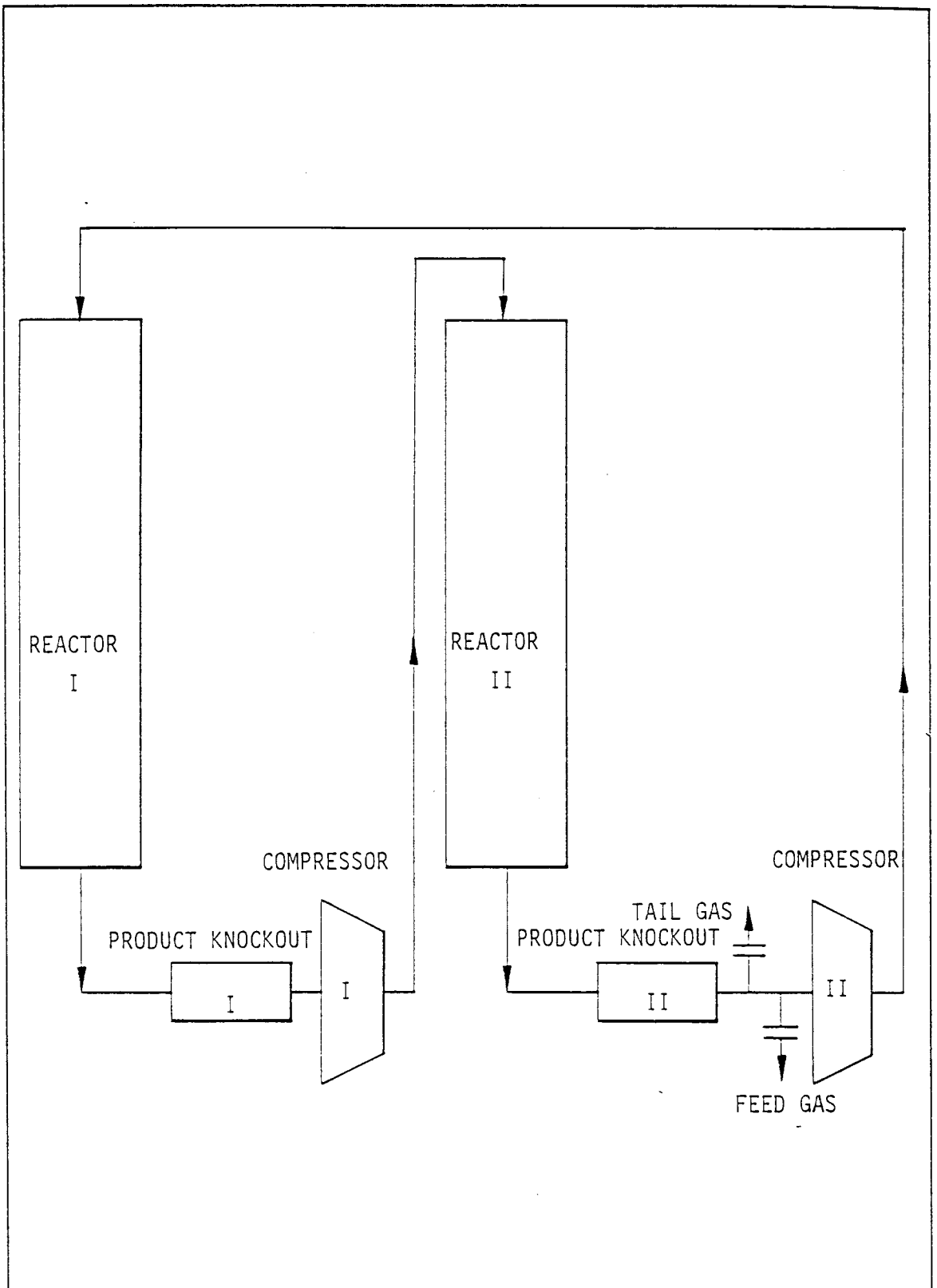

Figure 4.2. Flow sheet for the second reactor setup

identical reactor tubes, operated at precisely the same experimental conditions to ensure the validity of the comparison tests. In each test a fresh unused catalyst is compared with three experimental catalysts, i.e. used catalyst bed samples in order to have a common reference point.

The catalysts were kept on line until the activity, as measured by the daily (every 24 hours) drainages of water and hydrocarbon products stabilized. The activity was calculated as a function of the water produced.

4.2.3 Reproducibility of the data obtained from the laboratory micro reactors

The micro reactor system (Section 4.2.2.) was used to compare the used experimental catalysts from the reactors with an unused catalyst (fresh catalyst) in order to obtain trends. The reproducibility of these reactors and the suitability of the micro reactor setup to be used with an iron Fischer–Tropsch catalyst was determined.

The activity results are shown in Table 4.1.. For easier interpretation, the amount of water produced in a tube chosen at random ("standard tube") was assigned the arbitrary value of 100.

From the results in Table 4.1. it is evident that the activity of the fresh catalyst from the three experimental reactor tubes compare very well with that of the standard reactor tube. The accuracy is $\pm$ 1,5 % for the water measurement. This difference is so small that it is assumed that there is not a statistical difference.

	STANDARD TUBE	EXPERIMENTAL TUBES		
	1	2	3	4
WATER	100	97	100	97

Table 4.1. Relative activity, calculated as a % of the first reactor tube

From all this evidence, the author believes that the experimental results obtained from this micro reactor system are valid. The system is therefore capable of comparing the activities of used catalyst samples (from various sections of the pilot plant reactor tube) with those of a standard (fresh) catalyst.

4.3. References

1. Methods developed by the Sasol One Analytical Group
2. G.W. Ewing, *Instrumental Methods of Chemical Analysis*, 5th Edition, McGraw–Hill Book Company, New York, 1985, 199, 401
3. A.L. Chaffee, I. Campbell and N. Valentine, *Appl. Catal.*, *47*, 1989, 253
4. E. Ruckenstein, *Metal–support interactions in Catalysis, Sintering and Redispersion*, Van Nostrand Reinhold Company, New York, 1987, 230 – 236, 239 – 241, 271, 287, 291 – 294, 296

CHAPTER 5

DEACTIVATION OF A LOW TEMPERATURE FISCHER–TROPSCH PRECIPITATED IRON CATALYST IN A FIXED BED REACTOR

5.1 Introduction

The objective of this chapter is to investigate the effect that parameters, like time and reactor bed position, have on the chemical and physical properties of an iron catalyst unloaded from a fixed bed reactor.

Among the main factors[1] that determine when to end a Fischer–Tropsch reaction, is the catalyst activity. Therefore, this observed variable was monitored and correlated with the catalyst surface properties to obtain a better understanding of the changes taking place in the behaviour of the iron catalysts performance during hydrocarbon synthesis. The catalyst was unloaded and experimentally tested as explained in the experimental section (see Chapter 4).

Catalyst activity for an iron catalyst typically declines with time, as is shown in Figure 5.1.. This deactivation is similar to that published for other catalytic systems in literature[2]. The deactivation shows a rapid initial loss in catalyst activity, whereafter the activity stabilizes with time and later gradually decreases.

The initial sharp decline in activity is of little concern, as most catalysts need time to stabilize, but the decline in activity later on, as the run progresses, has an important effect on the actual lifetime of the catalyst. It is therefore important to identify the factors influencing this part of the deactivation profile in order to be

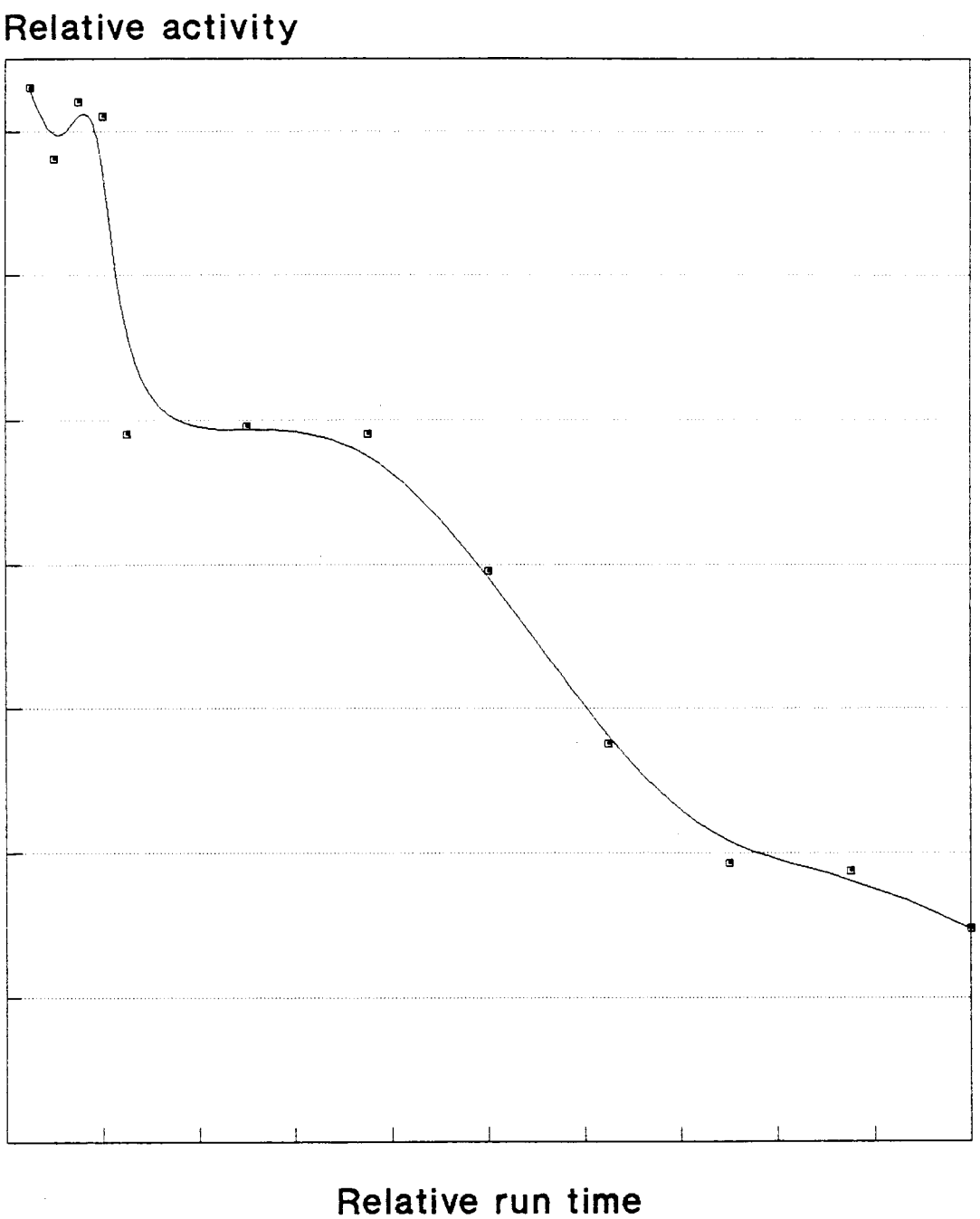

Figure 5.1. Deactivation profile of a fixed bed reactor

able to take preventative action and therefore lengthen the total running life time of the catalyst.

Progressing through this chapter, the decline in activity for an iron catalyst in a fixed bed reactor will be investigated and logical explanations for the observed changes will be given.

5.2. Fixed bed activity profile

After unloading the catalyst bed section by section for fixed bed reactors of different run lengths, as already mentioned, activity profiles over the length of the catalyst bed were obtained to determine each section's contribution towards the total performance of the catalyst. The results obtained are given in Figure 5.2. in which it is clearly shown that the activity of each section decreases with run time, i.e. for 1 time unit (tu) through to 1000 time units (tu).

Another observation from Figure 5.2. is, that for each case analyzed, (1 tu to 1000 tu), the top section of the reactor bed has a low activity. This low activity increases to a maximum activity one quarter from the top of the fixed bed reactor. Thereafter there is a gradual decrease in catalyst activity down the catalyst bed.

The effect of the catalyst deactivation is shown most clearly by the catalysts which spent the longest time on line, i.e. 1000 tu. Therefore, to simplify the remaining part of this discussion, only this profile (given in Figure 5.3.), except when mentioned otherwise, will be discussed further.

A final observation made from the deactivation profiles in Figure 5.2. is that the top

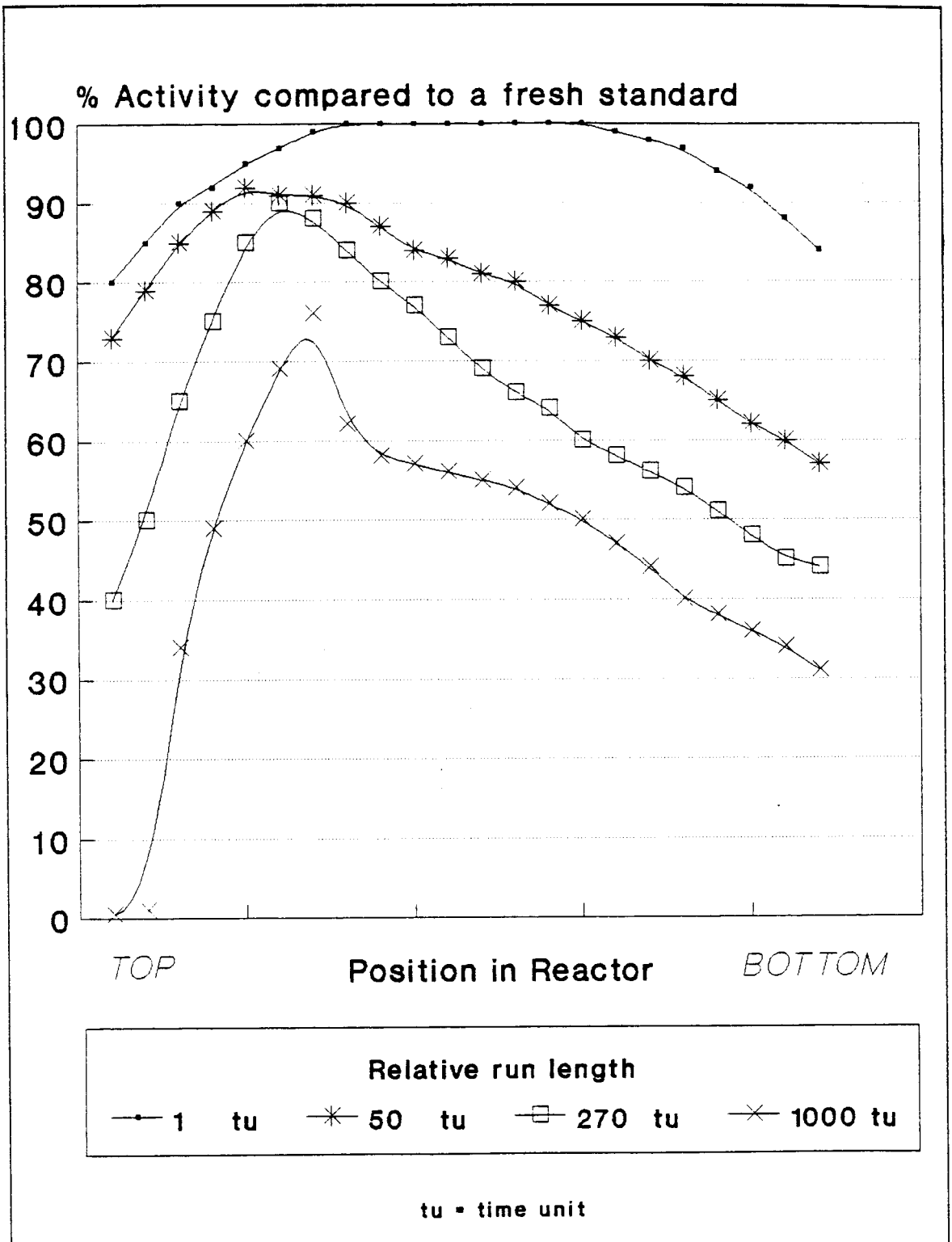

Figure 5.2. Activity profile through the reactor bed for catalysts of different run lengths

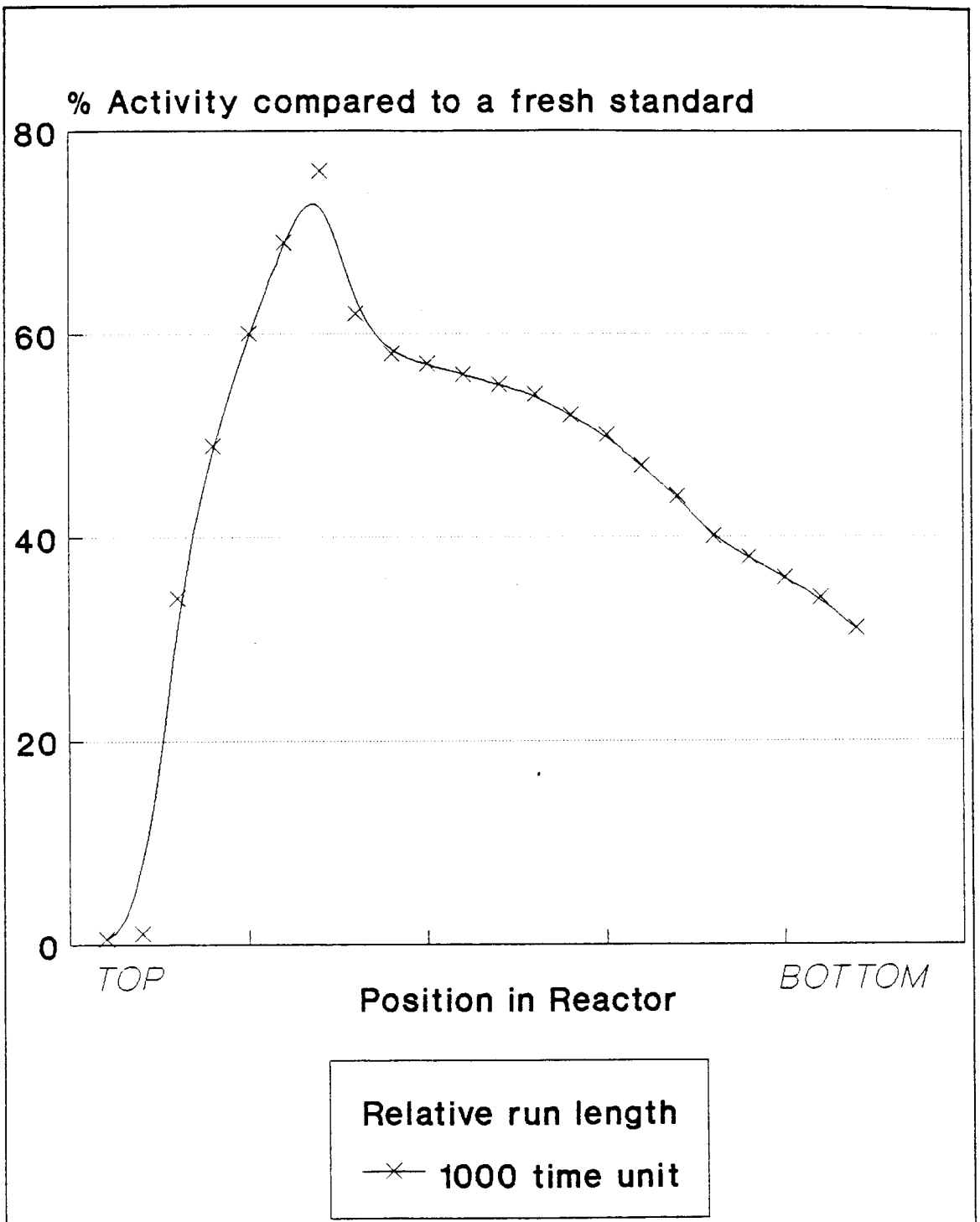

Figure 5.3. Deactivation profile for the discussion of catalyst deactivation

section of the catalyst bed deactivates more rapidly with time than the bottom section, and that the rate of deactivation at one quarter from the top of the catalyst bed is remarkably lower. This is clearly illustrated by Figure 5.4., which shows a semi logarithmic plot of the relative activity for different sections of the catalyst bed versus time on stream. This graph shows that the deactivation process is more severe in the top section and less drastic in the bottom section of the catalyst bed. The reason for this behaviour will be explained in Section 5.4.1..

The observation that the catalyst is more active one quarter from the top of the reactor, correlates well with the findings reported by Kölbel and Engelhard[3] for a fixed bed reactor and for the Fischer–Tropsch process in general.

Kölbel and Engelhard[3] reported that of the CO converted during the Fischer–Tropsch process in a fixed bed reactor, 80 % was converted in the first third of the catalyst bed and that a minimal increase in Fischer–Tropsch products occurred in the remaining two thirds of the catalyst bed. They also observed the highest concentration of Fe^m (metal + carbide) phase to be found in that region. As is well known[4] (see literature review in Chapter 2) iron metal and carbide phases are considered as the active phases for the Fischer–Tropsch process.

Furthermore, predicted data for a fixed bed reactor shows (see Figure 5.5.) a similar temperature profile down the reactor bed as that reported by Denbigh et al.[5] for a fixed bed reactor. The higher conversion obtained in this section, one quarter from the top of the reactor bed, corresponded with the highest temperature zone in the reactor. Temperature is well known as one of the parameters influencing the activity of a catalyst.

The reasons for the very low activity at the top of the catalyst bed and the gradual

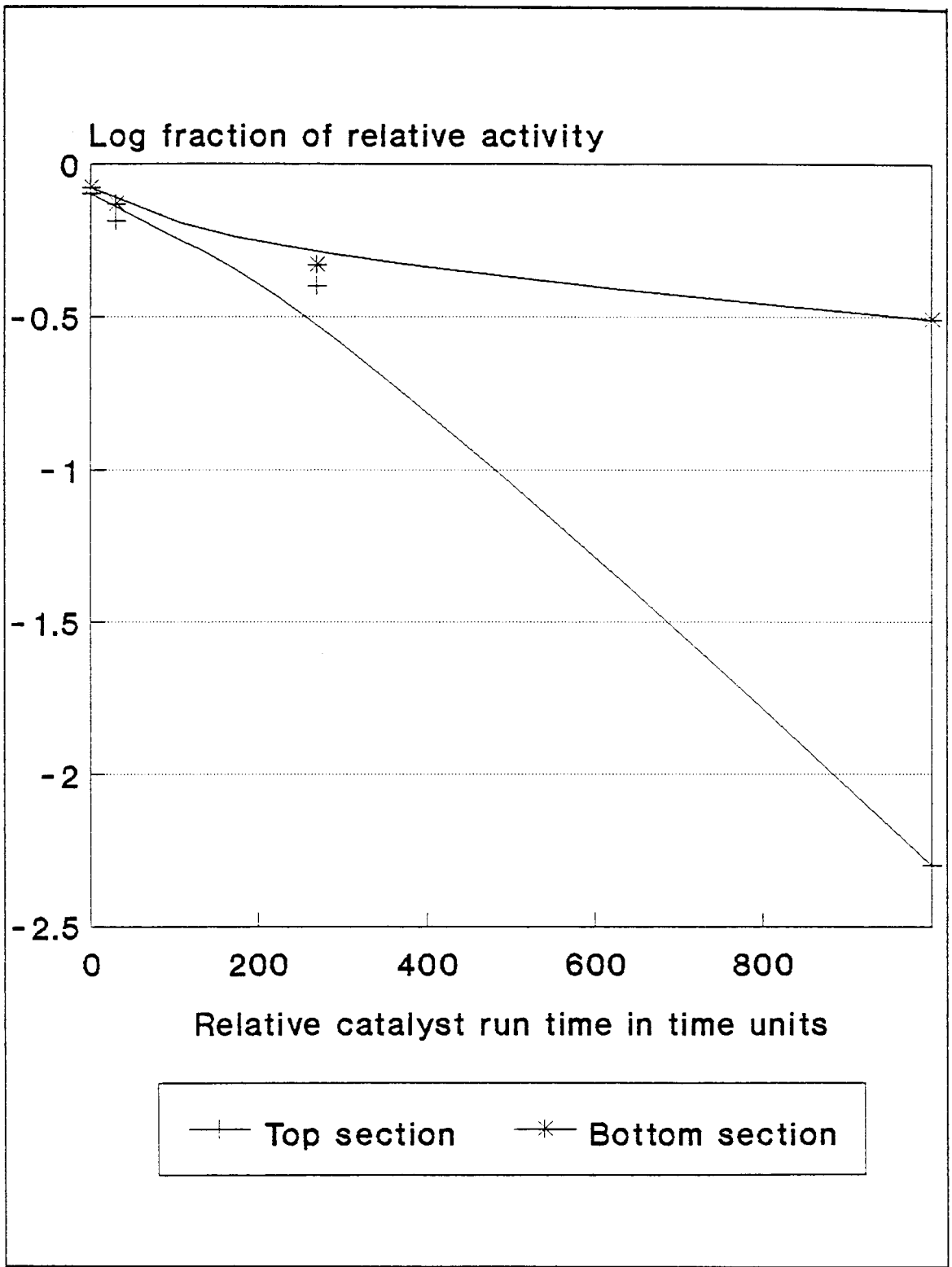

Figure 5.4. Activity of the top and bottom sections of the reactor vs the time the catalyst spend on line

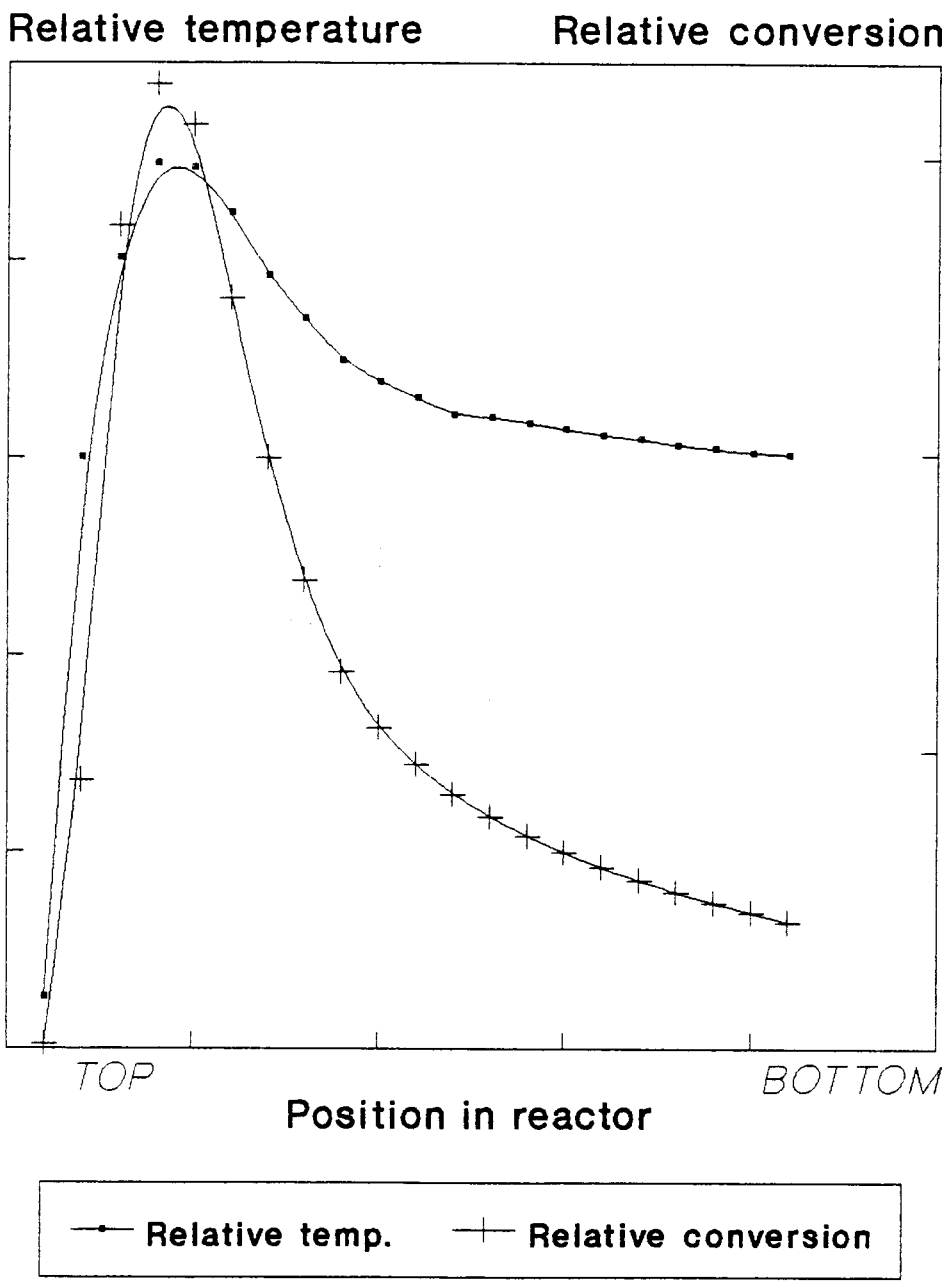

Figure 5.5. Relationship between the temperature and conversion profiles of a fixed bed reactor

decrease in activity one quarter from the top of the catalyst bed downwards will constitute the main discussion in the remaining part of this chapter and explanations will be given for this behaviour.

5.3. Physical properties of the catalysts samples from different sections of the catalyst bed.

The catalysts unloaded from the different sections of a tubular reactor were submitted for various tests, which included elemental, sulphur and carbon analysis by the analytical techniques described in the experimental section. The catalysts were also submitted for XRD, and area and pore volume examinations to obtain information and a better understanding of the effects that the Fischer–Tropsch synthesis have on an iron catalyst.

5.3.1. Sulphur content

As shown by Figure 5.6., high concentrations of sulphur were found in the top sections of the catalyst bed and basically no sulphur was detected in the remaining part of the catalyst bed.

5.3.2. Carbon content

The relative concentration of carbon (excluding the very top part of the reactor) seems to be very constant until the bottom part of the reactor, where it shows a small decrease. This trend is illustrated in Figure 5.7..

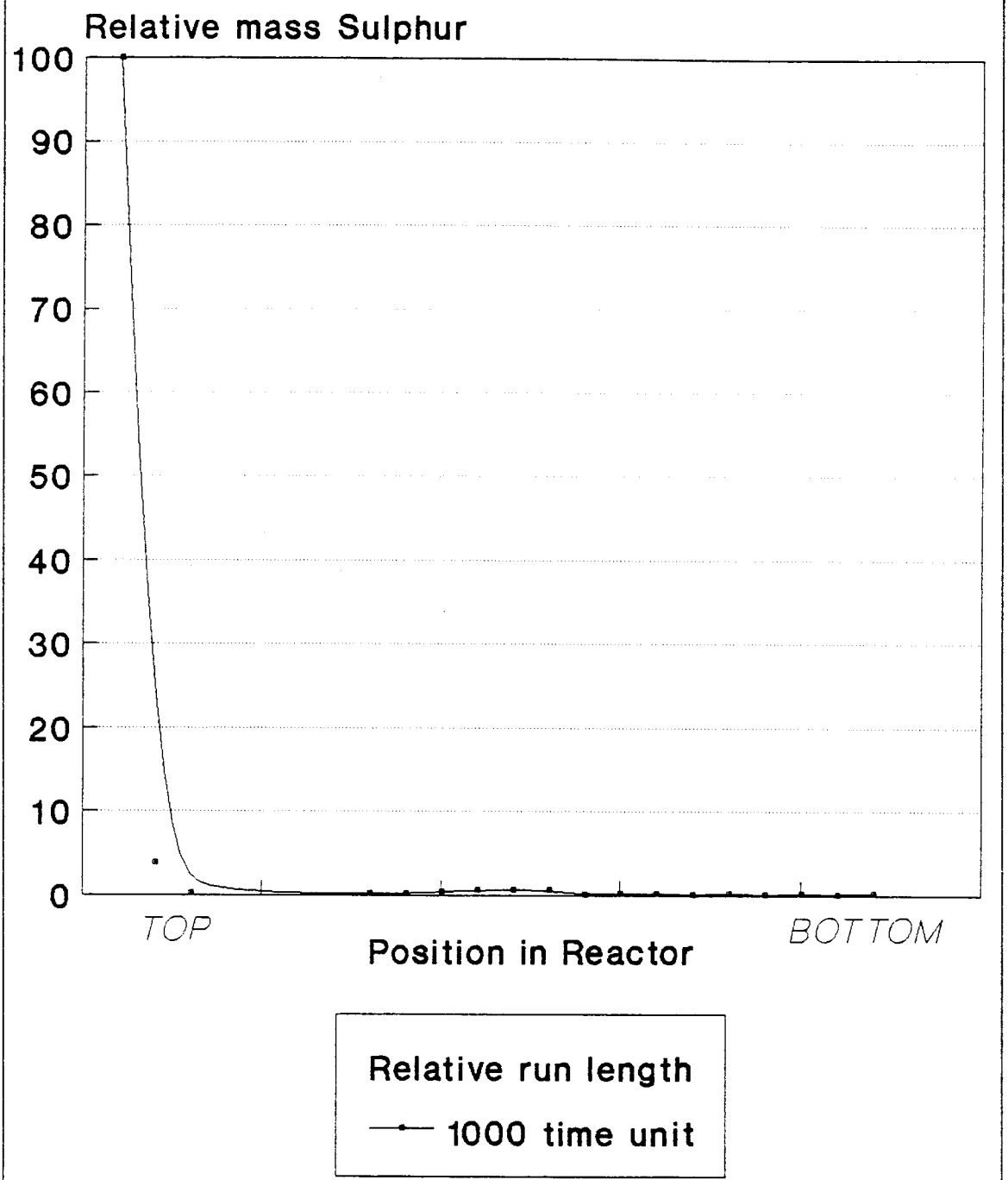

Figure 5.6. Sulphur profile for a fixed bed reactor catalyst bed

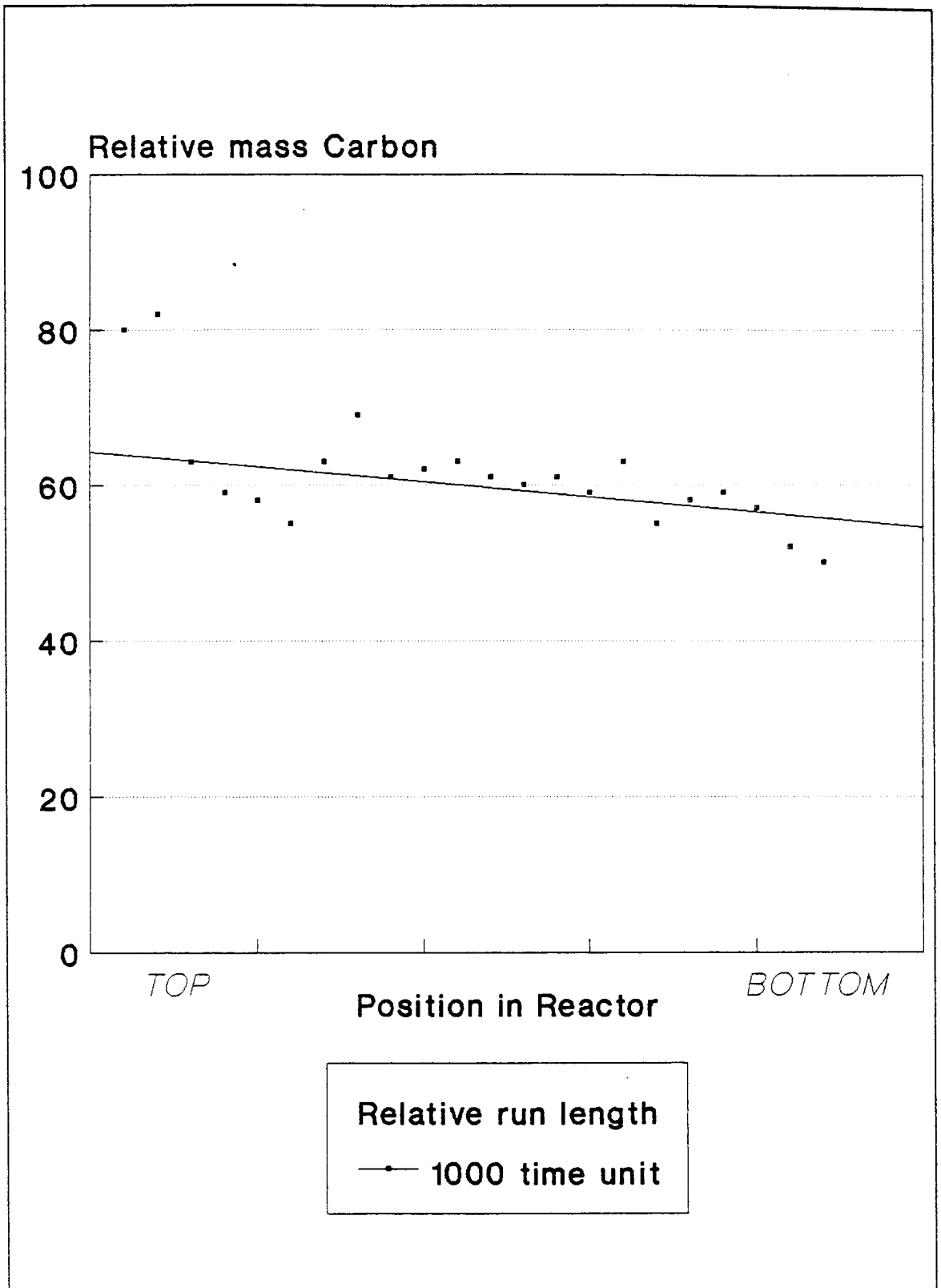

Figure 5.7. Carbon profile for a fixed bed reactor catalyst bed

5.3.3. Oxidation and crystallite size

XRD analysis done on the catalysts samples, revealed mainly the presence of magnetite (Fe_3O_4) throughout the catalyst bed. Figures 5.8. and 5.9. show the effect of synthesis on the magnetite concentration and crystallite size through the catalyst bed, respectively.

The amount of magnetite was shown to increase with catalyst run time and also on descending the catalyst bed. The crystallite size, calculated from the magnetite peaks, showed a similar tendency of size increase with catalyst run time and on descending the catalyst bed.

5.3.4. Area and pore volume

Area analysis (see Figure 5.10.) of the catalysts from the different sections in the catalyst bed, showed a definite decrease in the catalyst area down the reactor bed, while the pore volume analysis (see Figure 5.11.) showed an increase in total pore volume.

5.4. Discussion of results

The results obtained in Section 5.3. can be rationalized by the factors mentioned in the literature study in Chapter 3. It will be shown that these analytical results tie in with the catalyst deactivation behaviour observed during hydrocarbon synthesis using an iron catalyst run in a pilot plant fixed bed reactor.

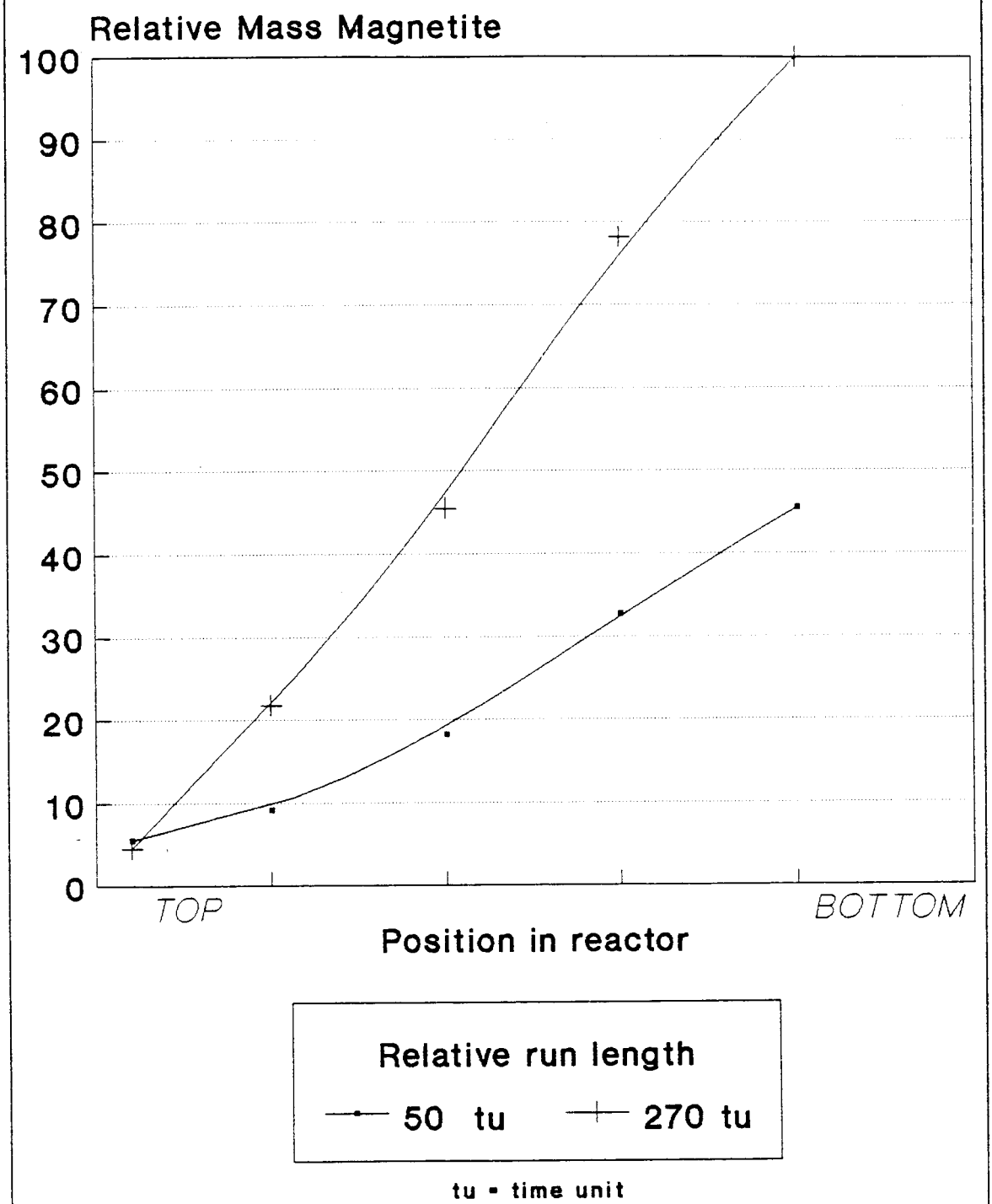

Figure 5.8. Mass magnetite through reactor bed

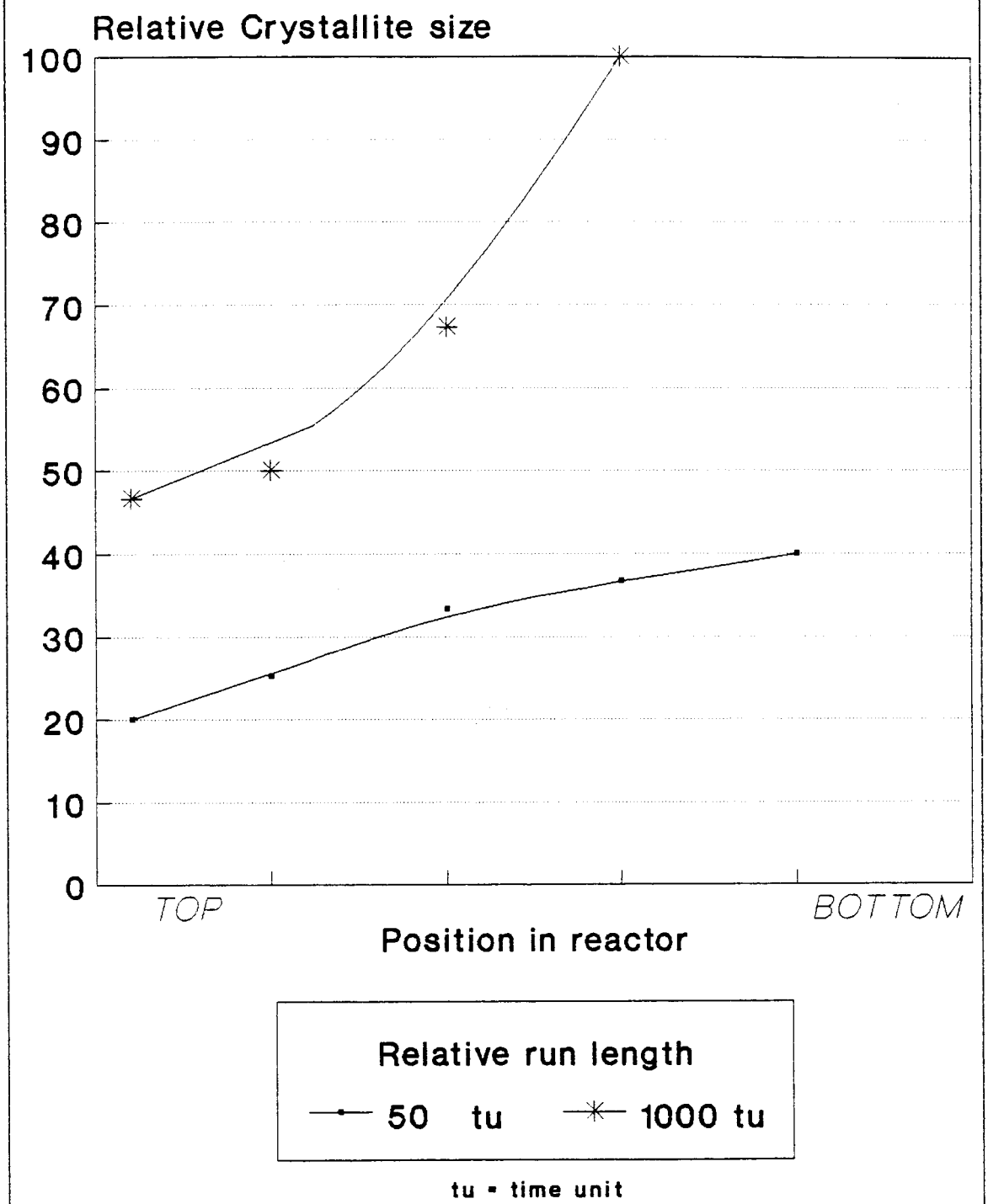

Figure 5.9. Crystallite size through reactor bed

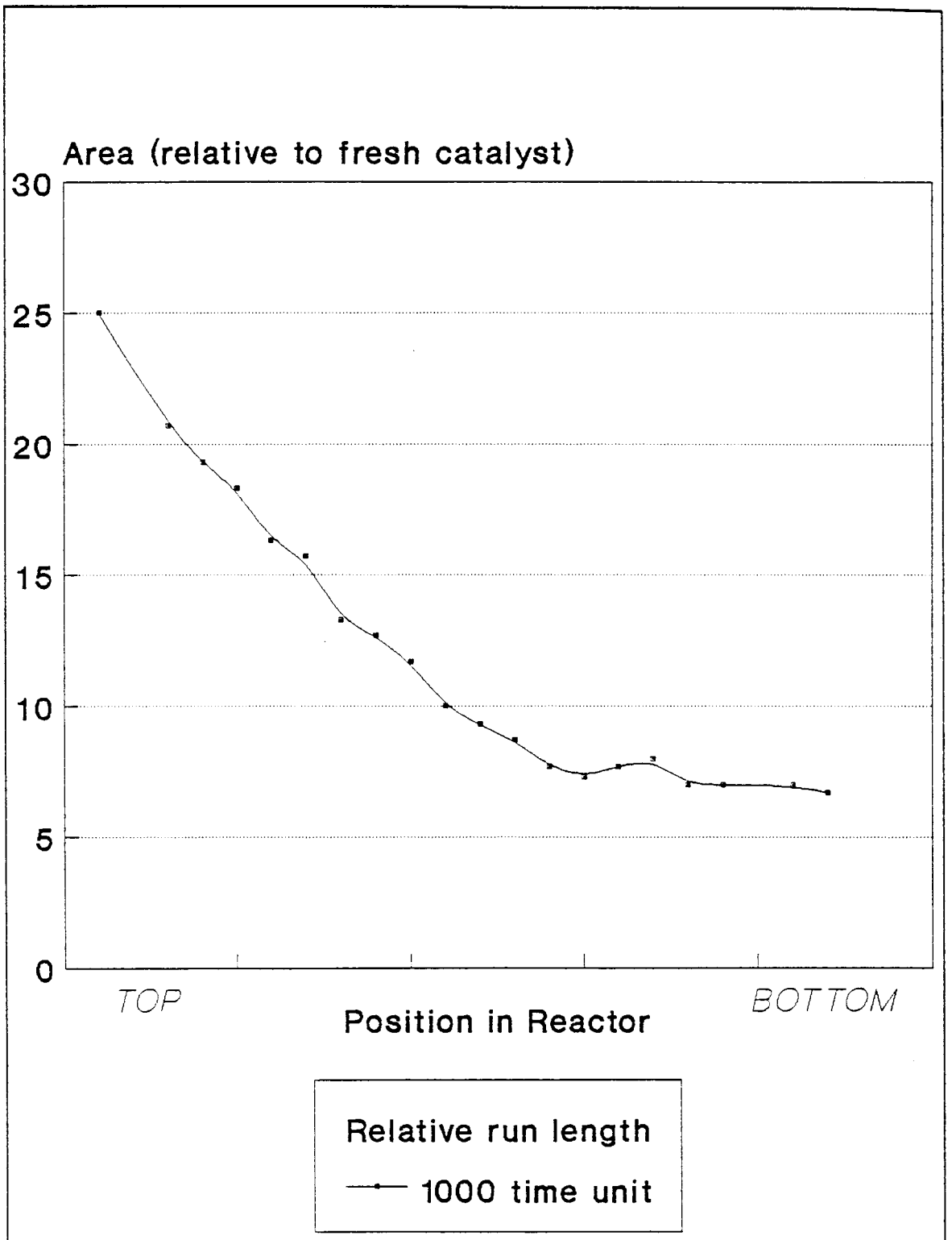

Figure 5.10. Surface area of the catalyst through reactor bed

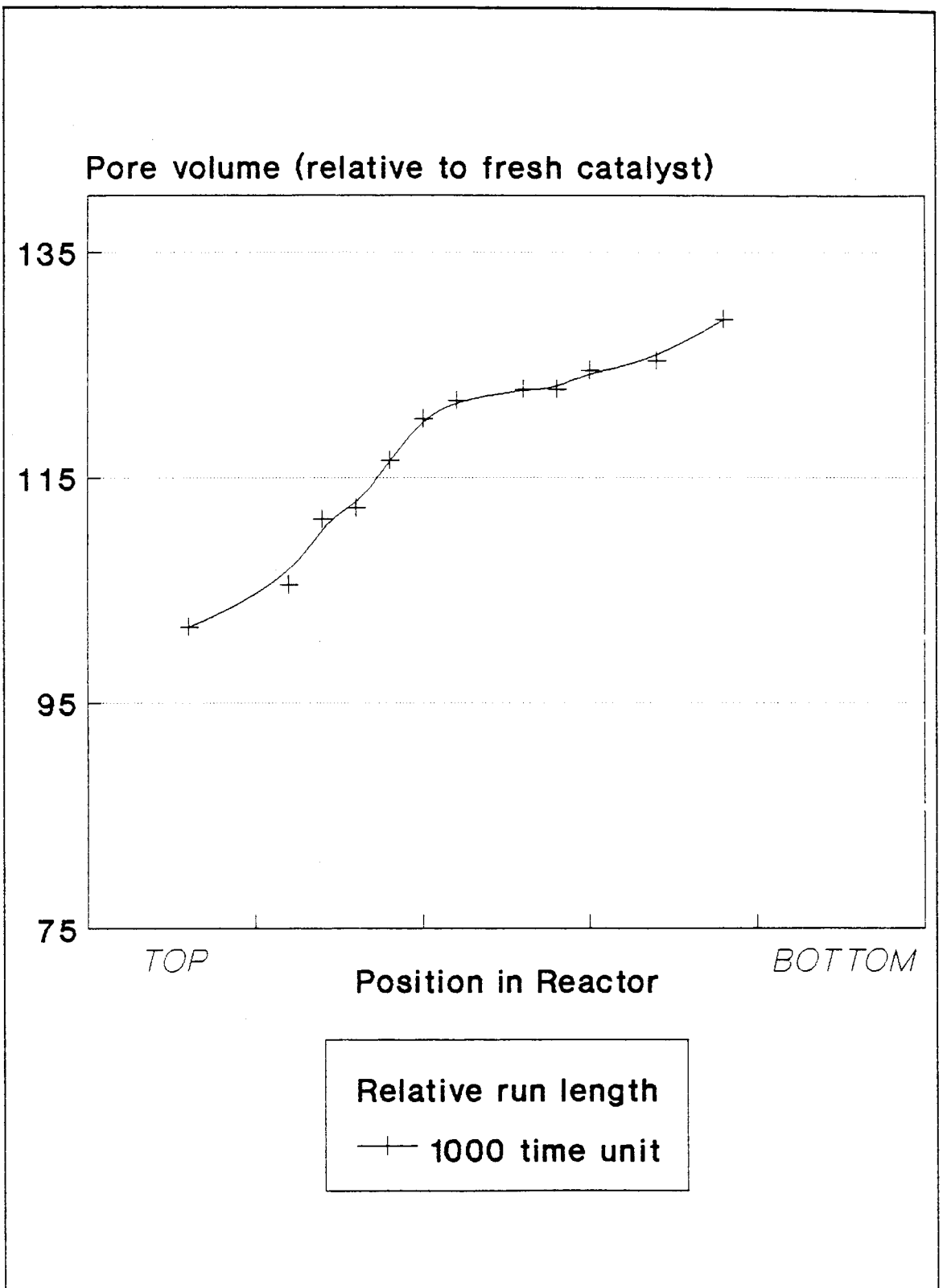

Figure 5.11. Pore volume of the catalyst through the reactor bed

In our discussion we will mainly describe the catalyst profiles for the catalysts that spent the longest time on line (270 tu and 1000 tu), as the deactivation trends are more clearly observed with these runs. In each case, the results obtained will be compared directly to the activity profile as shown previously in Figure 5.3..

5.4.1. Catalyst bed deactivation profile : top section

Plotting the sulphur profile (Figure 5.6.) and the activity profile (Figure 5.3.)on the same graph (Figure 5.12.) clearly shows that the high sulphur concentration obtained in the top section of the catalyst bed corresponds to the low activity for the corresponding sections in the catalyst bed. None of the other analytical results correlate with the decline in activity as shown for the top section of the catalyst bed. Further, sulphur has been positively identified as a poison for Fischer–Tropsch catalysts[6,7] (see Literature survey, Section 3.2.). We conclude that the presence of sulphur correlates with the low activity in the top section of the catalyst bed.

The finding that sulphur is only found to be present in the top section of the catalyst bed has been observed previously. Similar results have been reported by Chaffee et al.[8] for a manganese/iron catalyst system (making use of XRD and XPS techniques) and by Madon and Taylor[9] on a cobalt catalyst. Madon and Taylor deliberately poisoned a fixed bed reactor containing a cobalt catalyst and found sulphur was trapped only in the top 20% of the fixed bed reactor catalyst bed. The sulphur concentration, as in our case, decreased rapidly further down the catalyst bed.

Deactivation profiles reported by Denny and Twigg[10] for a copper based low temperature shift catalyst and results obtained by Bartholmew and Bowman[11] and

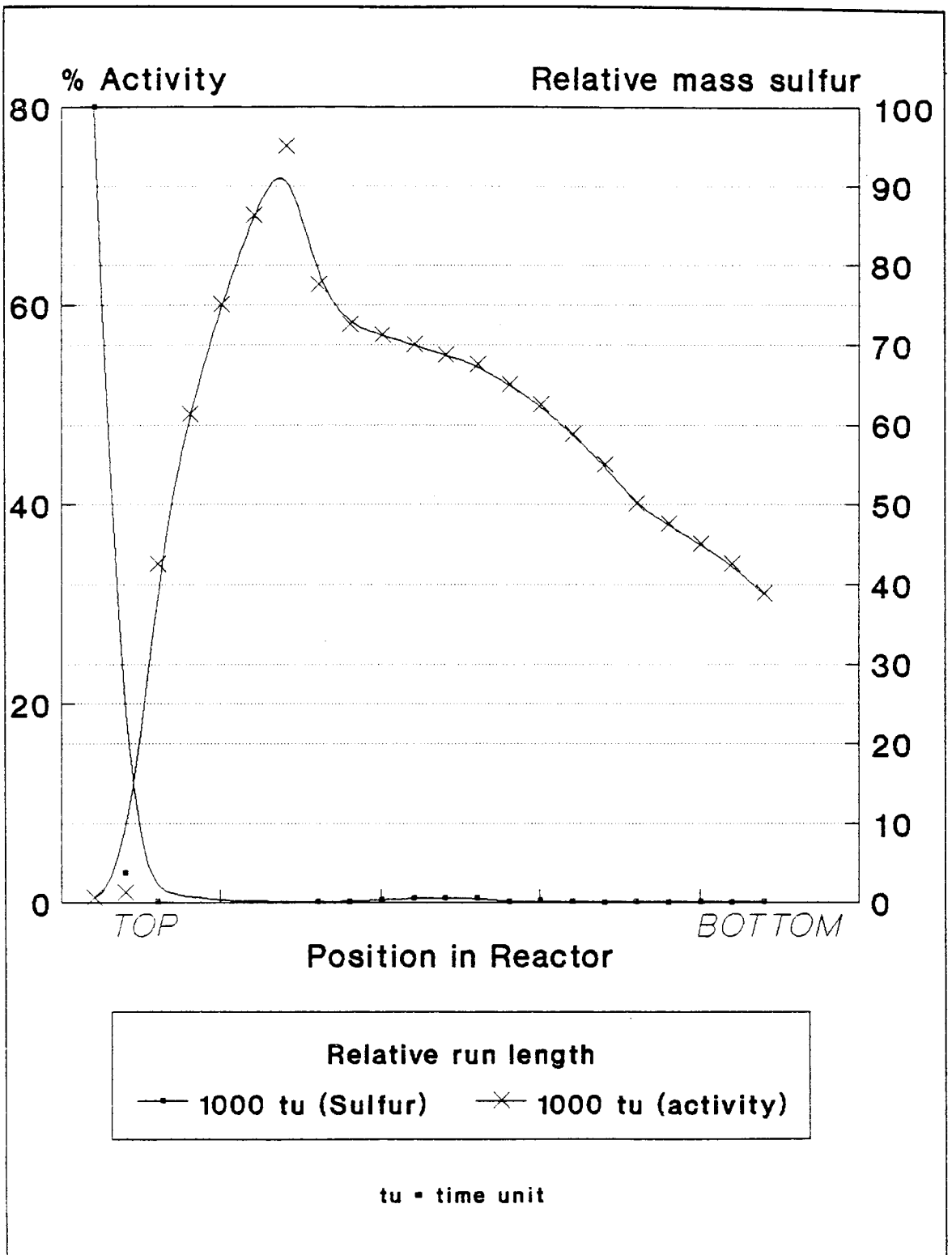

Figure 5.12. Effect of sulphur on the activity profile of a fixed bed reactor catalyst bed

Agrawal et al.[12] for iron based catalysts poisoned by H_2S, concentrations as low as 13 ppb to 2 ppm, have also given similar results.

5.4.2. Catalyst deactivation profile : middle and bottom sections

Two main causes for the deactivation of the catalysts in these sections of the catalyst bed can be identified. These are firstly, the oxidation of the reactive iron metal phase to mainly the Fischer–Tropsch unreactive magnetite (Fe_3O_4) phase, and secondly, iron crystallite growth which can contribute to the loss in surface area of the catalyst, i.e. total and active surface area of the catalyst.

(i) Oxidation

The water produced as a product during the Fischer–Tropsch reaction (see Section 3.3.) can oxidize the catalyst. The active iron metal phase (Fe^m) needed for the synthesis reaction is obtained by reducing the iron oxide catalyst with hydrogen at mild temperatures and pressures (see Chapter 2) before the actual synthesis gas is introduced to the catalyst[13]. If oxygenates, like water, are produced during the synthesis reaction, the catalyst will be oxidized when in contact with these products, resulting in the Fischer–Tropsch unreactive iron oxide phases[3]. These unreactive phases (see Section 5.4.4., as analyzed by XRD) proved to be hemeatite (Fe_2O_3) and magnetite (Fe_3O_4). Magnetite is the most abundant of the phases.

As already shown in Figure 5.8., the amount of magnetite increases with an increase in catalyst run time, but also increases down the catalyst bed. The reason[3] for this is that the partial pressure of water increases down the catalyst bed and therefore a more severe oxidizing atmosphere is present further down the catalyst

bed.

Correlating the relative amount of magnetite found through the catalyst bed with the corresponding activity profile, as is shown in Figure 5.13., it is obvious that the oxidation of the iron metal phase to magnetite could be contributing to the loss in catalyst activity one quarter from the top of the catalyst bed downwards.

Kölbel and Engelhard[3] also reported, that catalysts are more oxidized towards the bottom of the catalyst bed and that the higher the activity of the catalyst, the more water is produced, which in effect implies that a higher level of oxidation is to be expected. This also correlates with the oxidized phases found during our experiments, being in the catalyst sections immediately downstream of the most active section of the catalyst bed (see Section 5.4.4. on the XRD analysis of the unreactive and reactive phases found through the catalyst bed). These researchers[3] also remarked that catalysts oxidized by steam cannot be reactivated by re–reduction under synthesis conditions.

(ii) Iron crystallite growth – sintering

As shown in Figure 5.10., there is a marked decrease in the total surface area of the catalyst as the depth in the catalyst bed increases. This may also be explained by the increase in the crystallite size as determined by XRD (Figure 5.9.). This relationship between increasing crystallite size and decreasing catalyst surface area is also mentioned by Hughes[14] (see Section 3.3.).

Therefore, if the surface area's decreasing profile is matched with that of the

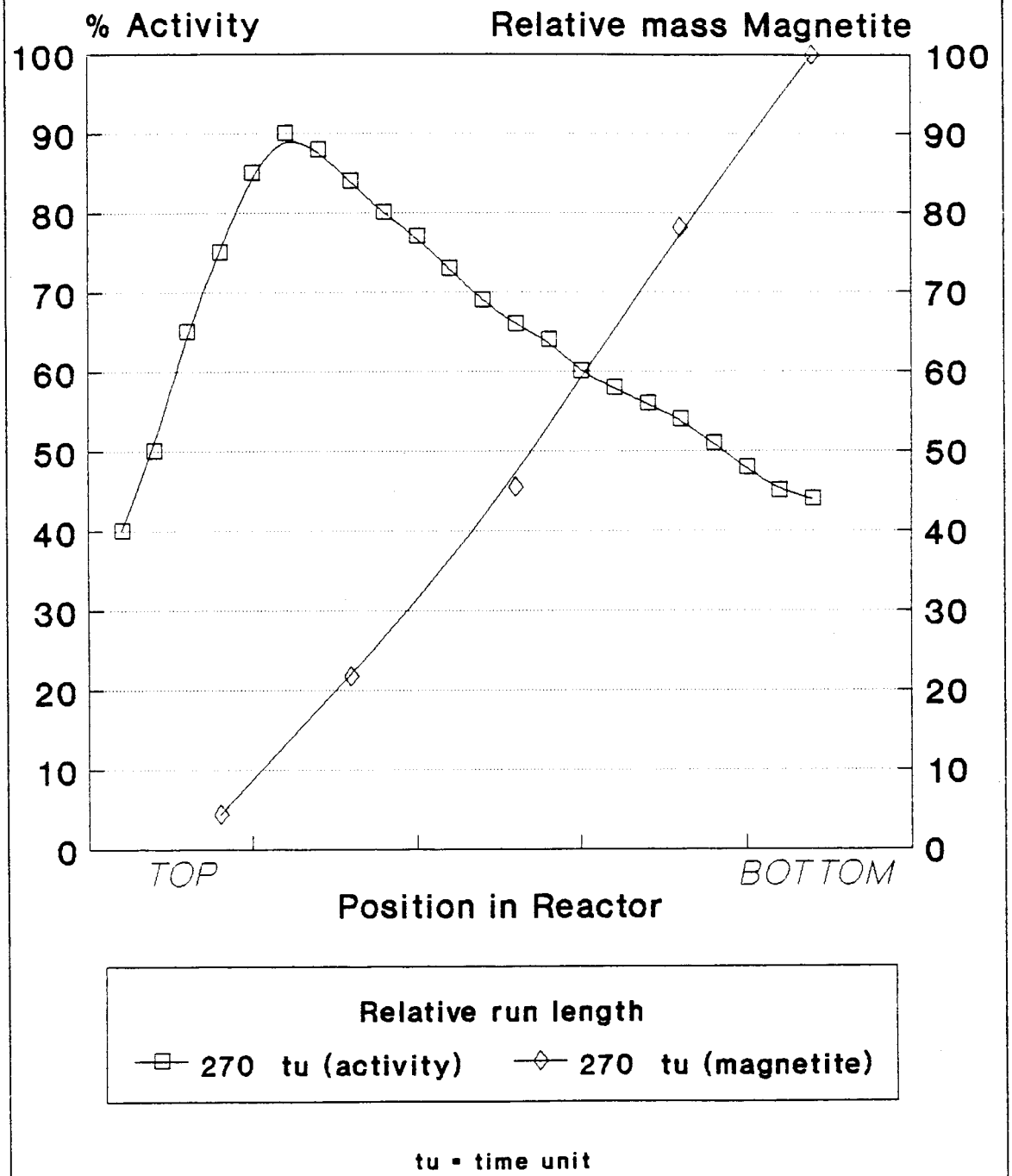

Figure 5.13. Effect of the amount of magnetite on the activity of a fixed bed reactor catalyst bed

activity profile as given in Figure 5.14., it can clearly be established that the loss of total surface area through increasing iron crystallite size, is definitely a contributing reason for the gradual decrease of the catalyst activity from one quarter from the top of the catalyst bed downwards. The same result, decreasing activity with an increase in metal crystallite size, is reported in the literature[1] for a low temperature copper shift catalyst.

As mentioned earlier and well described in the literature[1], the growth of iron crystallites results in a loss of active surface area.

As indicated in the literature survey on the growth of metal crystallites in Section 3.3., it is known that oxygen containing polar molecules like water can adsorb into metal oxides as a first step in the process for the growth of metal crystallites[15,16,17]. As already mentioned, water, a product of the Fischer–Tropsch reaction, oxidizes the active iron carbide phase to magnetite, which is a suitable metal oxide on which polar water molecules can adsorb to form larger iron crystallites. These larger iron crystallites therefore result in a decrease of the total and active surface area of the catalyst and subsequently result in a loss of the activity of the catalyst.

A final result, confirming that sintering is taking place during the synthesis process on this iron catalyst, is the increase in pore volume, as the growth of iron crystallites leads to a loss of the catalyst micro–pores. This expected behaviour is illustrated by Figure 5.11.. The growth of iron crystallites eliminates the micro–pore structure of the catalyst to yield a more stable lattice configuration.

As mentioned earlier, water produced from the Fischer–Tropsch reaction, will lead to an increase in the partial pressure of water down the catalyst bed and an increased degree of crystallite growth of the iron crystallites should occur. This

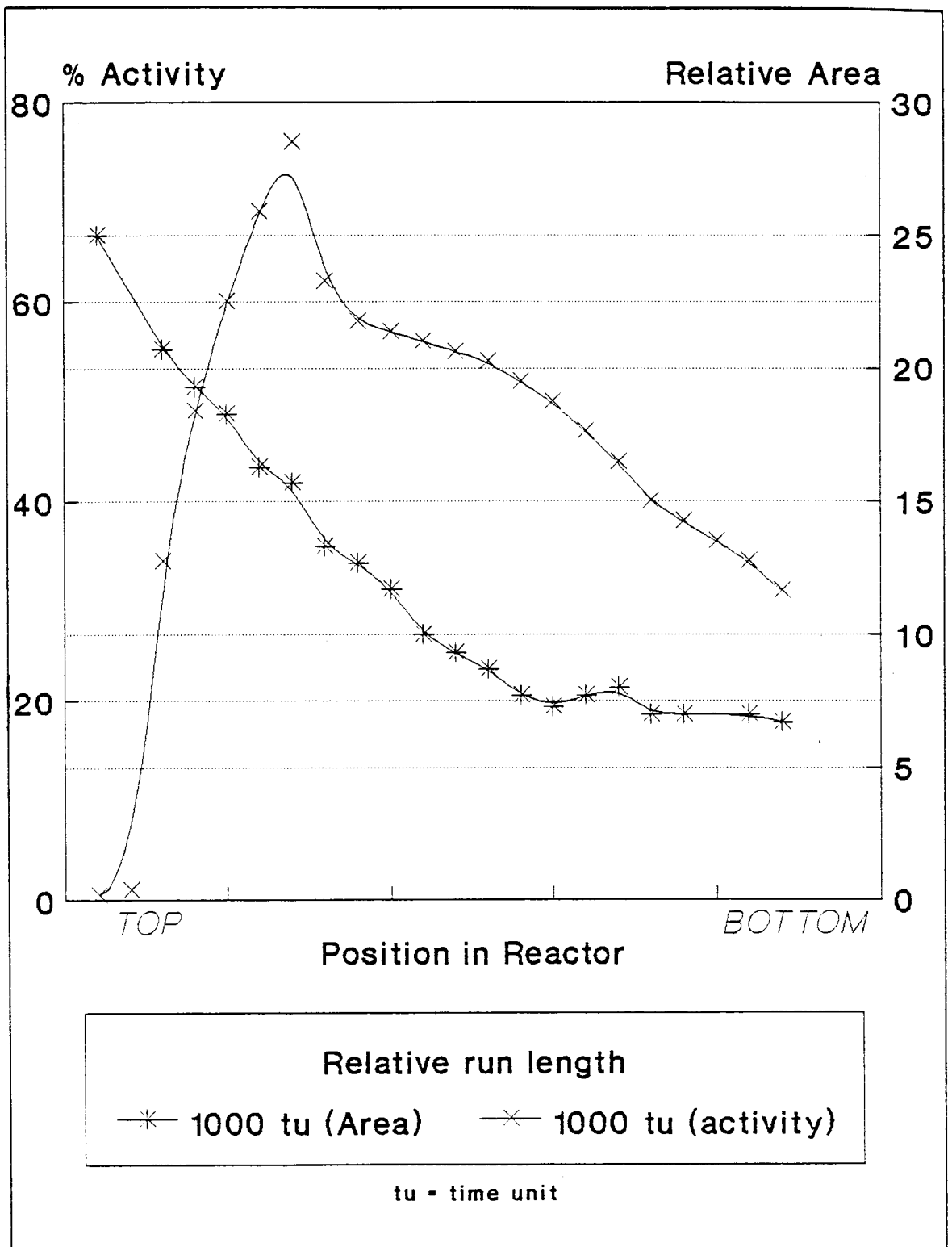

Figure 5.14. Effect of catalyst area on the activity of a fixed bed reactor catalyst bed

effect is indeed demonstrated by our results as shown in Figure 5.9.. These results also clearly show that crystallite growth is time dependent in that the degree of crystallite growth increases with the amount of time that the catalyst has spent on line. This also implies that crystallite growth, i.e. sintering of metal crystallites, is a typical catalyst aging process.

5.4.3. Fouling of the iron catalyst

The carbon concentration profile, shown in Figure 5.7., and the activity profile (Figure 5.3.) are shown together in Figure 5.15.. A very weak relationship is observed. In fact, if we exclude the very top section of the reactor (where we have shown that the influence of sulphur is high), the relative carbon concentration remains constant in a region where a big decrease in activity is observed. We therefore conclude that although coking of this catalyst does occur, it is not believed to play a large role in the deactivation behaviour.

The nature of this "carbon" as deposited, has been investigated by means of FTIR, and the results are shown in Table 5.1..

Wave number	Compound	% Transmittance
3500	$OH^- + H_2O$	medium
—	Aromatics	zero
2800	Aliphatics	low
1600	C=O	low

Table 5.1. Compounds identified in the carbon residue by means of FTIR

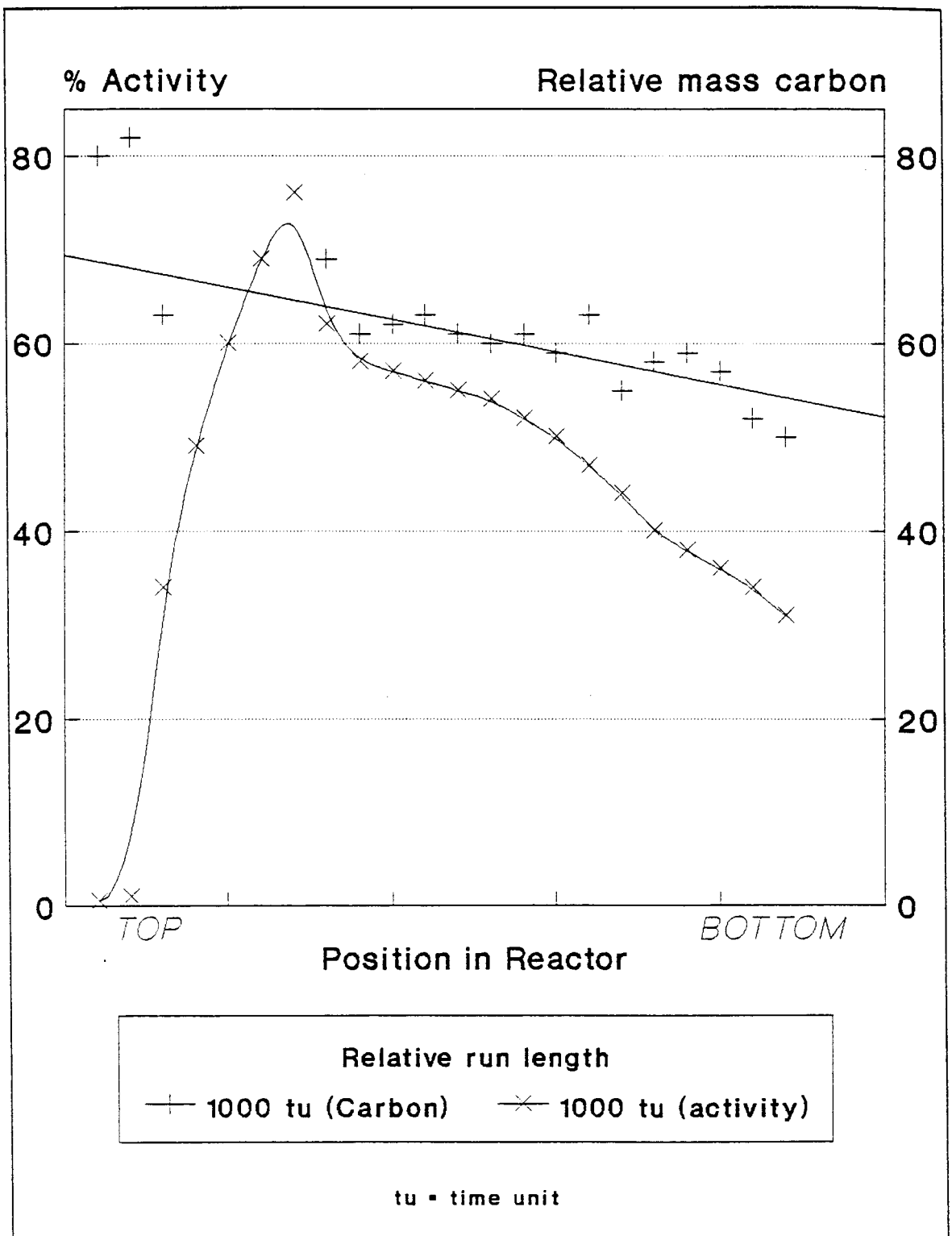

Figure 5.15. Effect of carbon on the activity profile of a fixed bed reactor catalyst bed

Although not calculated, the ratio of carbon to hydrogen appears to be very small. The carbon hydrogen ratio reported in the literature[18] for coke, is typically CH_1 and $CH_{0,5}$. The presence of aliphatic and C=O bonds, but no aromatics, is in line with the fact that this iron catalyst is not expected to form any aromatic products at this low operating temperature (see Chapter 2). It is believed that this "carbon" is a mixture of insoluble high molecular mass hydrocarbons and free carbon[7].

It may also be, as reported by Kissinger and Khang[19] and Galiasso et al.[20], that these carbon deposits may play a role in blocking the initial existing micro–pores and therefore contribute to the drop in initial activity as shown in Figure 5.1..

Therefore, deactivation by severe fouling from coking is unlikely, although, as concluded in our literature survey on fouling, the existence of high temperature zones in the catalyst pores may not be ruled out, as this could deposit small quantities of free carbon which block the catalytic active sites from the synthesis reaction.

5.4.4. Iron phases present on the different sections of the catalyst bed

A typical XRD spectrum is shown in Figure 5.16.. From the literature[21] it is known that all these phases are present in an used iron catalyst.

XRD phase analysis on the used catalysts from the different sections in the catalyst bed mainly showed Hägg's carbide (Fe_5C_2) and magnetite (Fe_3O_4) to be present in the catalyst bed. Hägg's carbide is predominant at the top of the reactor, while the

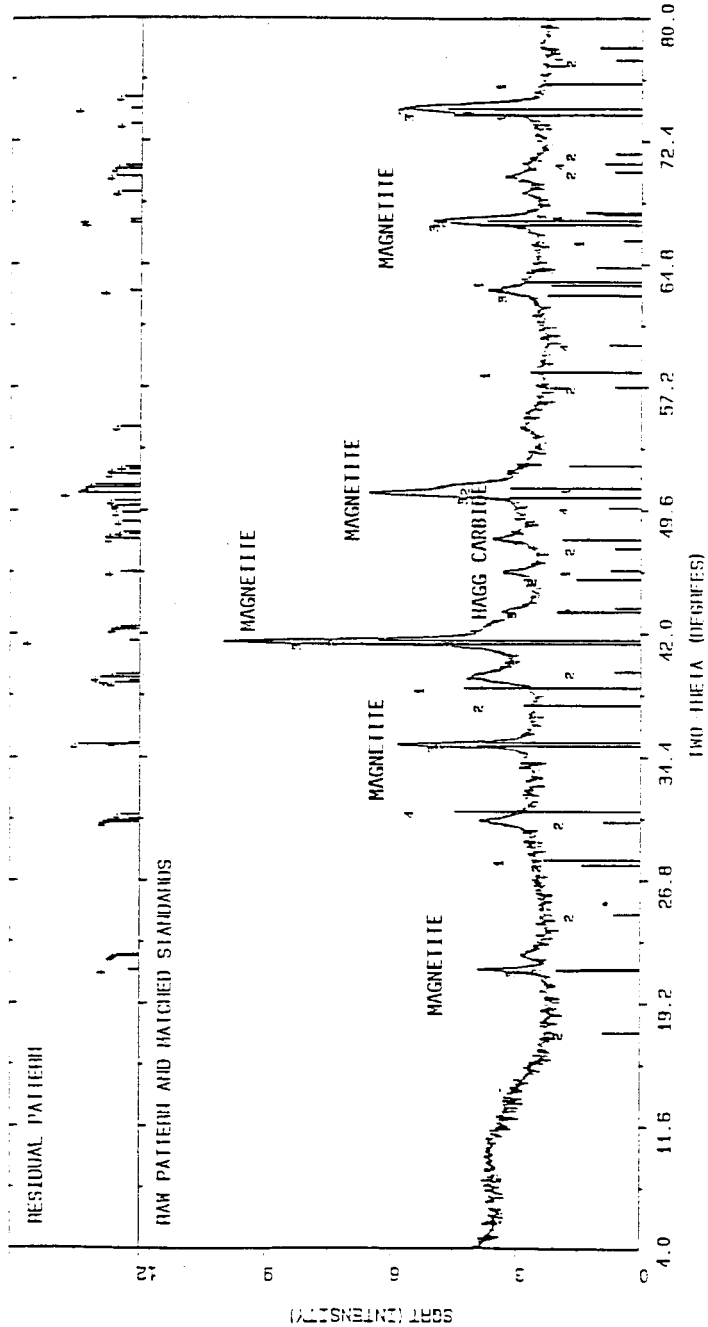

Figure 5.16. Typical XRD spectrum for the phases present in the catalyst

bottom section consists mainly of magnetite.

The gradual appearance of magnetite as we travel from the top to the bottom of the reactor bed, and the gradual disappearance of Hägg's carbide are illustrated in Figures 5.17. and 5.18.. These changes can be explained in terms of a gradual increase in the oxidative properties of the gases surrounding the catalyst, as reaction water is formed in increasing quantities while the hydrogen is being consumed. Therefore, if we exclude the strong poisoning effect of the sulphur in the uppermost part of the catalyst bed, these results tie in with the deactivation profile shown in Figure 5.3..

As mentioned in the literature section, the active phase for the Fischer–Tropsch reaction is believed to be the carbide phase, while the magnetite does not participate in the Fischer–Tropsch synthesis. It is logical then to expect that the catalyst that shows a higher concentration of Hägg's carbide (top section) would have a higher activity for the Fischer–Tropsch reaction than the catalyst that contains mainly magnetite (at the bottom of the reactor).

5.6. References

1. M.S. Spencer, *Catalysis Handbook*, (M.V. Twigg, ed.), Wolfe Publishing Ltd., London, 1989, 71
2. W.J. Lywood, *Catalysis Handbook*, (M.V. Twigg, ed.), Wolfe Publishing Ltd., London, 1989, 98
3. Von H. Kölbel and F. Engelhard, *Erdol und Kohle*, *3*, *11*, 1950, 529

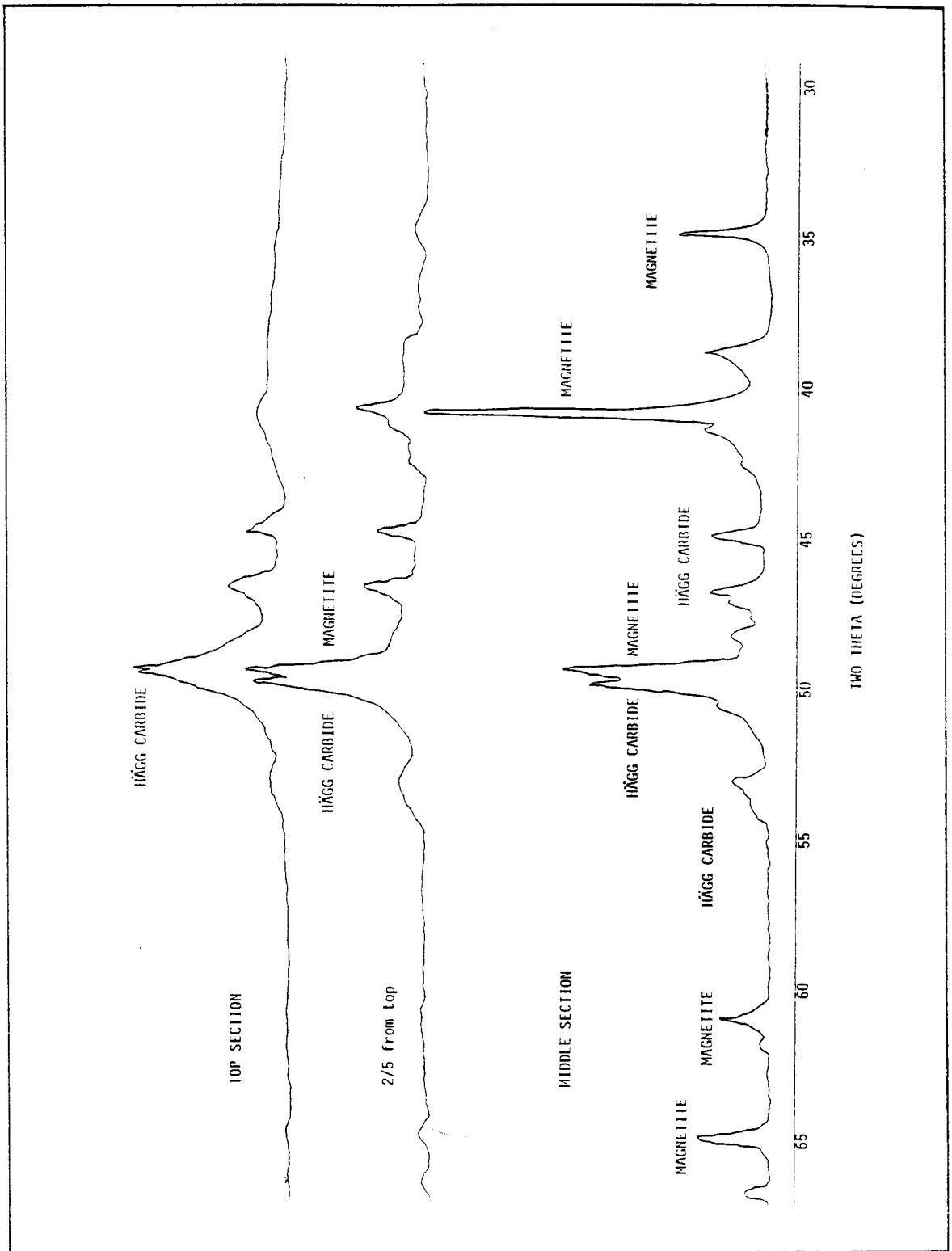

Figure 5.17. Gradual phase changes taking place through the catalyst bed

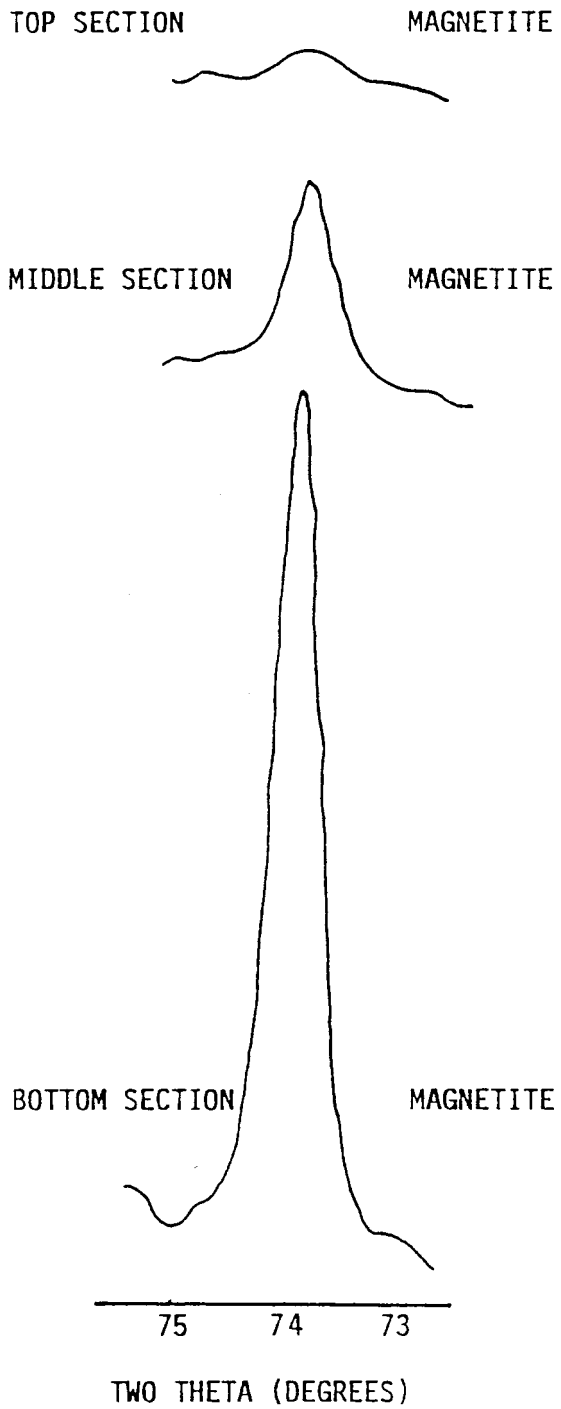

Figure 5.18. The increase in magnetite concentration observed down the reactor

4. H.H. Storch, N. Golumbic and R.B. Anderson, *The Fischer–Tropsch and related synthesis*, John Wiley and Sons, Inc., New York, 1951, 578

5. K.G. Denbigh and J.C.R. Turner, *Chemical Reactor Theory – an Introduction*, 3rd Edition, Cambridge University Press, London, 1984, 6

6. J.A. Linton and G.C. Tisdall, *Coke and Gas*, April, 1958, 148

7. M.E. Dry, *Catalysis – Science and Technology, Vol. 1*, (J.R. Anderson and M. Boudart, eds.), Springer–Verlag, Berlin, 1981

8. A.L. Chaffee, I. Campbell and N. Valentine, *Appl. Catal.*, *47*, 1989, 253

9. R.J. Madon and W.F. Taylor, *Hydrocarbon Synthesis*, 1979, 98

10. P.J. Denny and M.V. Twigg, *Catalyst Deactivation 1980*, (B. Delmon and G.F. Froment, eds.), Elsevier Science Publishers B.V., Amsterdam, 1980, 580

11. C.H. Bartholomew and R.M. Bowman, *Appl. Catal.*, *15*, 1985, 59

12. P.K. Agrawal, W.D. Fitzharris and J.R. Katzer, *Catalyst Deactivation 1980*, (B. Delmon and G.F. Froment, eds.), Elsevier Science Publishers B.V., Amsterdam, 1980, 179

13. C.D. Frohning, H. Kolbel, M. Ralek, W. Rottig, F. Schnur and H. Schulz, *Chemierohstoffe aus Kohle*, (J. Falbe, ed.), G. Thieme–Verlaag, 1977, 247

14. R. Hughes, *Deactivation of Catalysts*, Academic Press, Inc. Ltd., London, 1984, 1

15. D.A. Dowden, *Progress in Catalyst Deactivation*, (J.L. Figueiredo, ed.), Martinus Nijhoff Publishers, The Hague, 1982, 283, 298 – 305

16. S.E. Wanke, and P.C. Flynn, *Catal. Rev. – Sci. Eng.*, *12*, *1*, 1975, 93

17. E. Ruckenstein, *Metal–support interactions in Catalysis, Sintering and Redispersion*, Van Nostrand Reinhold Company, New York, 1987, 230 – 236, 239 – 241, 271, 287, 291 – 294, 296

18. C.N. Satterfield, *Heterogeneous Catalysis in Practice*, McGraw–Hill Book Company, New York, 1980, 14, 136 – 141

19. S.L. Kissinger and S. Khang, *Chem. Eng. Sci.*, *44*, *2*, 1989, 418

20. R. Galiasso, R. Blanco, C. Gonzalez and N. Quinteros, *Fuel*, *62*, *7*, 1983, 817

21. H.H. Storch, R.B. Anderson, L.J. Fischer, C.O Hawk, H.C. Anderson and N. Golumbic, *Synthetic Liquid Fuels from Hydrogenation of Carbon Monoxide*, United States Government Printing Office, Washington D.C., 1948, 131–172

CHAPTER 6

THE EFFECT OF EMPLOYING A TWO STAGE SYNTHESIS PROCESS

6.1. Introduction

The results obtained in Chapter 5 suggest that the loss of performance of the catalyst is mainly due to two factors; the poisoning of catalytic active sites by sulphur and the loss of active sites by oxidation and sintering.

By employing a two stage synthesis process as described in Section 4.2., both these effects can be verified. In this two stage synthesis system, two half reactor catalyst beds are linked in series, that is, the tail gas of the first half catalyst bed is fed directly into the inlet of the second half catalyst bed. By doing this, the first half catalyst bed simulates the top half of a full length catalyst bed and the second half catalyst bed simulates the bottom half of the same full length catalyst bed. However, during the synthesis process, water and hydrocarbons are knocked out after the first half catalyst bed. As is already known, poisonous sulphur compounds are trapped only in the top section of the top half of a full length catalyst bed and therefore it should also be removed from the second half catalyst bed.

As both the major contributors to the loss of catalyst performance are removed, the second half catalyst bed is expected to perform much better than the first half. The first and second half catalyst beds will hereafter be referred to as the "first" and "second stage reactors", respectively.

A discussion of the results obtained, which are very similar to those obtained in Chapter 5 follows. These findings will be used to explain and confirm the results obtained. A superior XRD apparatus than that employed to analyze data reported in the Chapter 5 was used. Thus, a more detailed explanation on the phases present in the used catalyst from the two catalyst beds is given.

6.2. Laboratory tests of the catalysts from the two stage synthesis process

6.2.1. Sulphur profiles for the two reactor stages

The immediate question to ask is : how is the sulphur profile of the second stage reactor catalyst bed influenced by employing a two stage synthesis process ? Both a positive and a somewhat negative result was obtained.

The sulphur content of the second stage reactor catalyst bed was drastically reduced, as shown by Figure 6.1.. Excluding the first two readings (see later), the sulphur content throughout the bed is the same as that of the lower section of the first catalyst bed. Overall, the second stage has 95 % less sulphur than the top section in the first stage reactor. This shows clearly that the iron oxide catalyst is a very effective sulphur removing agent. The sulphur content for the top two sections of the catalyst bed of the second stage reactor is unusually high and needs to be explained.

As mentioned in Chapter 3.2.4., sulphur compounds have a tendency to contaminate experimental equipment. Although the pilot plant reactor and associated piping were cleaned thoroughly, it is believed that these two sections of the catalyst bed were contaminated by hydrogen sulphide from the reactor system (from the previous

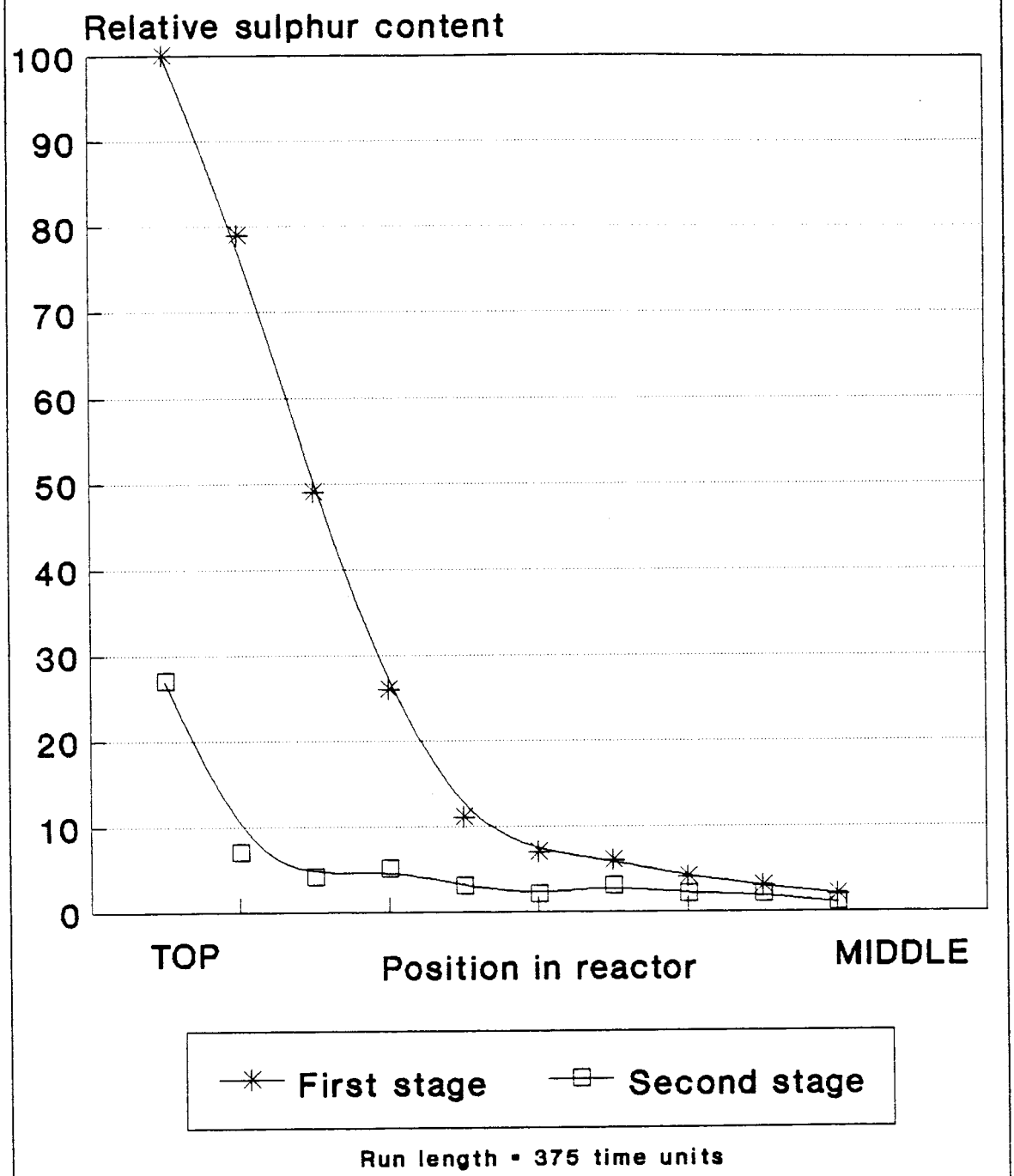

Figure 6.1. Sulphur content through the first and second stage reactor catalysts beds

experiments) and not from the synthesis gas. A further reason why it is believed that an external sulphur source, other than the hydrogen sulphide in the feed gas, existed, is the fact that such low levels of sulphur were present at the bottom section of the first stage reactor and therefore a constant sulphur level is to be expected through out the second stage reactor catalyst bed. Therefore, if the first two points on the sulphur profile of Figure 6.1. for the second stage reactor catalyst bed are removed, it is evident that the sulphur profile throughout the second stage reactor catalyst bed is constant. This is illustrated by Figure 6.2..

6.2.2. Laboratory micro reactor tests

Activity profiles from laboratory micro reactor tests, performed on the catalyst unloaded from the first and second stage pilot plant reactors, are displayed in Figure 6.3.. This figure shows that in general there is a good correlation between the activity of the catalysts and the sulphur content of the individual samples sections (see Figure 6.1.). Low activities are found at the top sections of both stages (which correspond with higher sulphur levels), and vice versa as we travel down the reactor bed.

This figure also shows that the first two points of the second stage have a low activity, but that the activity of the third point is already the same as the one for the most reactive section. This behaviour is strongly related with the sulphur content for the first two points, as shown in Figure 6.1.. We therefore believe that the lower activity for the uppermost two points on the second stage is due to sulphur contamination.

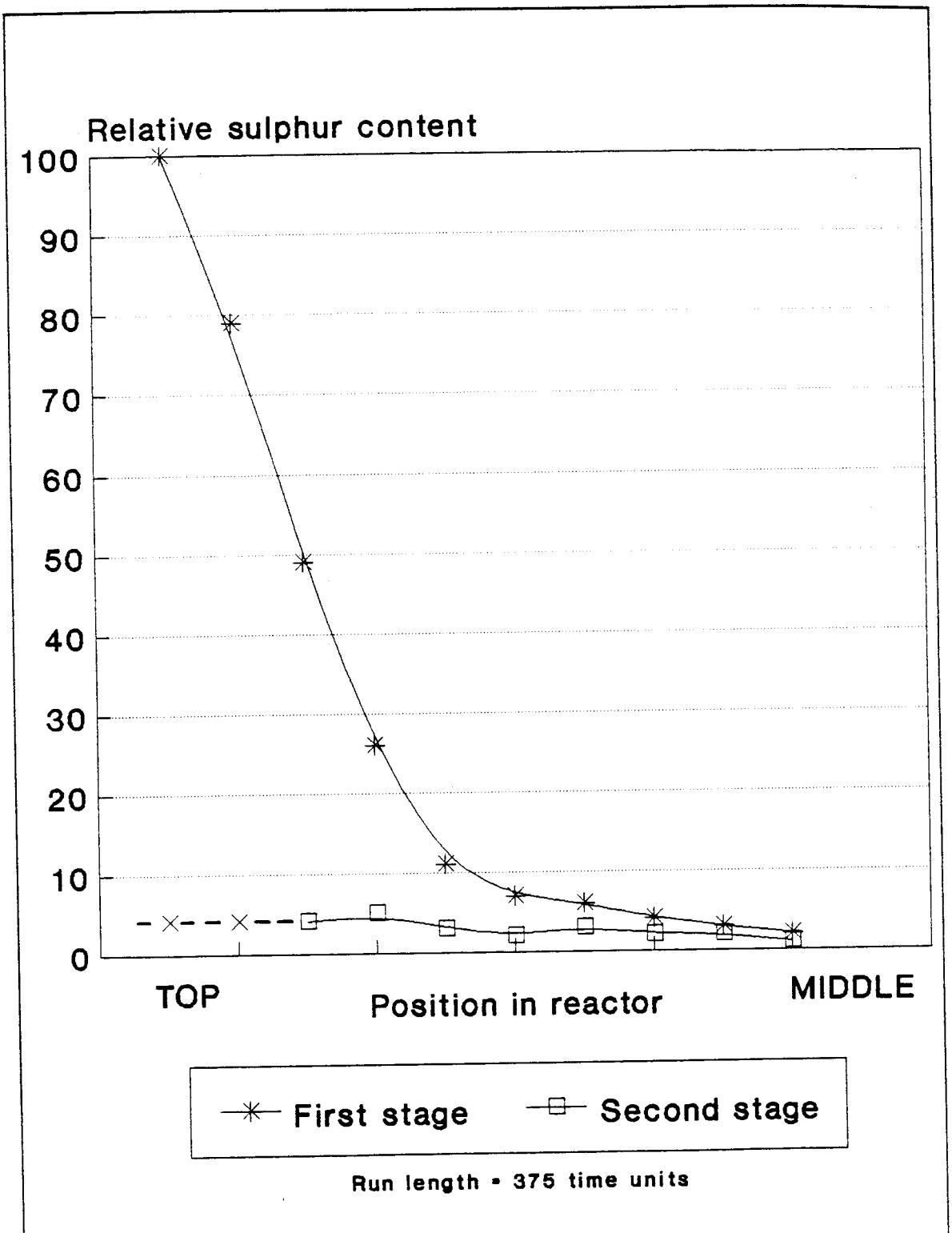

Figure 6.2. Sulphur content through the catalyst bed for the first and adjusted second stage reactors

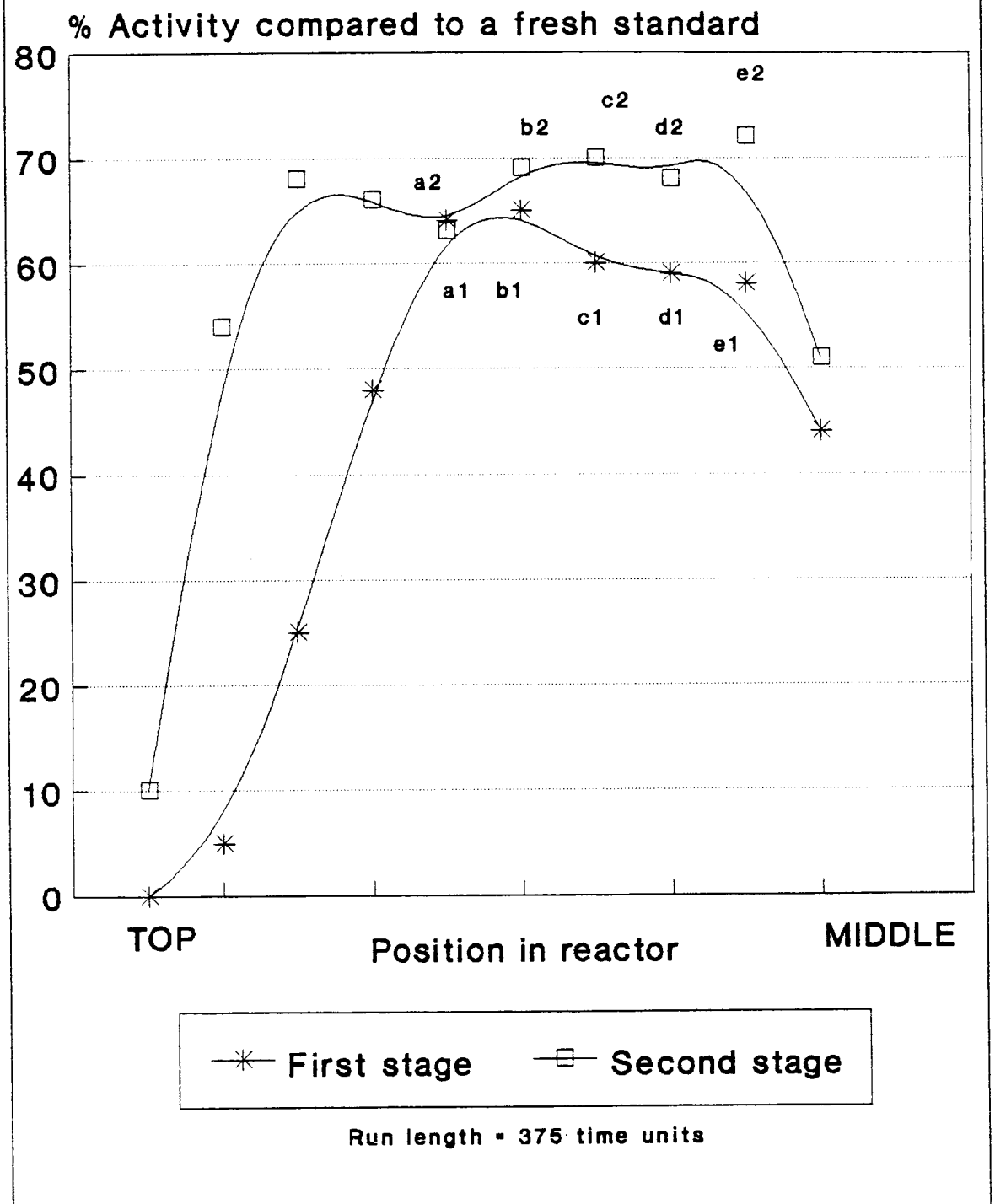

Figure 6.3. Activity profiles through the catalyst bed for the first and second stage reactors

The small difference in activity for the uppermost points of both stages seems odd, considering the big difference in their sulphur levels. This could be explained in terms of the sulphur threshold concept (see Chapter 3.2.3.). That is, if the level of "effective" sulphur contamination is exceeded, no further drastic decrease in activity will occur.

If the sulphur content of the first two sections of the second stage reactor catalyst bed is ignored, due to the reasons presented, an activity–sulphur profile similar to that proposed in Figure 6.4. is expected. Then the activity profiles for the first and second stage reactor catalyst beds would be as shown in Figure 6.5..

A detailed analysis of points "a" to "e" in Figure 6.3. shows two different tendencies. The first stage reactor shows a decline in activity starting with point "a", while for the second stage reactor this decline is delayed until right after point "e". After point "e", both stages show a definite drop in the catalyst activity which starts in the middle section of the catalyst bed (or the bottom of the half filled two stage reactors). We believe that this is not due to experimental error, as this drop is observed for both reactor stages. From our previous experiments (see Chapter 5), it is known that this drop in activity is due to oxidation of the reactive phase to the unreactive oxide phases and to the hydrothermal sintering of the catalyst, which takes place in these regions. Both these problems are present in the first and second stages, and they increase down the catalyst bed, as the partial pressure of water, which is a product of the Fischer–Tropsch reactor increases.

It seems therefore, that in the first stage this kind of deactivation is aggravated by the presence of a higher concentration of sulphur, contributing to an earlier start of the general deactivation pattern and that the effect of water becomes more apparent after point "e" in the catalyst bed.

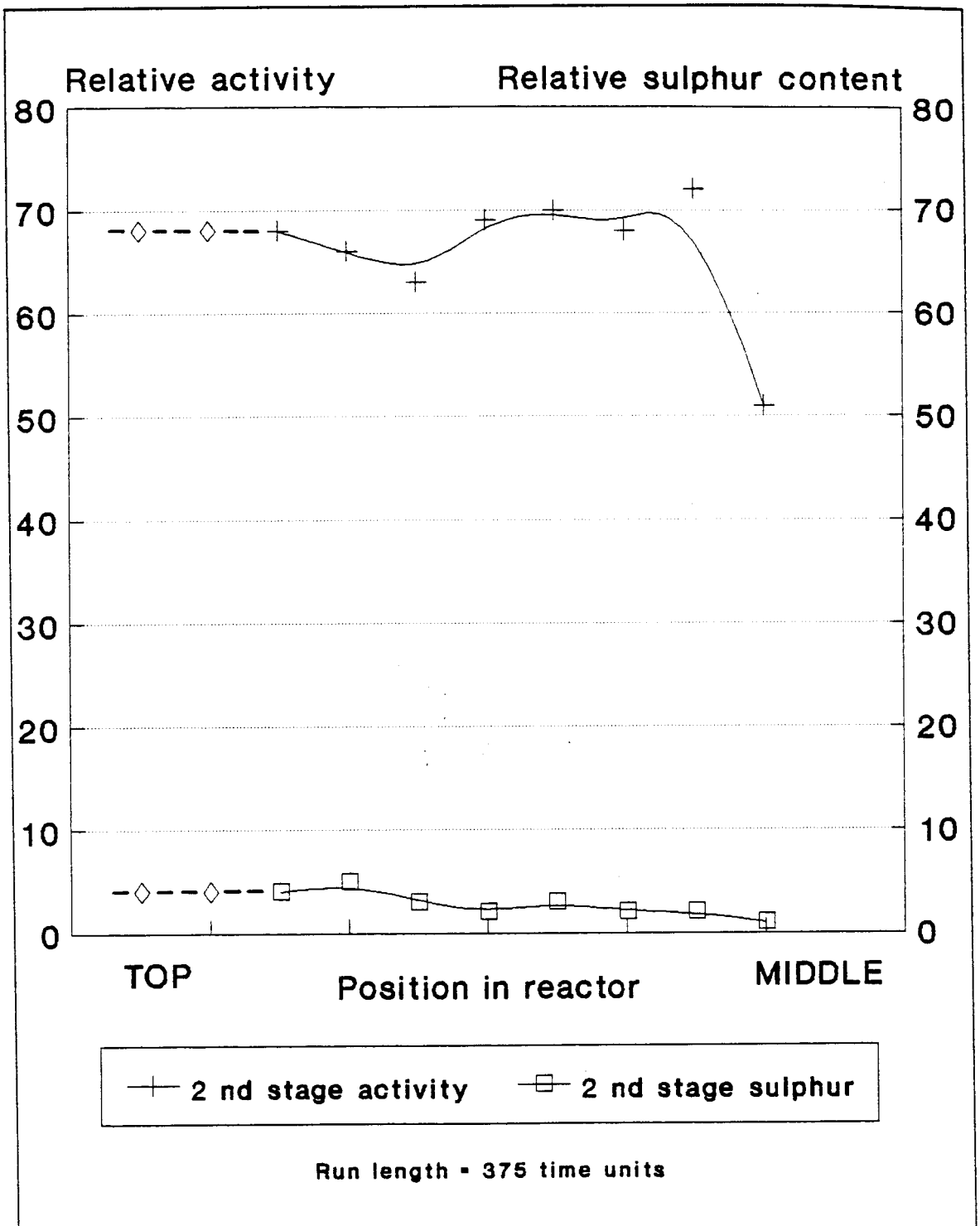

Figure 6.4. The effect of the adjusted sulphur content from the second stage reactor catalyst bed on the adjusted activity profile of the catalyst bed

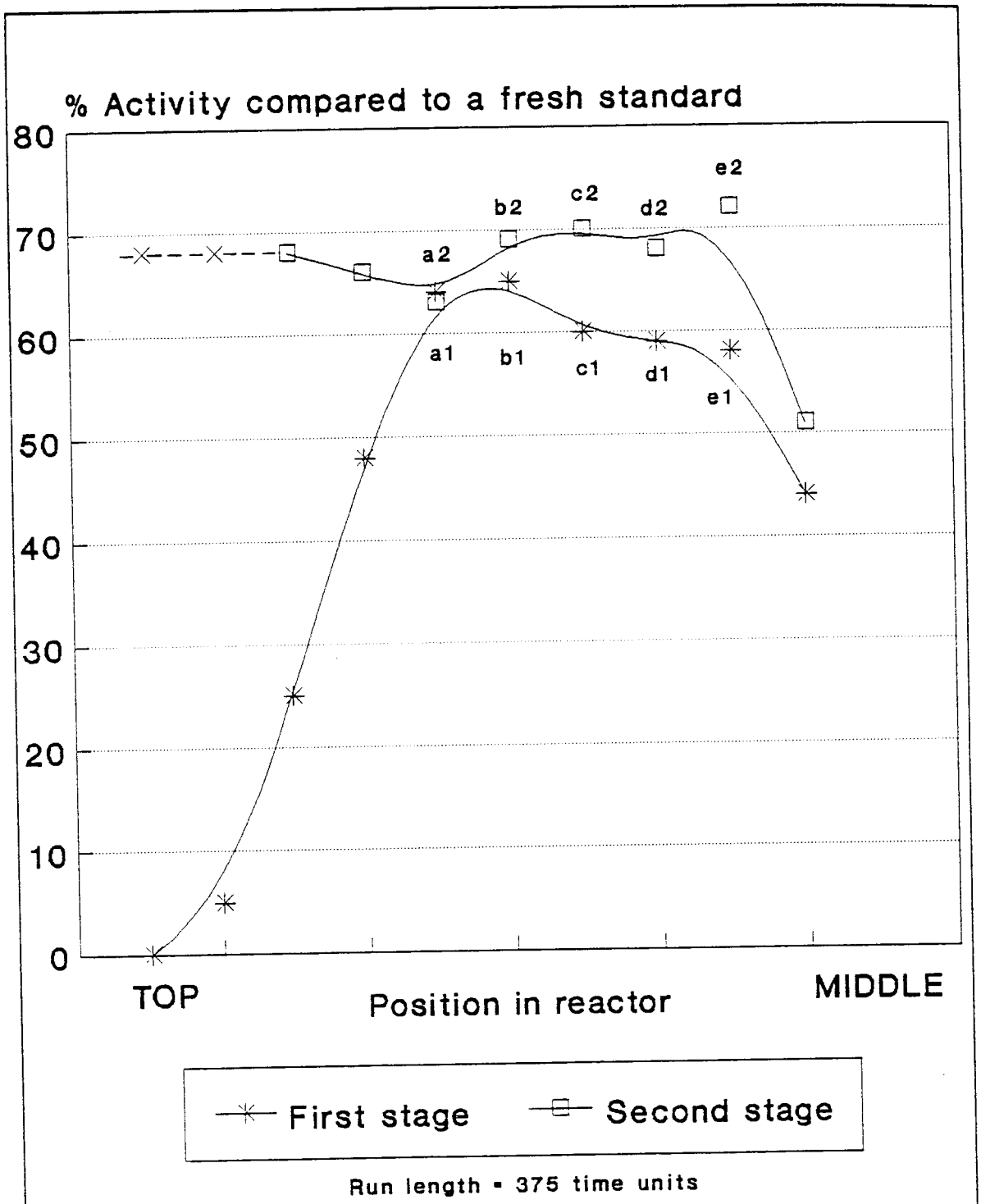

Figure 6.5. Activity profiles through the catalyst bed for the first and adjusted second stage reactors

6.2.3. Carbon content

No remarkable difference is observed for the first and second stage reactor catalyst bed carbon profiles (see Figure 6.6.). Similar to the profiles reported in Chapter 5 (Figure 5.7.), these profiles show a decreasing trend from the top section of the catalyst bed to the middle section of the catalyst bed.

6.2.4. Oxidation and crystallite growth

As already explained in Chapter 5.4.2., water is a product of the Fischer–Tropsch reaction. Water is an oxidizing agent, therefore the extent of the catalyst oxidation is expected to increase down the catalyst bed. This was illustrated in Chapter 5 (see Figure 5.13.) for the full loaded reactor. Here, and as expected, this effect is also present for both half stage reactors (see Figure 6.7.).

Again, we will use this result to help explain the loss of activity in the lower section of the reactor. In the top section of the reactor, the sulphur overshadows any negative effect of the catalyst oxidation on the activity. This is followed by a relative "flat" region (points "a" to "e" in Figures 6.3. to 6.5.), after which the slope for the decay in conversion increases. In view of this, we believe that the amount of magnetite in the upper regions of the catalyst bed is insufficient to cause a noticeable decrease in the activity of the catalyst.

As we approach the middle section of the reactor, i.e. after the most reactive section of the catalyst bed, the ever increasing concentration of magnetite begins to affect the activity in a noticeable and increasing manner (see Figures 5.13. and 6.5.).

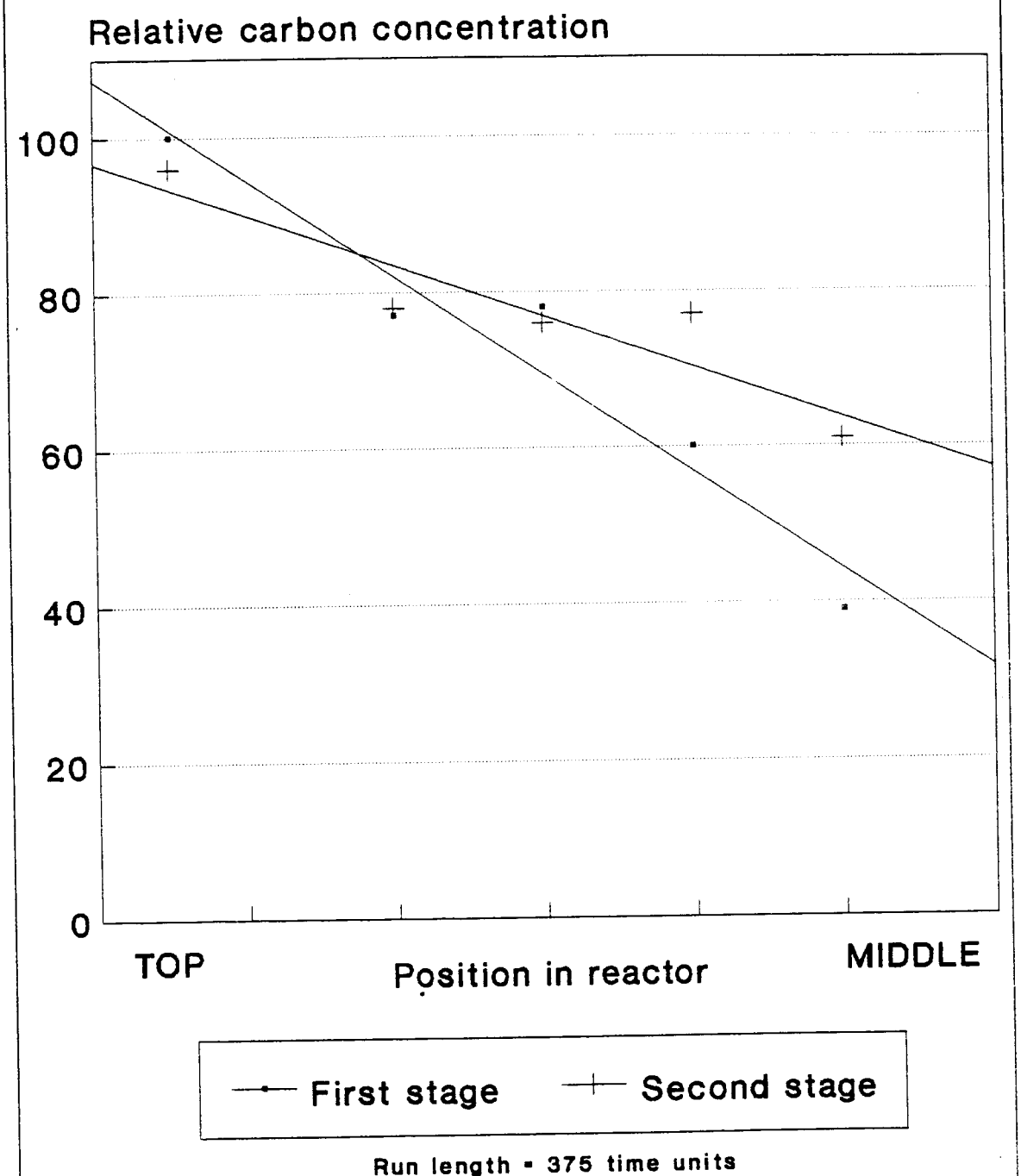

Figure 6.6. Carbon content for the first and second stage reactor catalyst bed sections

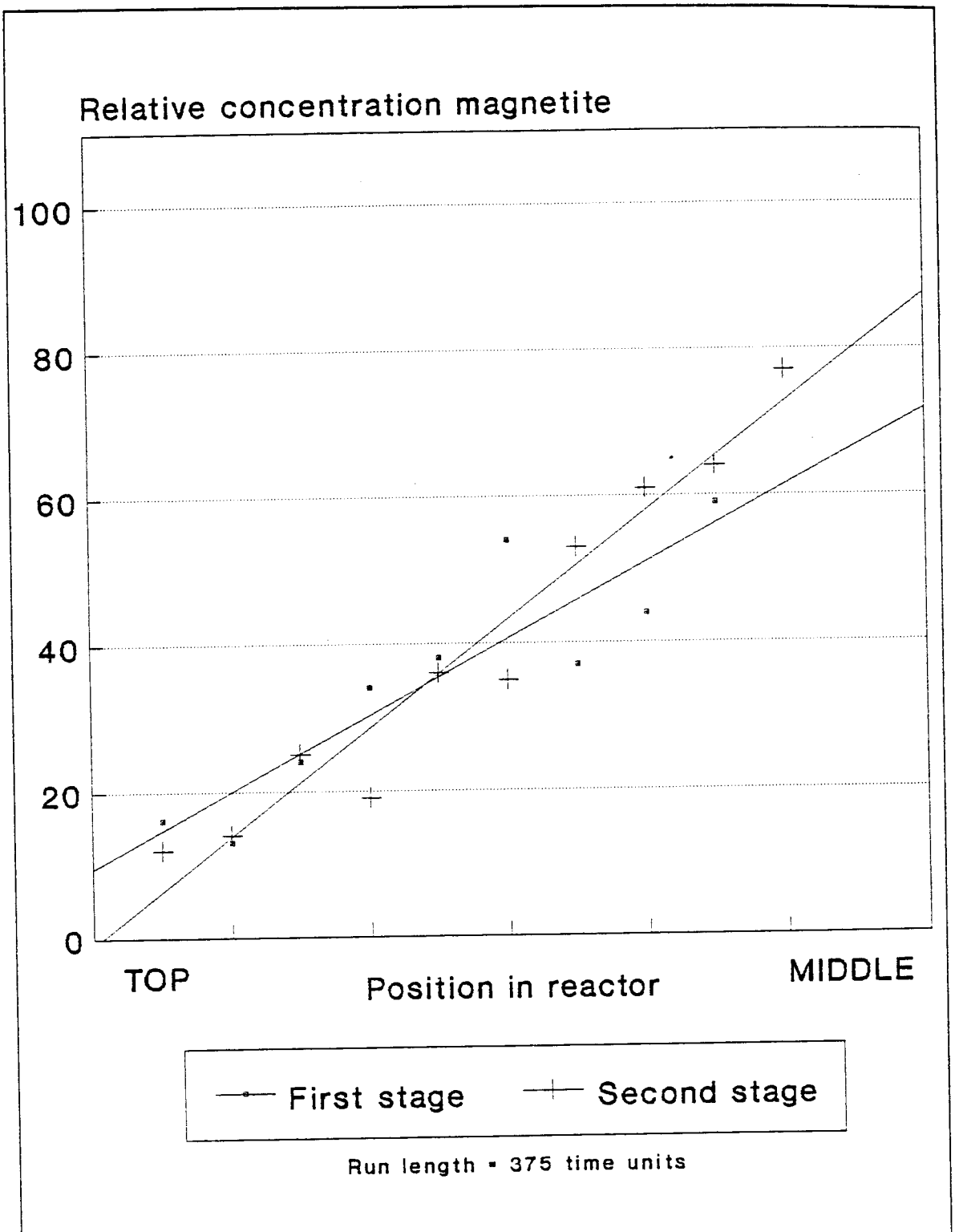

Figure 6.7. Magnetite concentration for the first and second stage reactor catalyst bed sections

Kölbel and Engelhard[1] reported that the effect of oxidation is to be expected to show more clearly just below the most reactive section of the catalyst bed.

Additionally, as already shown in Chapter 5 (Figure 5.13.), for the fully loaded reactor, water is expected to promote the growth of the iron crystallites (sintering).

The effect of hydrothermal sintering on the catalysts samples from both stages is clearly illustrated in Figures 6.8. and 6.9.. Figure 6.8. shows a gradual increase in the magnetite crystallite size (for both stages) as we move down the catalyst bed. This confirms the results obtained for the fully loaded reactor and will contribute to the global loss in activity. Furthermore, the B.E.T. surface area of the two reactor stages catalyst beds is illustrated in Figure 6.9., and show a decrease with catalyst reactor position. Surface area loss must therefore contribute to the loss of activity.

6.2.5. Pore volume

Similarly to what we reported in Chapter 5, the pore volume of the catalysts from both reactor stages, showed an increase down the catalyst bed. This is illustrated in Figure 6.10..

6.2.6. XRD phase analysis

XRD phase analysis for the different sections of both stages showed, as expected, similar results to those obtained in Chapter 5 (for the full catalyst bed).

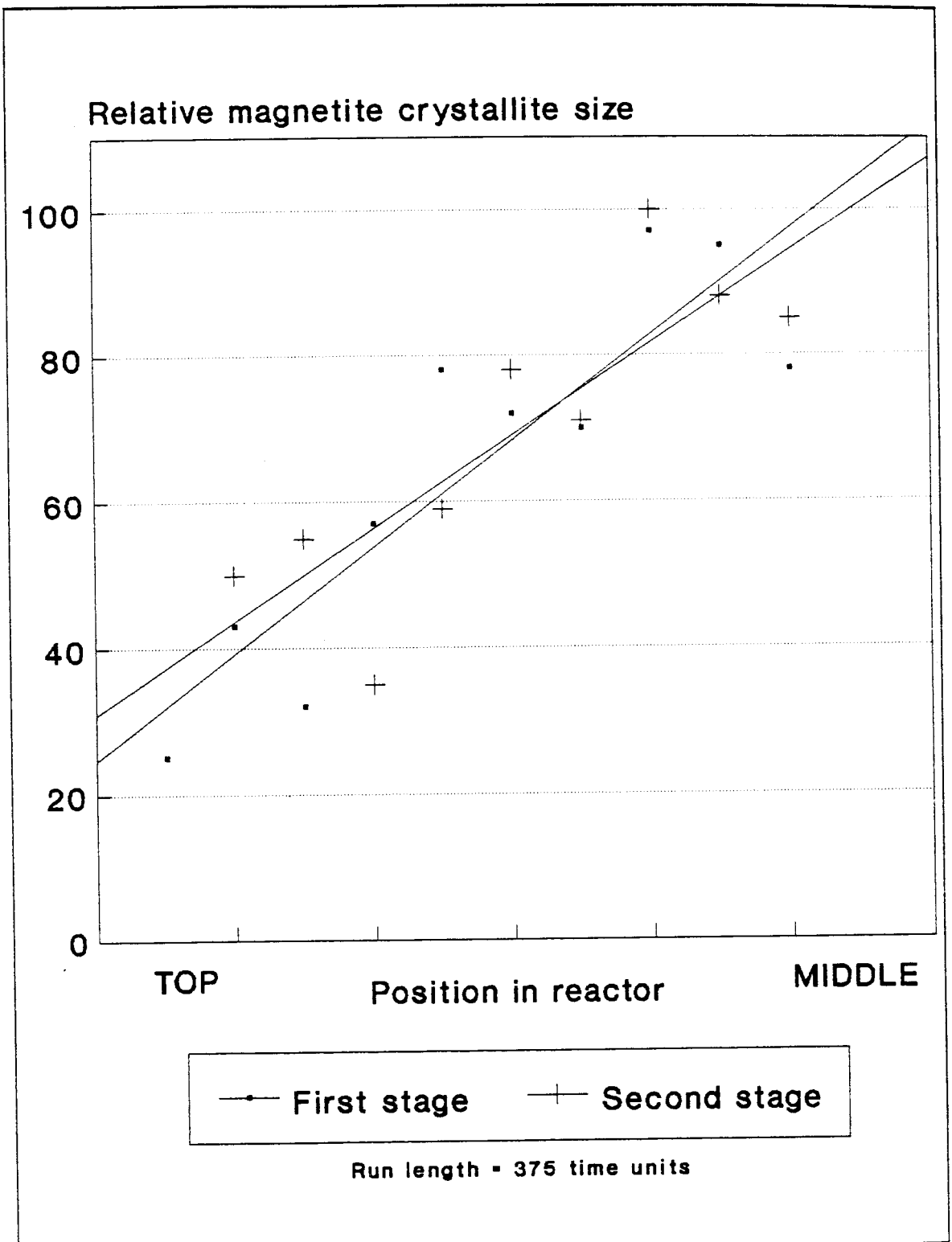

Figure 6.8. Magnetite crystallite size for the first and second stage reactor catalyst bed sections

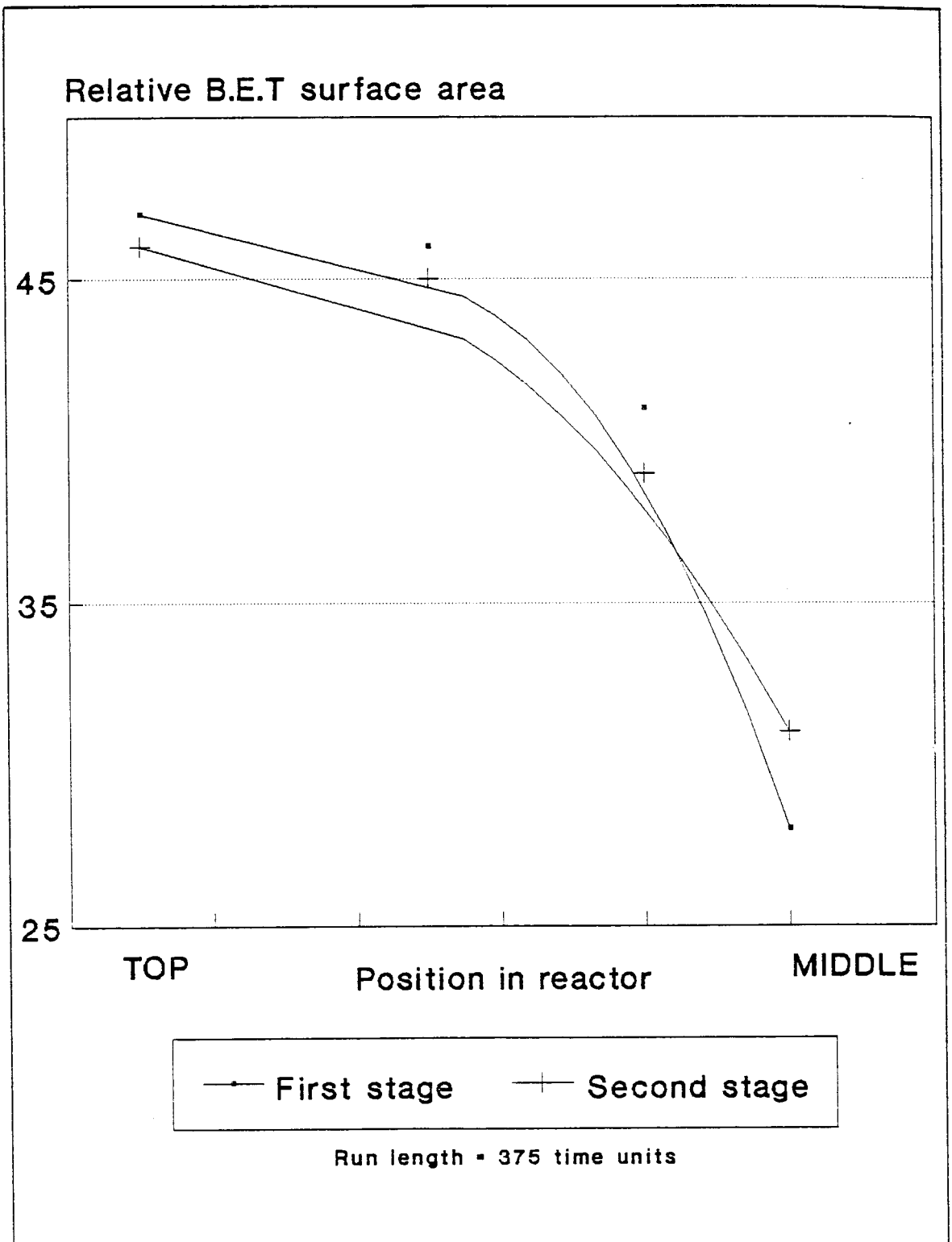

Figure 6.9. B.E.T. surface area for the first and second stage reactor catalyst bed sections

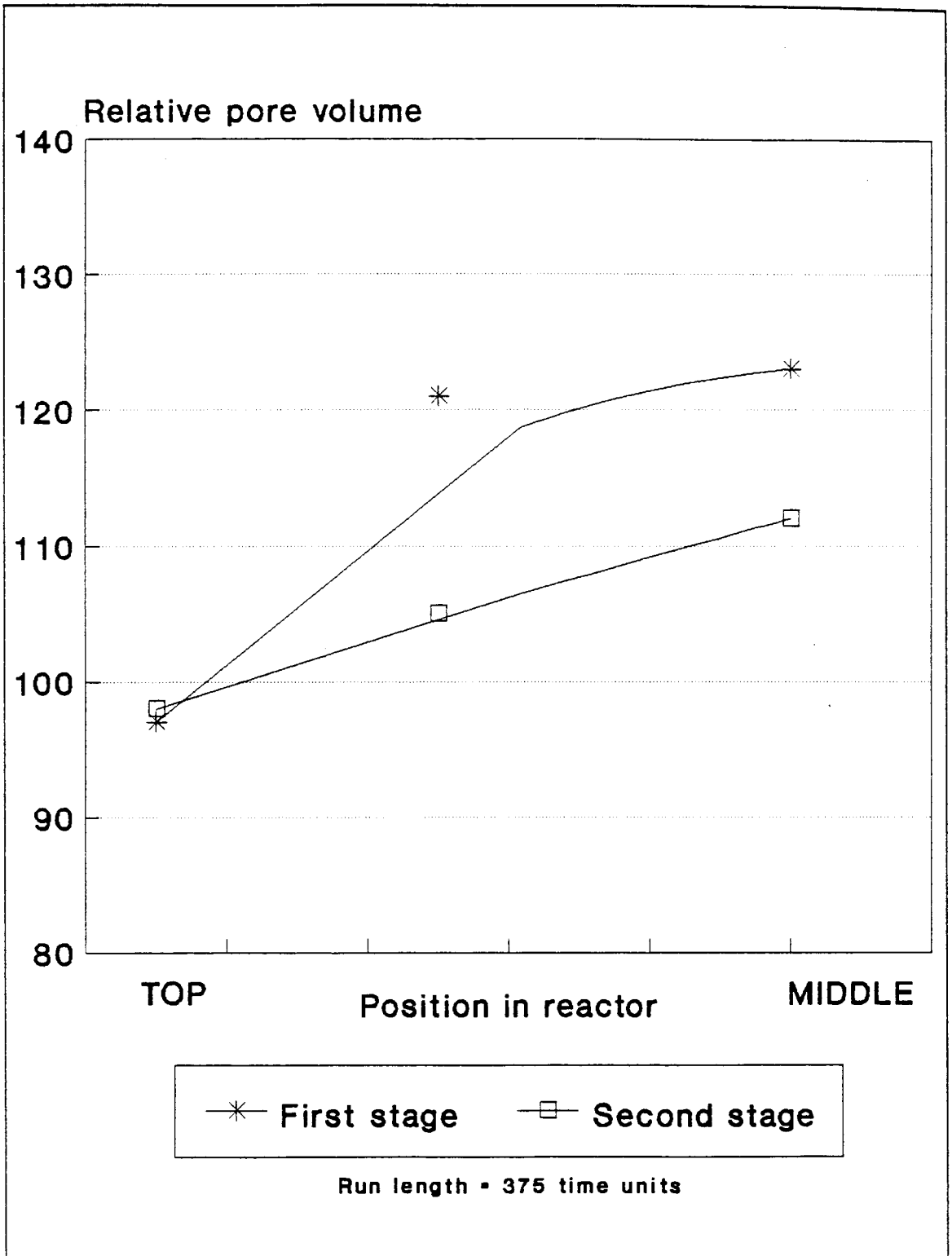

Figure 6.10. Pore volume for the first and second stage reactor catalyst bed sections

Figures 6.11. to 6.14. show the XRD analysis for the different sections of the catalyst bed of the second stage, while Figure 6.15. shows the same information for the first stage reactor.

Before discussing the XRD data, it is necessary to clarify the presence of the Fe_2O_3 phase in the top caption of the figures. The oxide phase as observed by the X–ray diffraction analysis, is γ–Fe_2O_3, maghemite. Maghemite is crystallographically related to magnetite. Both these phases have a cubic structure, but with different lattice spacings. Maghemite has a lattice constant of 8,35 A while magnetite's lattice constant is 8,40 A. Using photographic techniques, these two structures are easily confused, due to their similar diffraction patterns[2]. Therefore, due to the fact that this phase is not identified as maghemite with certainty, it should be assumed that it is the more commonly known magnetite phase. But, it should be kept in mind that the maghemite phase may exist in the used iron catalyst.

From Figures 6.11. to 6.14., it is evident that :

(i) Hägg's carbide is present in all the sections of the catalyst bed.

(ii) Magnetite (as discussed above) is hardly detected in the top section, but keeps increasing, until it becomes the predominant phase in the bottom section of the catalyst bed. This trend is shown more clearly in Figure 6.16.. As mentioned before, this behaviour is to be expected due to the increasing amounts of water as we travel down the reactor bed.

(iii) From the middle section downwards, a second carbide phase (sementite, Fe_3C) appears (see Figure 6.14.), although it shows no definite trend with the axial position in the catalyst bed.

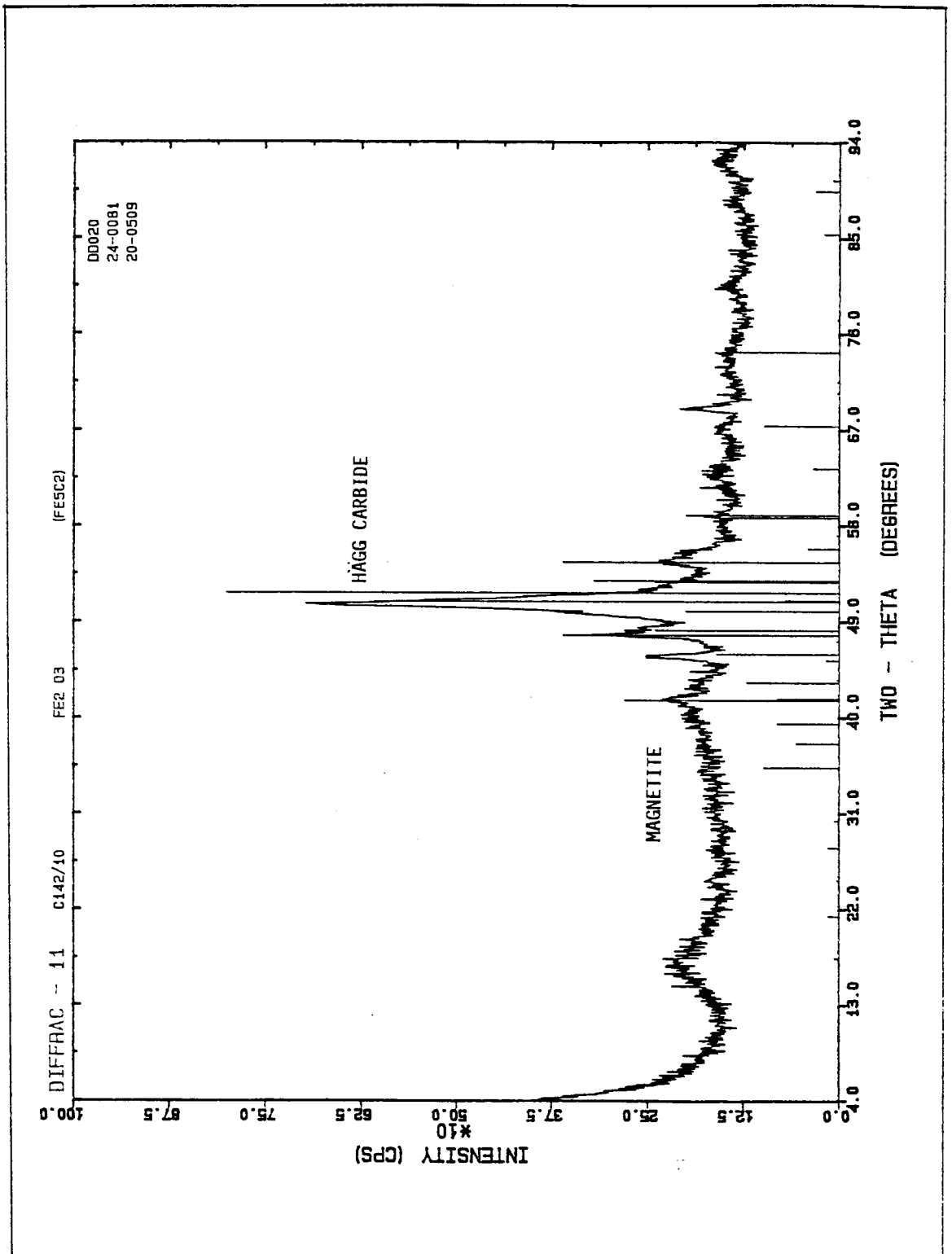

Figure 6.11. XRD phase analysis of the top section of the catalyst bed

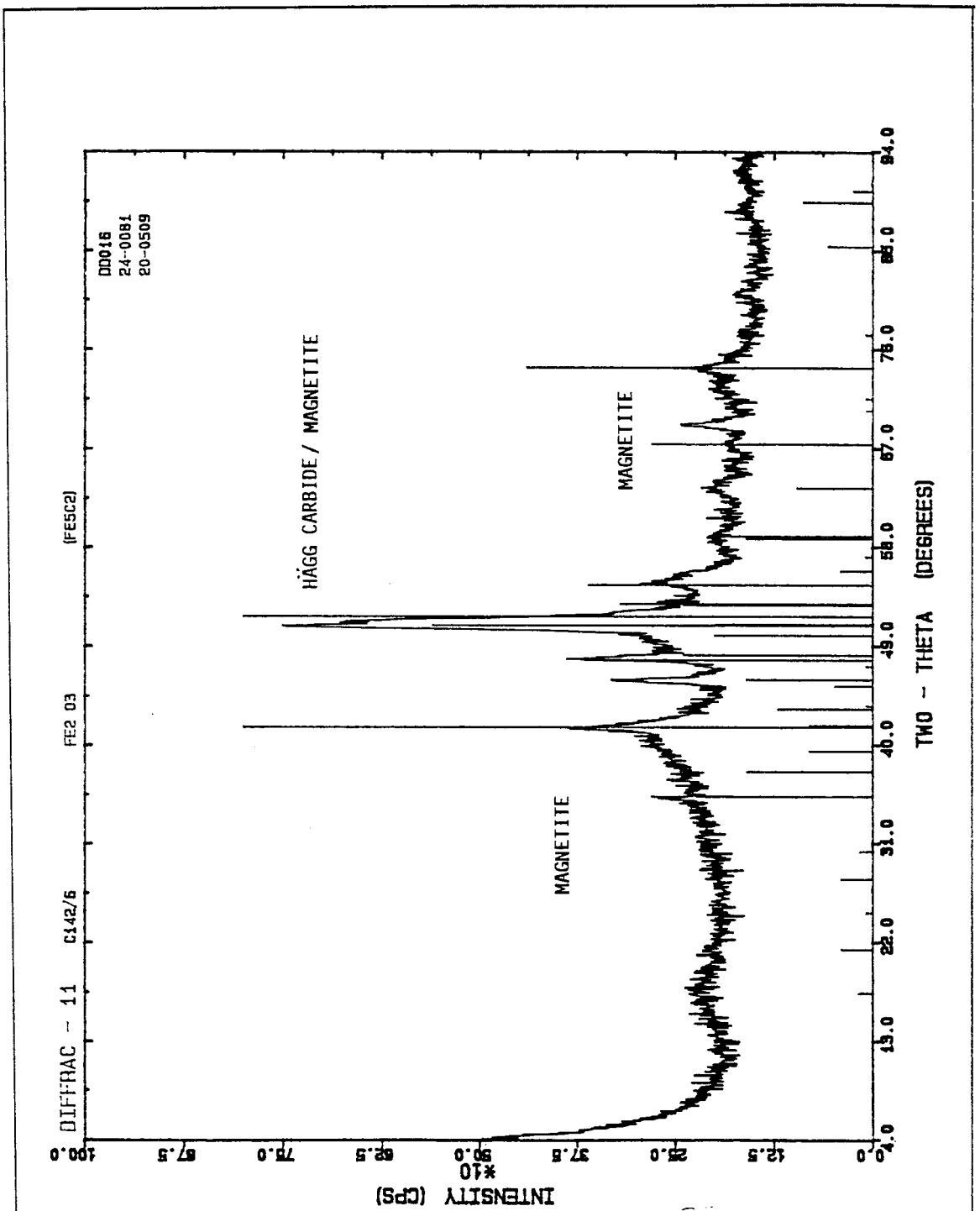

Figure 6.12. XRD phase analysis of $^{2}/_{5}$ from the top of the catalyst bed

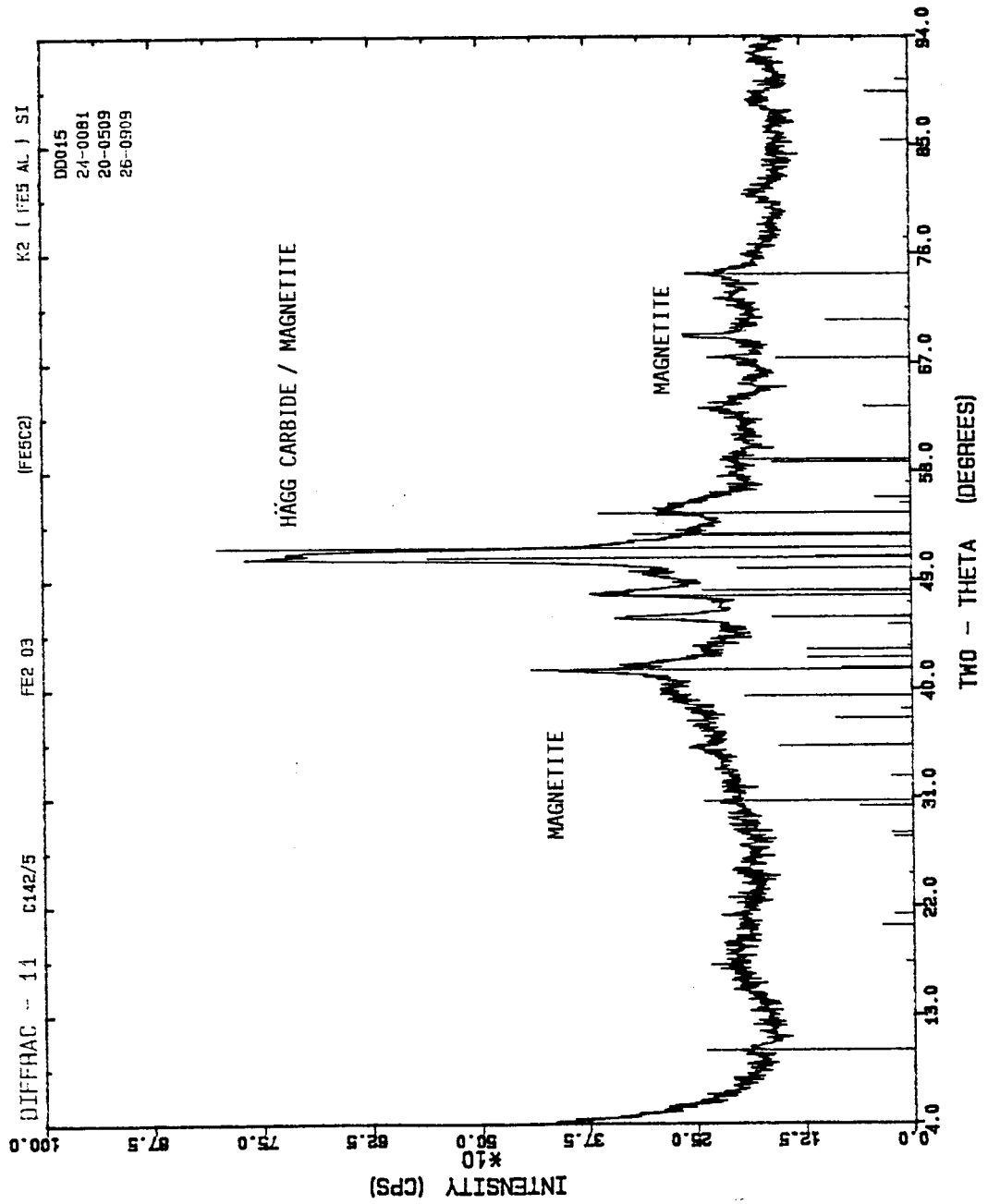

Figure 6.13. XRD phase analysis of the section $^{2}/_{5}$ from the middle of the catalyst bed

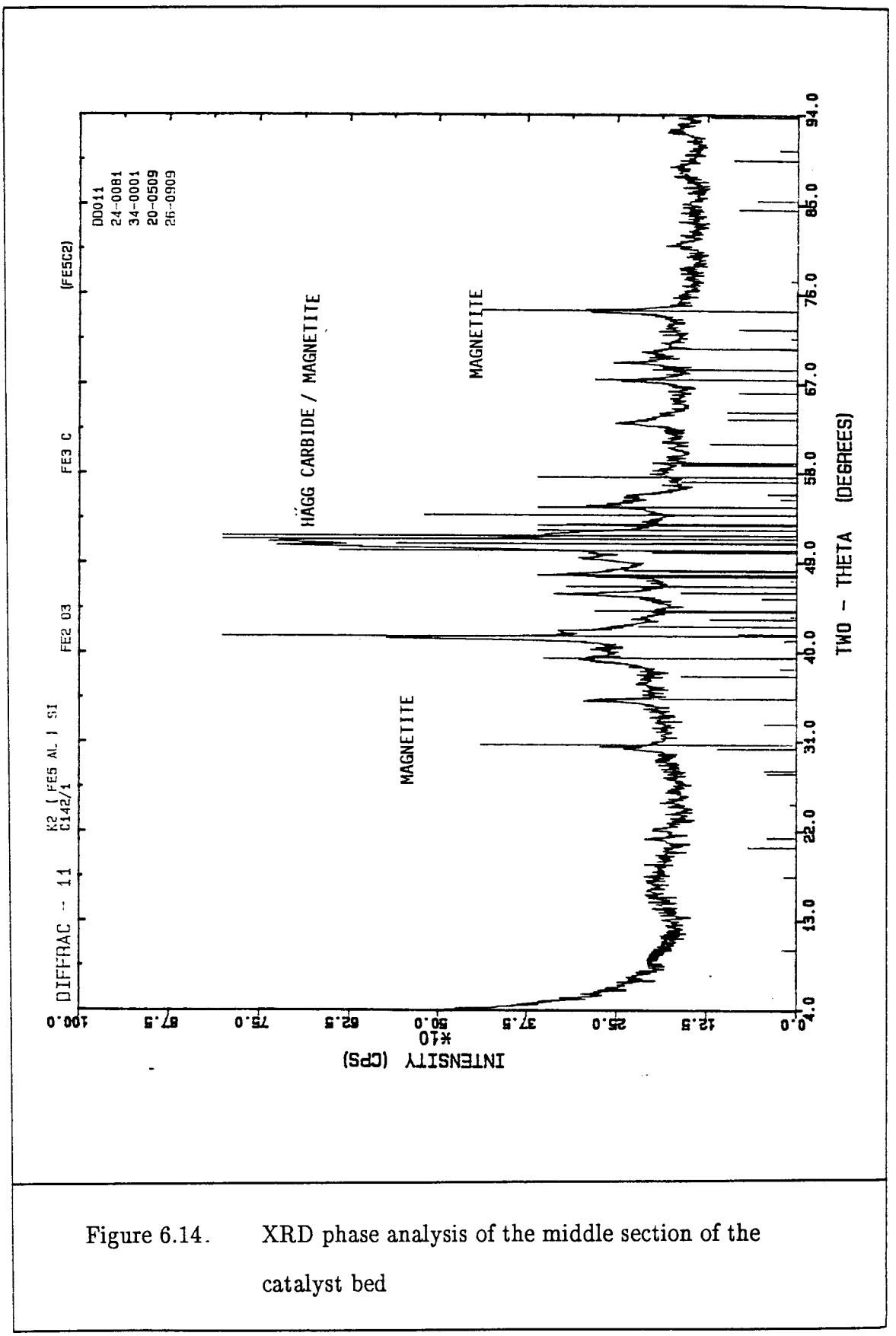

Figure 6.14. XRD phase analysis of the middle section of the catalyst bed

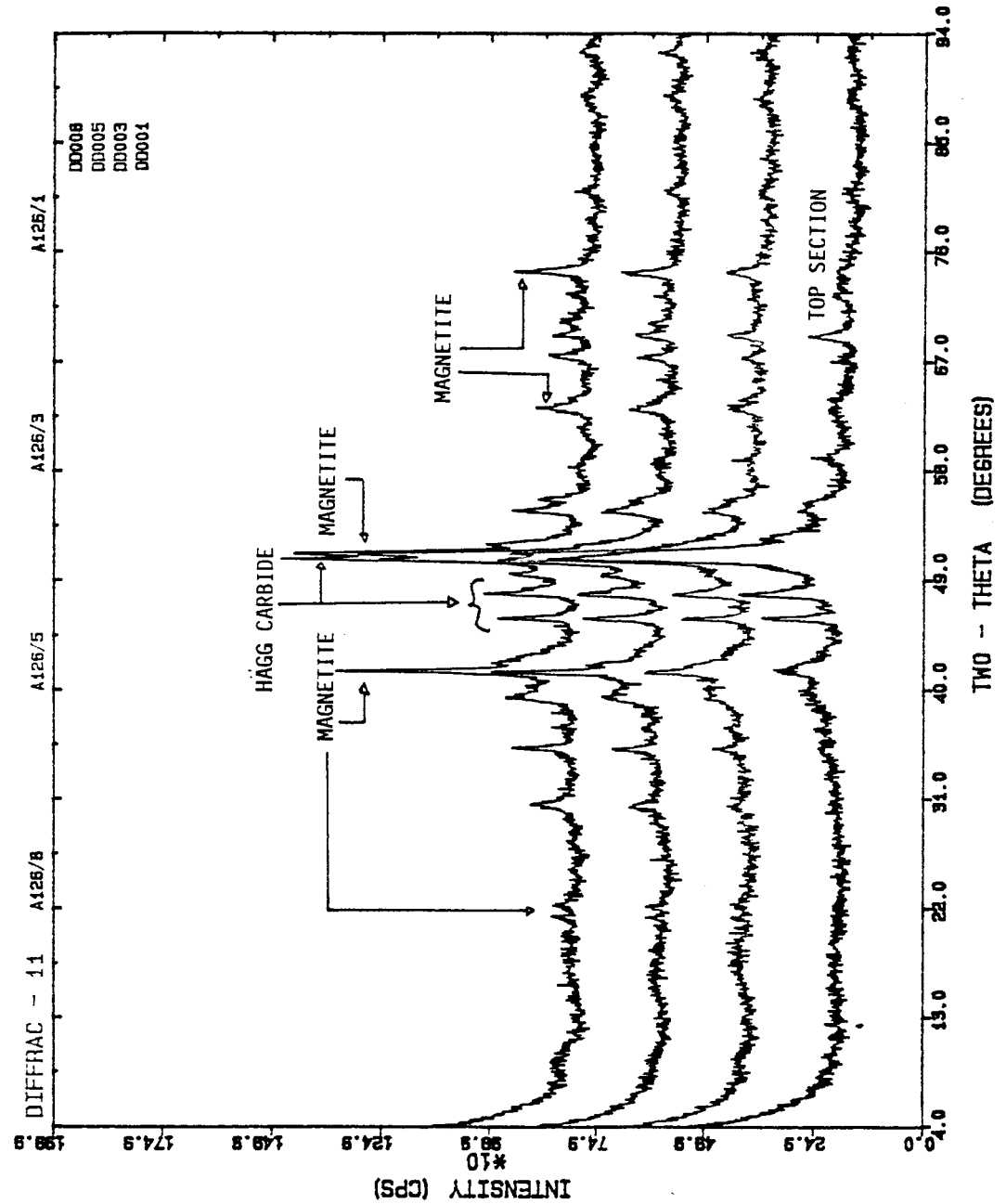

Figure 6.15. Phase changes through the first stage reactor catalyst bed

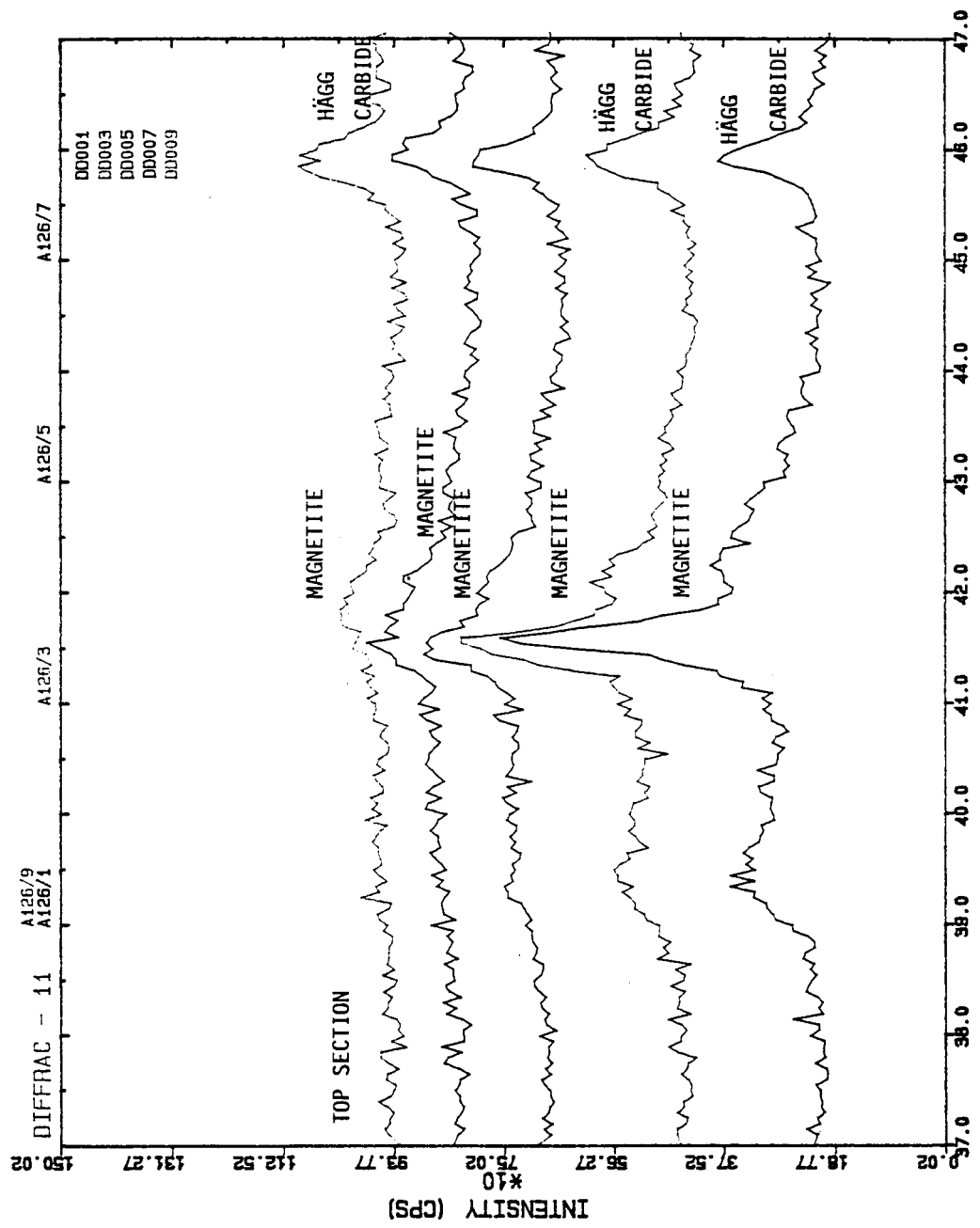

Figure 6.16. Change in magnetite concentration through the catalyst bed

6.3. References

1. H. Kölbel and F. Engelhard, *Erdöl und Kohle, 3, 11*, 1950, 529

2. H.H. Storch, R.B. Anderson, L.J. Fischer, C.O Hawk, H.C. Anderson and N. Golumbic, *Synthetic Liquid Fuels from Hydrogenation of Carbon Monoxide*, United States Government Printing Office, Washington D.C., 1948, 131–172

CHAPTER 7

SCANNING ELECTRON MICROSCOPY AND SECONDARY ION MASS SPECTROMETRY ANALYSIS

7.1. Introduction

Analysis of catalysts taken from a fixed bed reactor[1] clearly illustrated (see Chapters 5 and 6) that poisoning of the top section of the catalyst bed, and increased oxidation and sintering of the remaining part of the catalyst bed downwards, takes place on a low temperature Fischer–Tropsch iron catalyst. The purpose of this chapter is to illustrate how these phenomena may be identified, making use of Scanning Electron Microscopy (SEM)[2,3] and Secondary Ion Mass Spectrometry analysis (SIMS)[2] techniques. The purpose of this chapter is not to do a detailed study, but rather to show how these techniques could be used to identify phenomena like catalyst poisoning[4,5] and catalyst crystallite growth[6,7] (also known as sintering).

The SEM technique was used to obtain visual information of the used catalyst from the fixed bed reactor, therefore physically revealing, the changes taking place within the catalyst pellet during hydrocarbon synthesis. The SIMS technique was also used as it has powerful chemical analysis capabilities, much more sensitive than those of the SEM. Compounds like sulphur can be detected at very low concentrations.

From Chapters 5 and 6 it is known that :

(i) poisoning takes place only in the top section of the catalyst bed,

(ii) sintering progressively increases down the catalyst bed, and

(iii) both these phenomena were observed and identified in the top half of a fixed bed reactor catalyst bed.

Only the samples from the first stage reactor catalyst bed (see Chapter 6) were used for the SEM and SIMS analysis. The SIMS analysis was used mainly to confirm the presence of sulphur contaminants in the top section of the catalyst bed and to support the findings made with the SEM.

7.2. SEM characteristics of an used iron catalyst pellet

Figures 7.1. to 7.4. display four catalyst pellets which are representative of

(i) a reduced, but unused catalyst (Figure 7.1.),

(ii) an used catalyst sample from the top section from a catalyst bed (Figure 7.2.),

(iii) one quarter from the top of the catalyst bed (Figure 7.3.) and

(iv) the middle section (Figure 7.4.) of the catalyst bed.

The reduced unused catalyst pellet (Figure 7.1.) displays a smooth surface with the presence of fine cracks which might have resulted from the reduction process. SEM–EDAX analysis of the surface shows a homogeneous distribution of the catalyst active phase (iron).

Figure 7.2., as expected, displays a totally different picture. Here, the following characteristic features are identified :

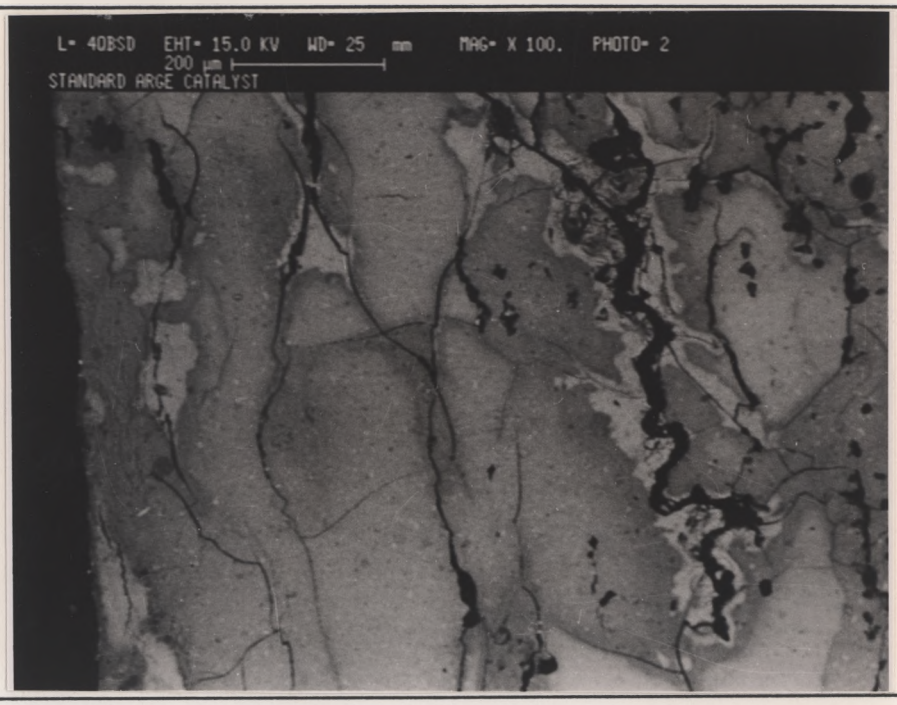

Figure 7.1. SEM photo of a reduced unused catalyst (MAG = x 100)

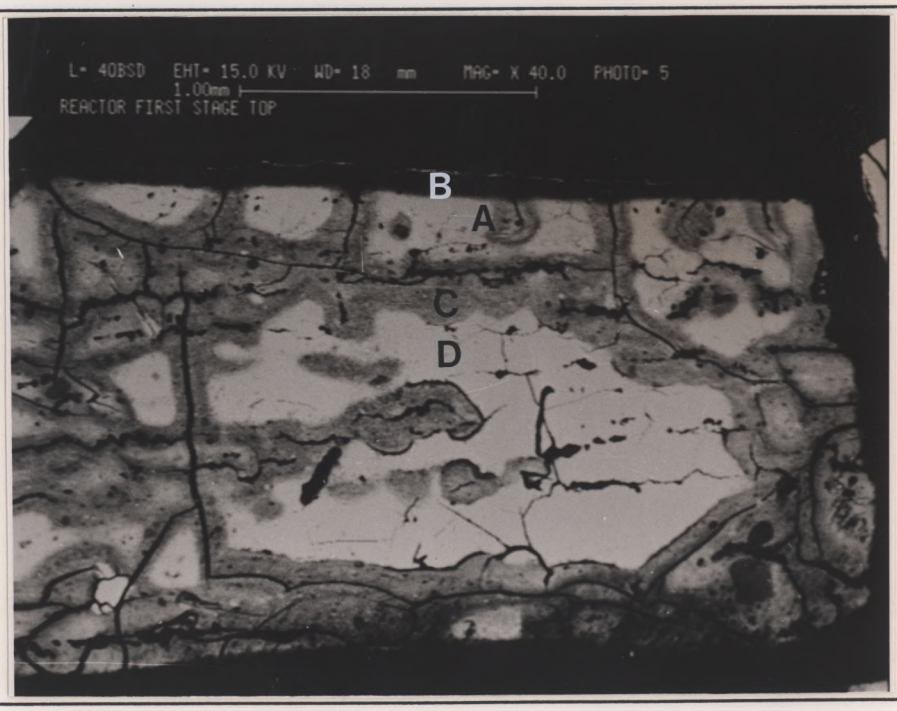

Figure 7.2. SEM photo of a used catalyst from the top section of a fixed bed reactor catalyst bed (MAG = x 40)

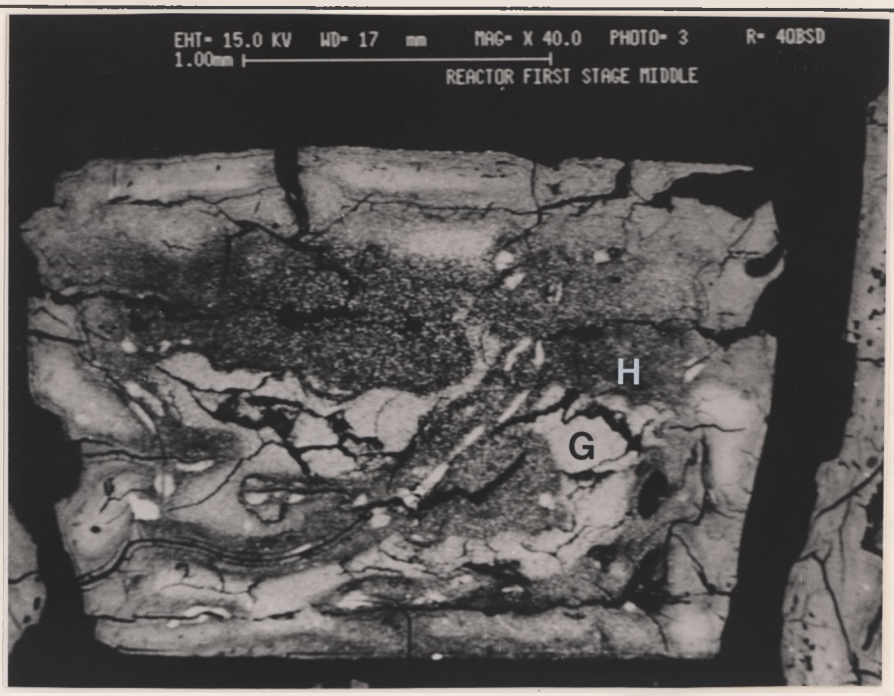

Figure 7.3. SEM photo of a used catalyst from one quarter from the top of the catalyst bed (MAG = x 40)

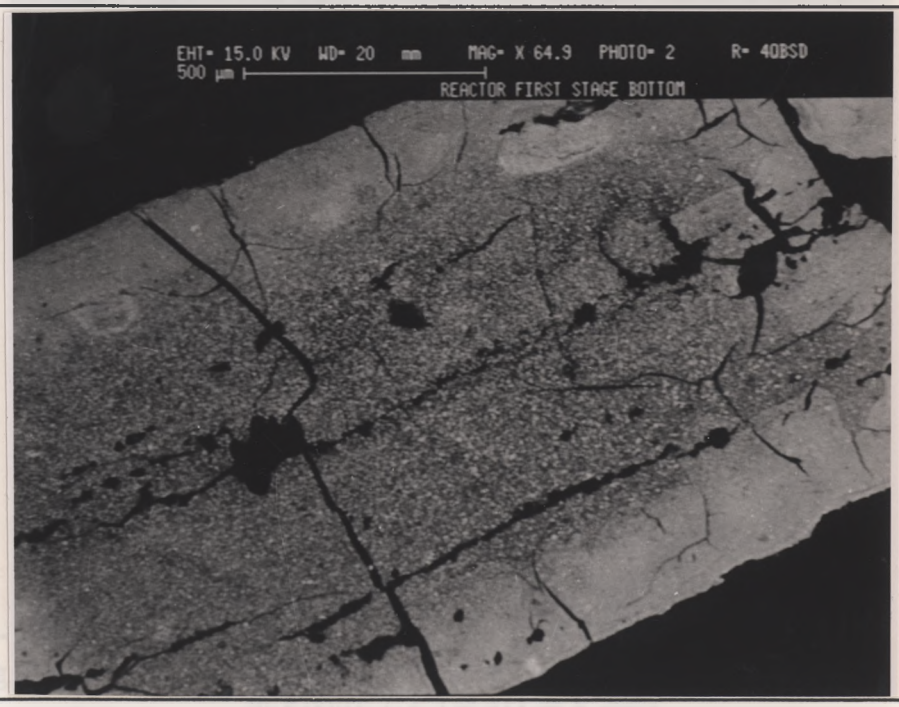

Figure 7.4. SEM photo of a used catalyst from the middle section of a fixed bed reactor catalyst bed (MAG = x 40)

1. a thin brighter outer rim,
2. a black outer rim,
3. grey areas – mostly along cracks leading to the interior of the pellet,
4. bright areas – mostly the catalyst interior and
5. more pronounced cracks than in Figure 7.1..

Figure 7.5. is a further enlargement (MAG x 200) of the "inkpot", a grey area marked "A" on Figure 7.2.. Enlarging the tip (MAG x 2000), marked "B" in Figure 7.5., resulted in Figure 7.6.. As this is next to the bright outer rim, a SEM–EDAX analysis was performed to characterize this bright region. As expected, sulphur was detected. This sulphur compound is believed to be iron sulphide. This is shown in Figure 7.7..

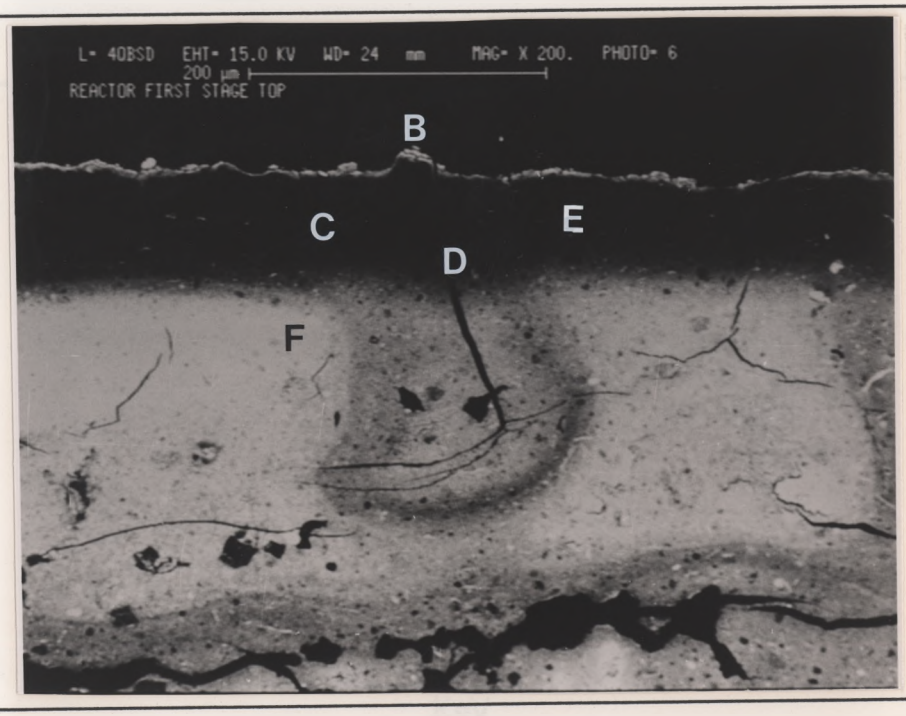

Figure 7.5. Enlargement of "inkpot", a grey area marked A in Figure 7.2. (MAG = x 200)

Figure 7.6. Enlargement of "tip", a black area marked B in Figure 7.5. (MAG = x 2000)

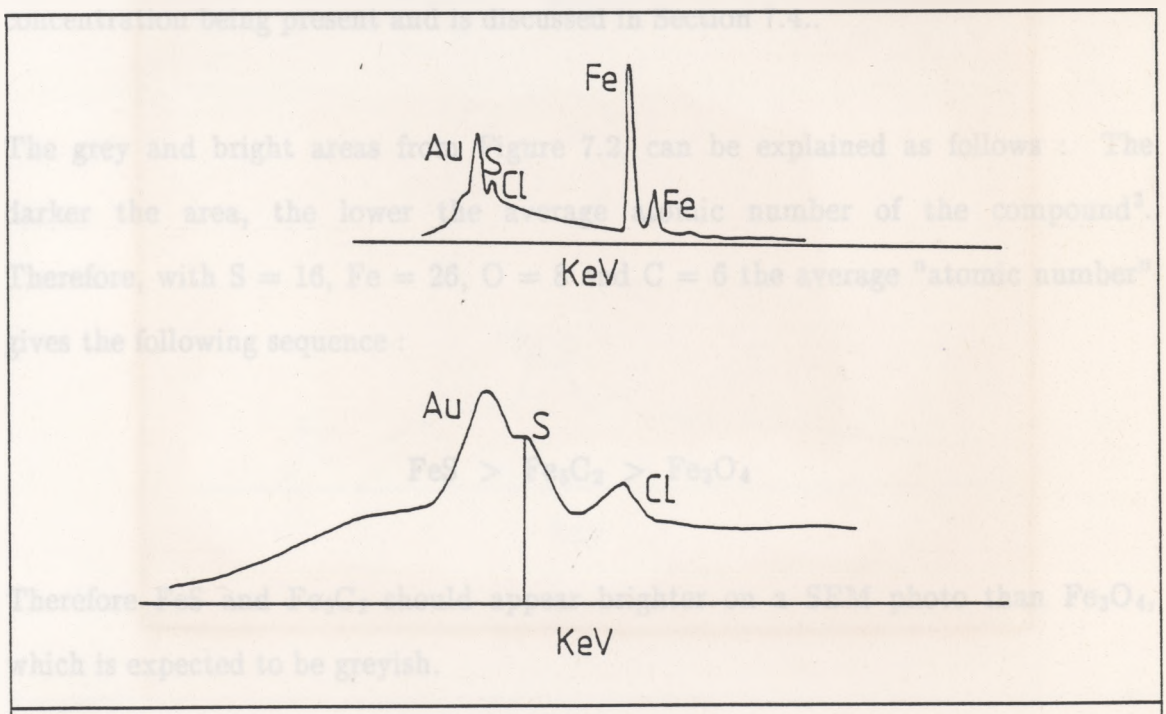

Figure 7.7. SEM–EDAX analysis within the black area as displayed in Figure 7.6.

* SEM–EDAX not operated in the window less mode. Therefore no oxygen detected.

It should be noted, that the sulphur peak is displayed as a shoulder in the gold peak, which is used as a conductor to improve the visual display of this catalyst, which is a poor conductor. When carbon was used as conductor, it did not improve the image of the catalyst sufficiently to get a good picture. Nevertheless, it is believed that the presence of sulphur is shown clearly as is also shown in Figure 7.8. for areas C, D and E of Figure 7.5.. Furthermore, it should be remembered that the sulphur analyzed in this section of the catalyst bed is present in very low concentrations and that the SEM–EDAX set–up has sensitivity problems in giving a clear chemical analysis at these low levels. Finally, no sulphur could be detected in the catalyst pellets shown in Figures 7.3. and 7.4.. This is in line with the results reported by Chaffee et al.[3] making use of SEM and XPS techniques for a similar catalyst system.

SIMS analysis of these catalyst pellets showed the same trends in sulphur concentration being present and is discussed in Section 7.4..

The grey and bright areas from Figure 7.2. can be explained as follows : The darker the area, the lower the average atomic number of the compound[3]. Therefore, with S = 16, Fe = 26, O = 8 and C = 6 the average "atomic number" gives the following sequence :

$$FeS > Fe_5C_2 > Fe_3O_4$$

Therefore FeS and Fe_5C_2 should appear brighter on a SEM photo than Fe_3O_4, which is expected to be greyish.

If Figure 7.2. is evaluated, using the above mentioned assumption, the following conclusions can be made :

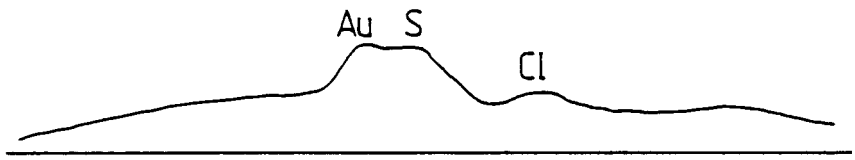

C

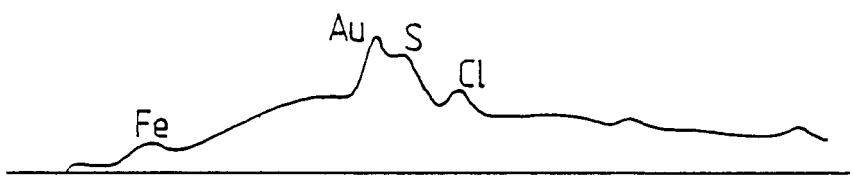

D

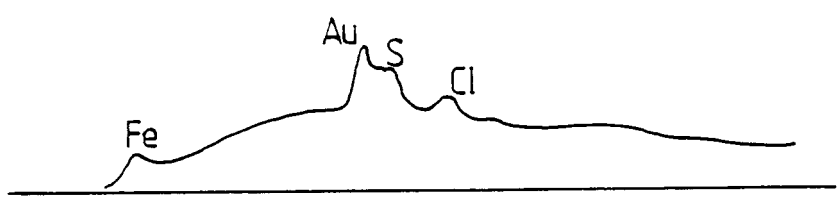

E

Figure 7.8. SEM–EDAX analysis within the black area, marked as C, D and E in Figure 7.5.

SEM–EDAX not operated in the window less mode. Therefore no oxygen detected.

1. The bright outer layer is iron sulphide, as has already been shown by the SEM–EDAX analysis of this area.
2. The larger bright area in the interior of the catalyst appears to be iron carbides (see discussion that follows).
3. The grey areas along the cracks appear to be iron oxides (It should be noted that the grey areas in Figure 7.2. are mostly found along the cracks within the catalyst pellet and that these cracks mostly lead from the outer surface to the interior of the catalyst.).

However, it is known[1] that when the synthesis gas (during the Fischer–Tropsch reaction) diffuses into the catalyst pellet, which is porous, the consumed H_2 and CO produces H_2O and CO_2. This therefore implies that the "reducing" synthesis gas (2H:1CO) progressively becomes more oxidizing as it penetrates into the catalyst.

Taking this into consideration, the former phase classification of Figure 7.2. may be incorrect as it would be expected that the outer surface of the catalyst should contain the active iron carbide phase (also along the cracks) and that the interior of the catalyst should mainly consist of iron oxides. This therefore implies that :

1. The grey areas next to the cracks are iron carbides, while
2. the brighter interior consists mainly of iron oxides.

In Figure 7.9. (Mag x 200), which is similar to that of Figure 7.2., the grey areas next to the cracks leading from the outer surfaces are clearly visible. Figure 7.10. is a 1470 times magnification of an area marked "A" on Figure 7.9.. The grey area next to the crack appears to be very porous. For a porous surface, the solid would be "bright", while the voids would be "black". If the voids are finely dispersed in

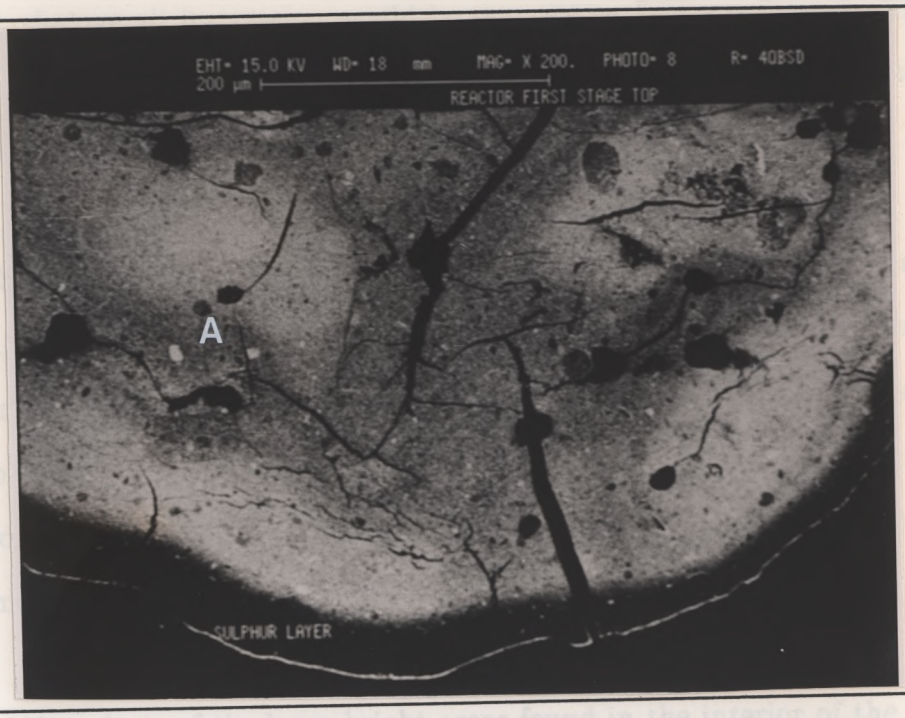

Figure 7.9. SEM photo of a used catalyst from the top section of a fixed bed reactor catalyst bed (MAG = x 200)

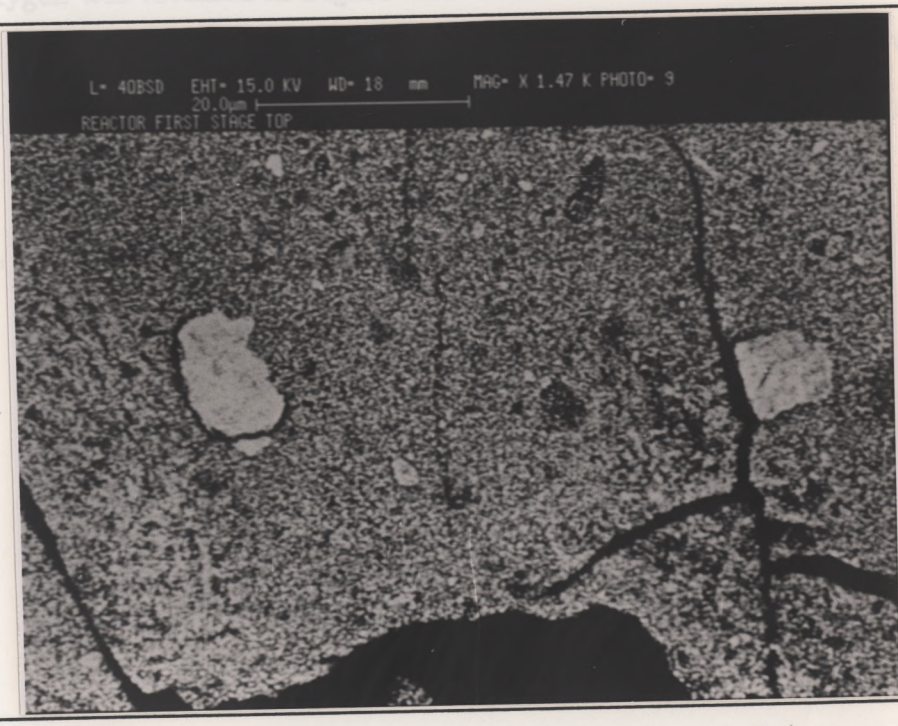

Figure 7.10. Enlargement of a porous area marked A on Figure 7.9. (MAG = x 1470)

the "solid", the overall impression would be that the surface was "grey". Thus the "grey" surface could in fact be porous iron carbide and the "bright" surface could be non–porous magnetite.

The fact that no carbon (which is associated with iron carbide) was detected in the grey areas, can be attributed to the fact that the SEM–EDAX analysis were not operated in the window less mode. The EDAX beam energy was too high to detect elements of low atomic number. However, if Figure 7.13. (displayed later) is taken into consideration, which is an SEM–EDAX analysis of a similar grey area, these lower atomic number elements (like carbon) are displayed.

SEM–EDAX analysis of the large bright areas found in the interior of the catalyst (Figure 7.5.) revealed the result given in Figure 7.11.. Again, large quantities of iron are revealed, which are believed to be associated with iron oxide. The fact that no oxygen was revealed in Figure 7.11. could be due to the same reason given previously for the absence of carbon associated with iron carbide. However, in a similar bright area (see Figure 7.12.), the presence of oxygen is demonstrated.

Therefore, the observations made from Figure 7.2., give the following conclusions :

1. The bright outer rim is iron sulphide.
2. The grey areas next to the cracks leading from the catalyst surface to the interior, consists mainly of iron carbide and also some iron oxide.
3. The bright areas in the interior of the catalyst pellet consists mainly of iron oxide.

Moving to Figure 7.3. (catalyst one quarter from the top of the bed) the picture changes drastically. The following characteristic features are identified :

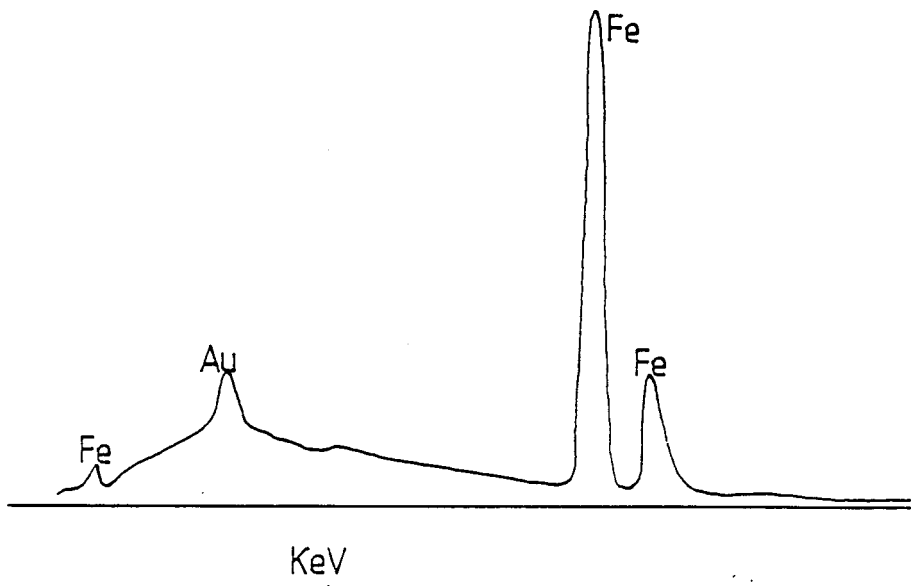

Figure 7.11. SEM–EDAX analysis within the bright area, marked F in Figure 7.5.

* SEM–EDAX not operated in the window less mode. Therefore no oxygen and carbon detected.

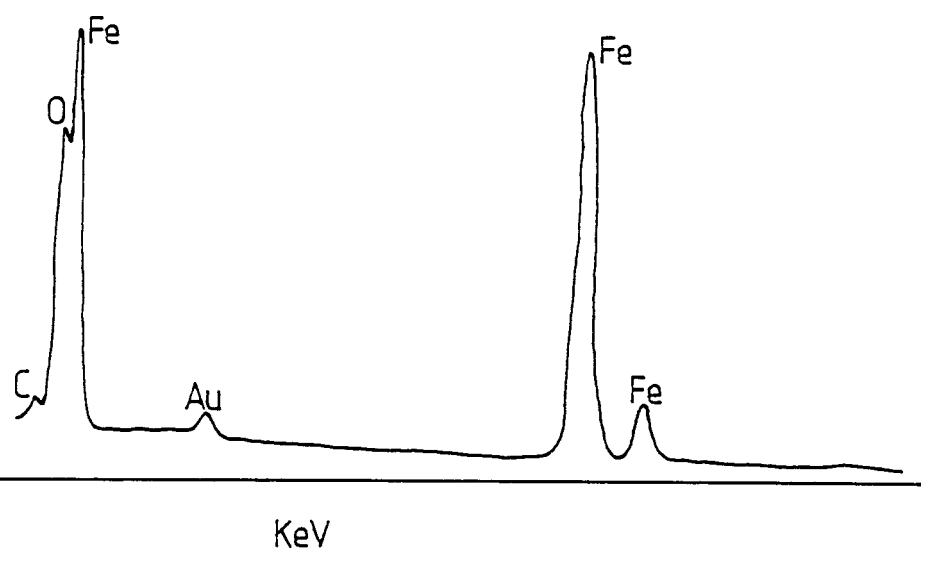

Figure 7.12. Iron rich area analyzed from the bright area, marked G in Figure 7.3.

1. no bright and black outer rim is observed,
2. a large portion is grey, previously shown to be iron carbide,
3. the catalyst pellet interior shows fewer bright areas, and
4. a granular type of texture is displayed.

No sulphur could be detected and no bright rim is present. As in Figure 7.2., the bright and grey areas are taken to be iron oxide and iron carbide respectively (see Figures 7.12. and 7.13., respectively). The granular texture (see Figure 7.14., which is Figure 7.3. two hundred times enlarged) is definitely absent from the previous set of figures (see Figures 7.2. and 7.5. to 7.7.) representing the top section of the catalyst bed. This observed granular texture will be explained later on.

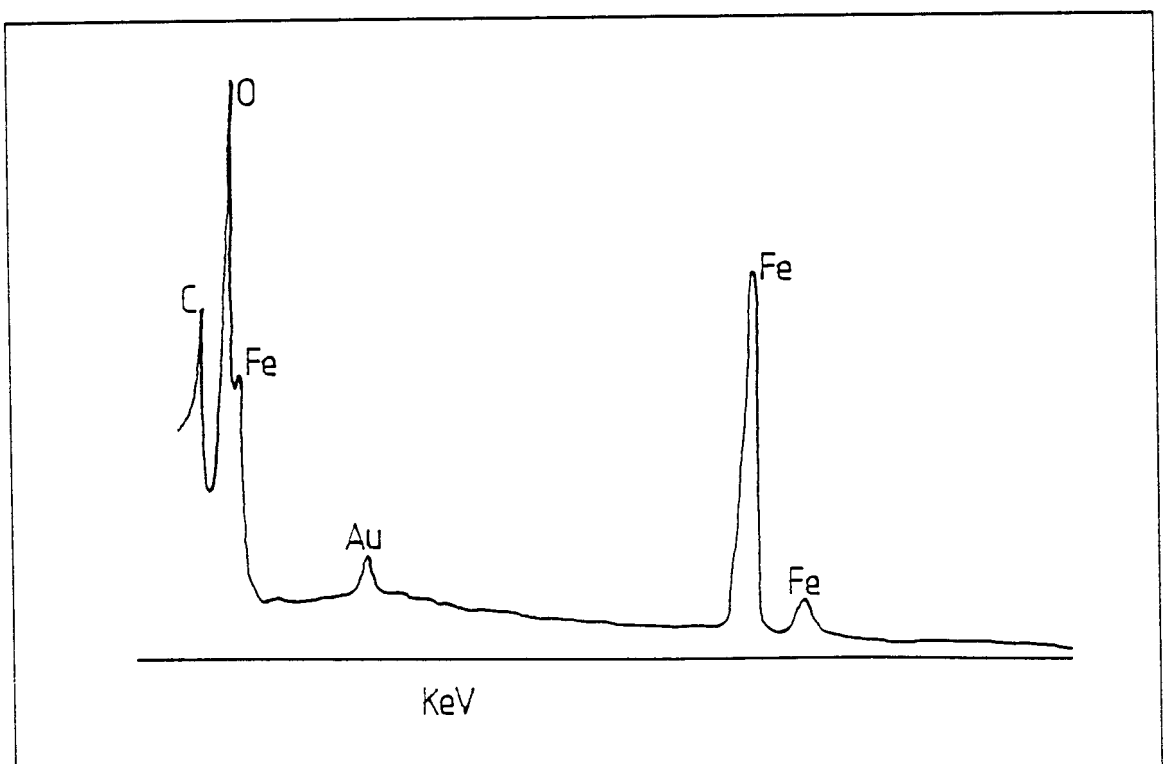

Figure 7.13. Oxygen and carbon rich area analyzed from the grey area, marked H in Figure 7.3.

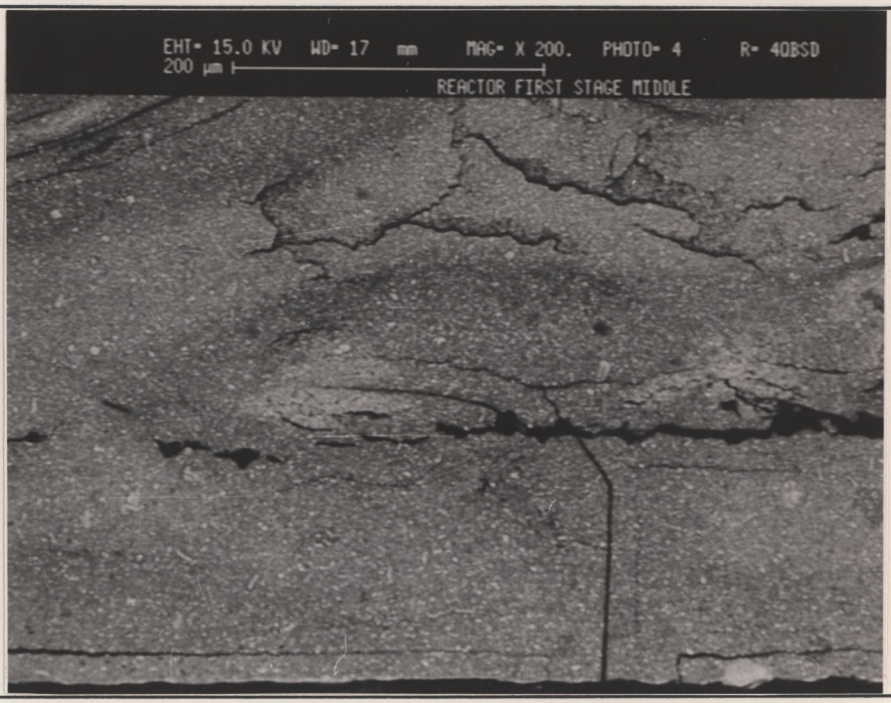

Figure 7.14. Granular texture of the interior of a catalyst pellet from two quarter from the top section of the catalyst bed (taken from Figure 7.3.) (MAG = x 200)

It is also observed in Figure 7.13. that large quantities of both carbon and oxygen are present in the grey area.

Finally, Figure 7.4. (middle section of the catalyst bed) reveals a totally different catalyst pellet analysis. Smooth outer rims are displayed with a granular like interior. The granular like image displays large quantities of small bright spots within a completely grey surface.

Figure 7.15. shows an further enlargement of Figure 7.4. (MAG x 200). Here, the outer rim has a smooth surface while the inside of the catalyst pellet shows a definite granular type of surface.

SEM–EDAX analysis of the different areas confirm that the bright areas are iron

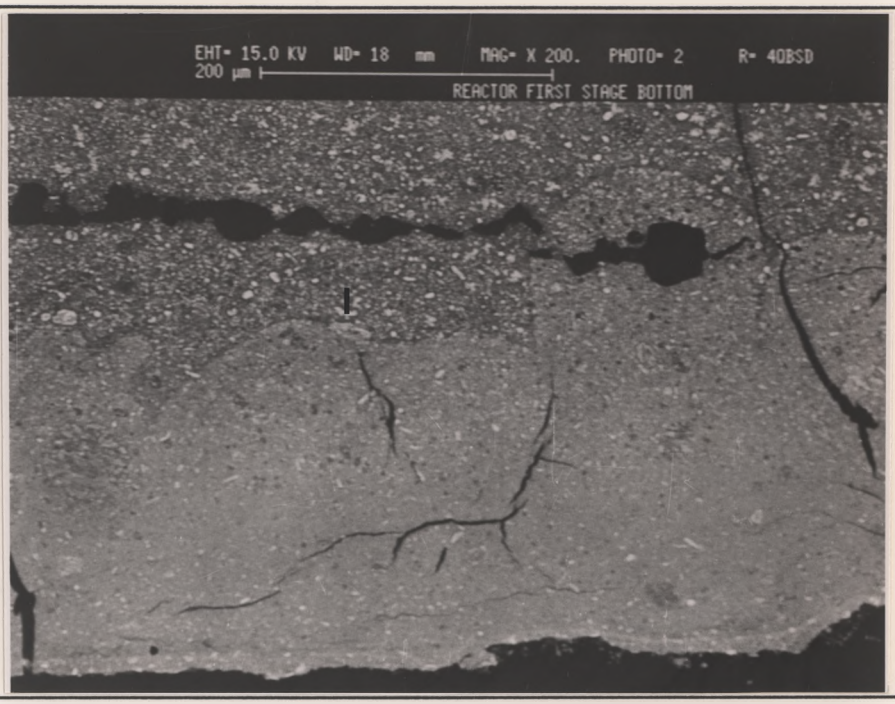

Figure 7.15. Granular texture of the interior and smooth texture of the outer rim for a catalyst pellet from the middle section of the catalyst bed (taken from Figure 7.4.) (MAG = x 200)

rich (Figure 7.16.) while the grey areas, which are already known to contain iron oxide and iron carbide (see Figure 7.13.). In the following section, this phenomenon, the increase in the size of the bright iron rich particles, will be discussed.

7.3. Iron crystallite growth

In this section it will be shown that the increase in the granular appearance shown in Section 7.2. can be related to an increase in iron oxide crystallite growth down the catalyst bed. This phenomenon has been discussed in Chapters 5 and 6.

In Figures 7.17. to 7.20. the following is displayed within a single photograph :

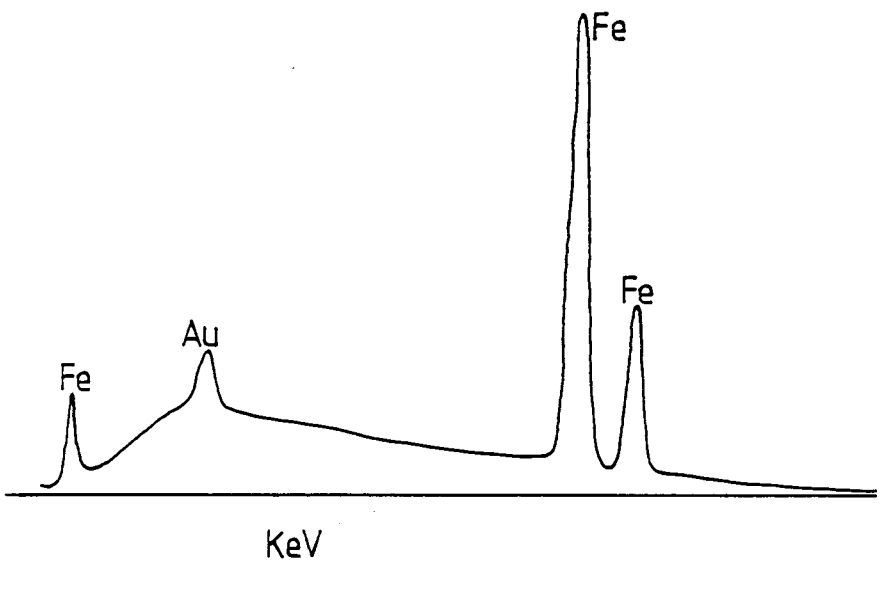

Figure 7.16. SEM–EDAX analysis of a bright area (iron rich), marked I in Figure 7.15.

* SEM–EDAX not operated in window less mode

1. Top left (TL): whole catalyst pellet at magnification x 25
2. Top right (TR): outer rim of catalyst pellet at magnification x 650
3. Bottom left (BL): interior of catalyst pellet at magnification x 650
4. Bottom right (BR): interior of catalyst pellet at magnification x 2500

These figures correspond to :

1. Figure 7.17. : Fresh, reduced catalyst
2. Figure 7.18. : Used catalyst, from the top section of the catalyst bed
3. Figure 7.19. : Used catalyst, $^1/_4$ from the top of the catalyst bed
4. Figure 7.20. : Used catalyst, the middle section of the catalyst bed

From these figures, it is evident that no major change is observed for the outer rim

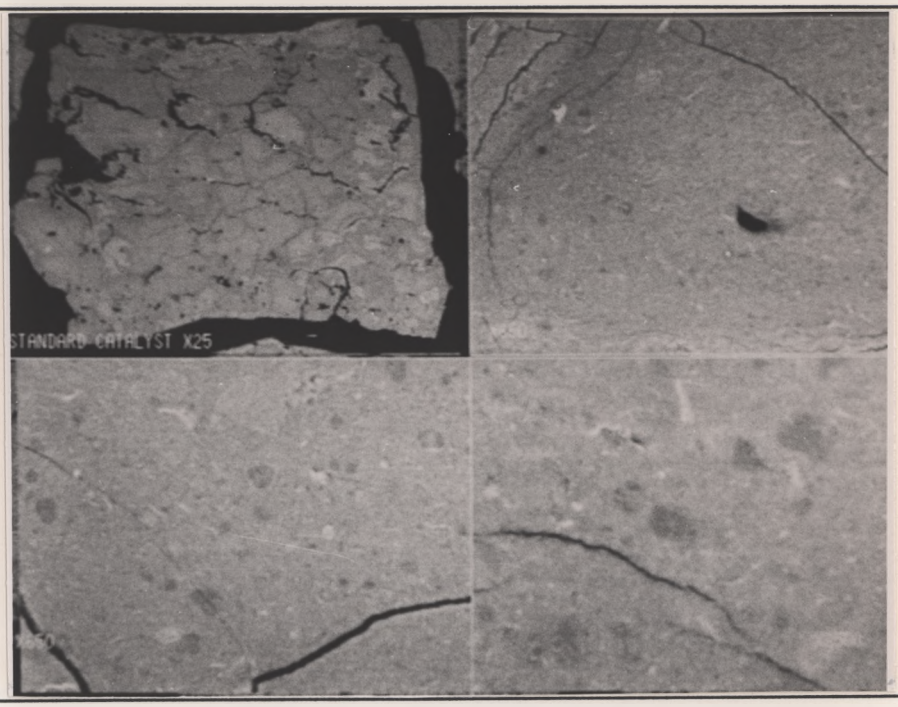

Figure 7.17. SEM photo of a reduced unused catalyst pellet as described on page 163 (MAG = TL x 25, BL x 650, TR x 650, BR x 2500)

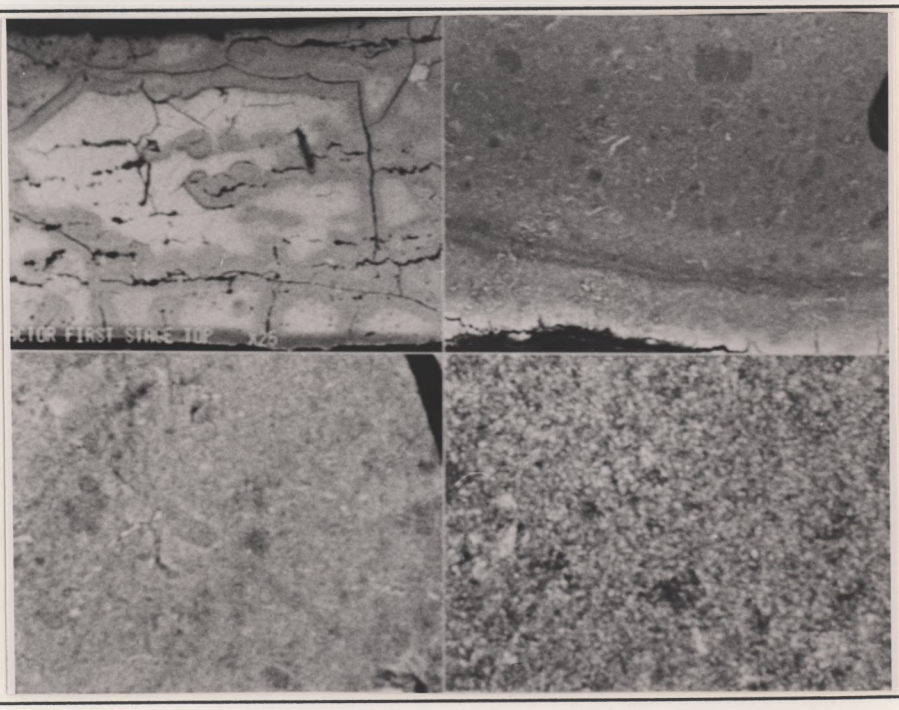

Figure 7.18. SEM photo of a catalyst pellet, representing the catalysts from the top section of the catalyst bed, as described on page 163 (MAG = TL x 25, BL x 650, TR x 650, BR x 2500)

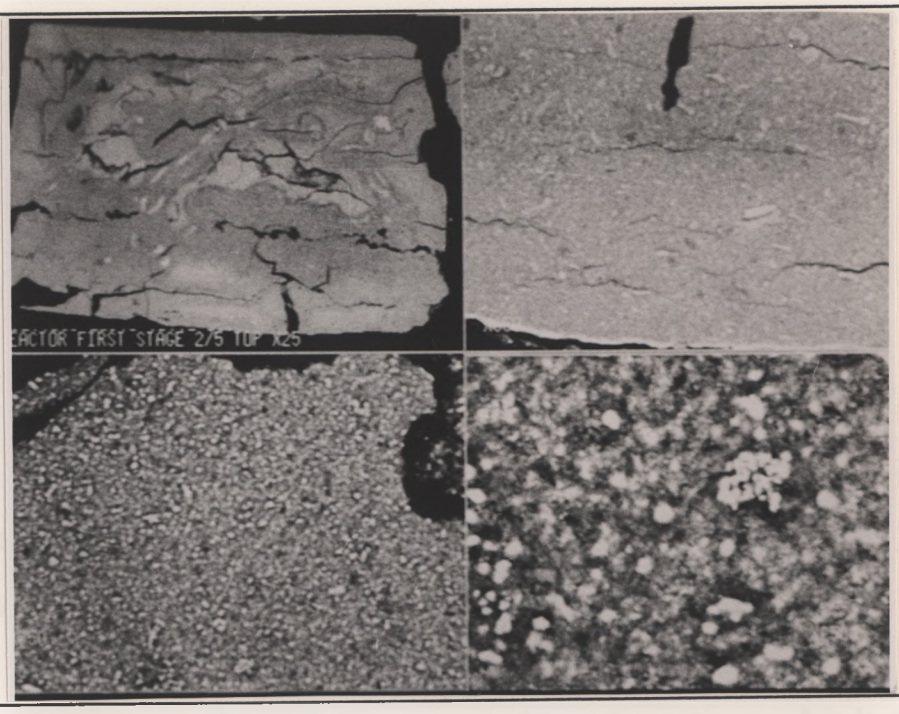

Figure 7.19. SEM photo of a catalyst pellet, representing the most reactive section of the catalyst bed, as described on page 163 (MAG = TL x 25, BL x 650, TR x 650, BR x 2500)

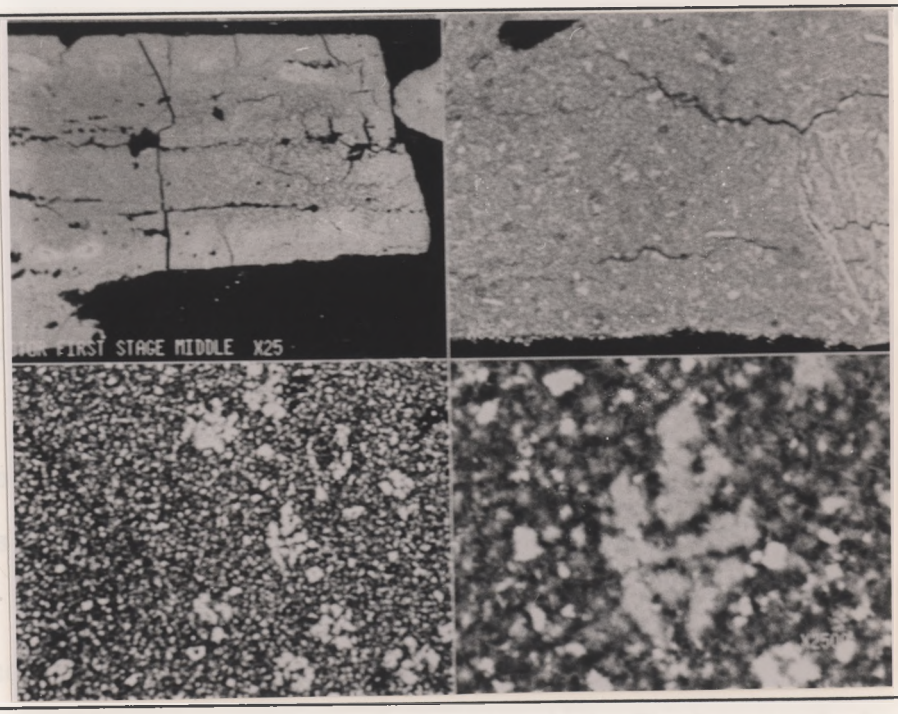

Figure 7.20. SEM photo of a catalyst pellet, representing the middle section of the catalyst bed, as described on page 163 (MAG = TL x 25, BL x 650, TR x 650, BR x 2500)

for each of these catalyst pellets, but that a totally different phenomena is observed for the interior of these used catalyst pellets. The bright areas increase in size as one moves down the catalyst bed. These areas are now known (Section 7.2.) to be iron rich. With the 2500 times magnification (bottom right)(Figure 7.18., 7.19. and 7.20.), it is clear that the iron rich phases increase in size with bed depth, up to a stage (Figure 7.20.) where large clusters are formed.

Enlarging the cluster displayed in Figure 7.20. (bottom right) 6000 times, gave the cluster displayed in Figure 7.21. SEM–EDAX analysis of this cluster at the regions marked A (grey area) and B (bright area) revealed the following.

The grey product (area A) is rich in oxygen and lean in carbon, and it is therefore believed that mostly iron oxide and no iron carbide is present (see Figure 7.22.). The brighter areas (area B) are rich in iron (see Figure 7.23.). Again it is believed that the carbon and oxygen present, correspond mostly to iron oxide and iron carbide.

Finally, SEM–LIA analysis of the particles found in the three sections of the catalyst bed (see Figures 7.18., 7.19., and 7.20.) revealed that an increase in the iron phase is observed with bed depth. Figures 7.24., 7.25. and 7.26., which are 7000 time magnification of Figures 7.18., 7.19., and 7.20., clearly show the increase in the iron crystallite size. Figure 7.27. shows the average diameter of the iron rich phase versus the actual position in the reactor.

To conclude, the SEM technique produced proof of a catalyst poison, sulphur, to be present mainly in the top section of the catalyst bed. Furthermore it showed that the growth of iron rich phases, also known as sintering, does take place in the catalyst bed, increasing in degree of bed depth.

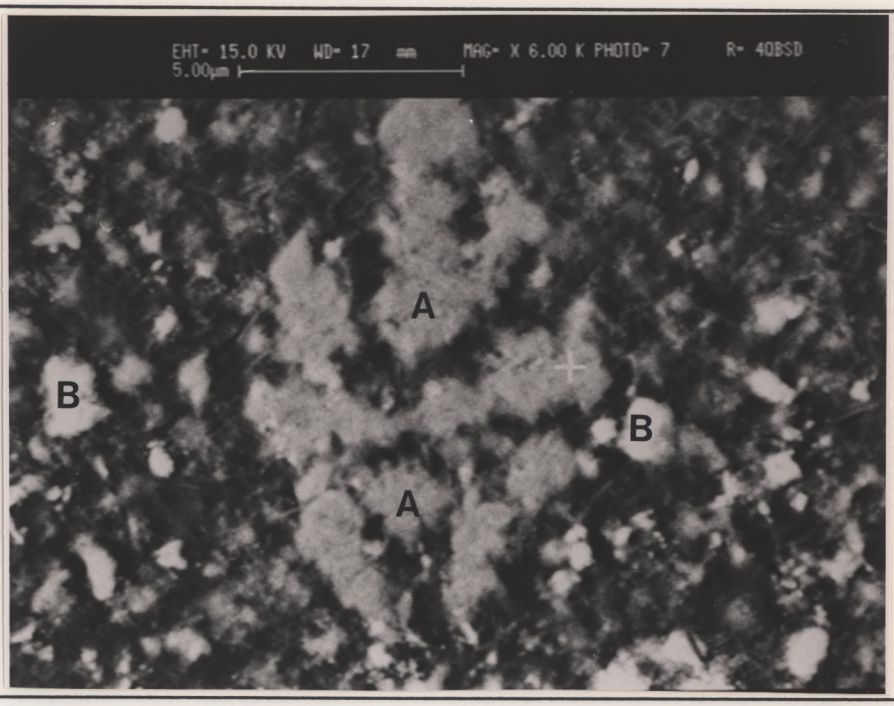

Figure 7.21. SEM photo of a sintered product (MAG = x 6000)

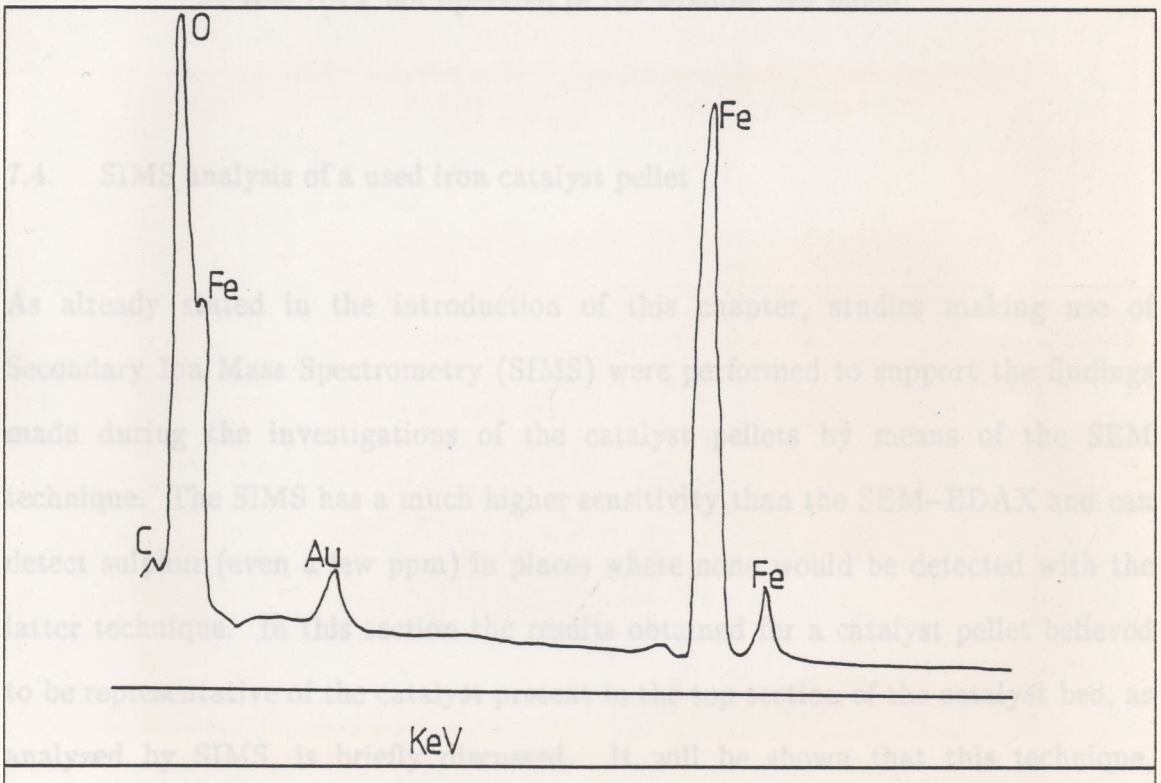

Figure 7.22. SEM–EDAX analysis of the grey sintered product (oxygen rich), marked A in Figure 7.21.

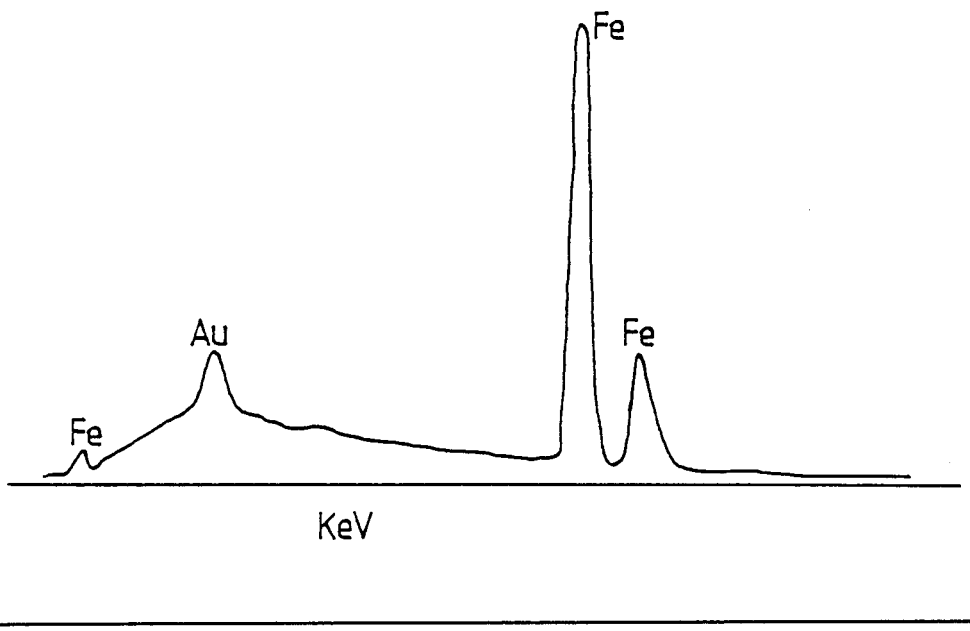

Figure 7.23. SEM–EDAX analysis of the bright area (iron rich), marked B in Figure 7.21.

* SEM–EDAX not operated in the window less mode

7.4. SIMS analysis of a used iron catalyst pellet

As already stated in the introduction of this chapter, studies making use of Secondary Ion Mass Spectrometry (SIMS) were performed to support the findings made during the investigations of the catalyst pellets by means of the SEM technique. The SIMS has a much higher sensitivity than the SEM–EDAX and can detect sulphur (even a few ppm) in places where none would be detected with the latter technique. In this section the results obtained for a catalyst pellet believed to be representative of the catalyst present in the top section of the catalyst bed, as analyzed by SIMS, is briefly discussed. It will be shown that this technique, combined with other surface techniques like SEM, can be used to obtain a better understanding of catalyst deactivation.

Figure 7.24. Magnification of the bright areas (iron crystallites) representing the top section of the catalyst bed, taken from Figure 7.18. (MAG = x 7000)

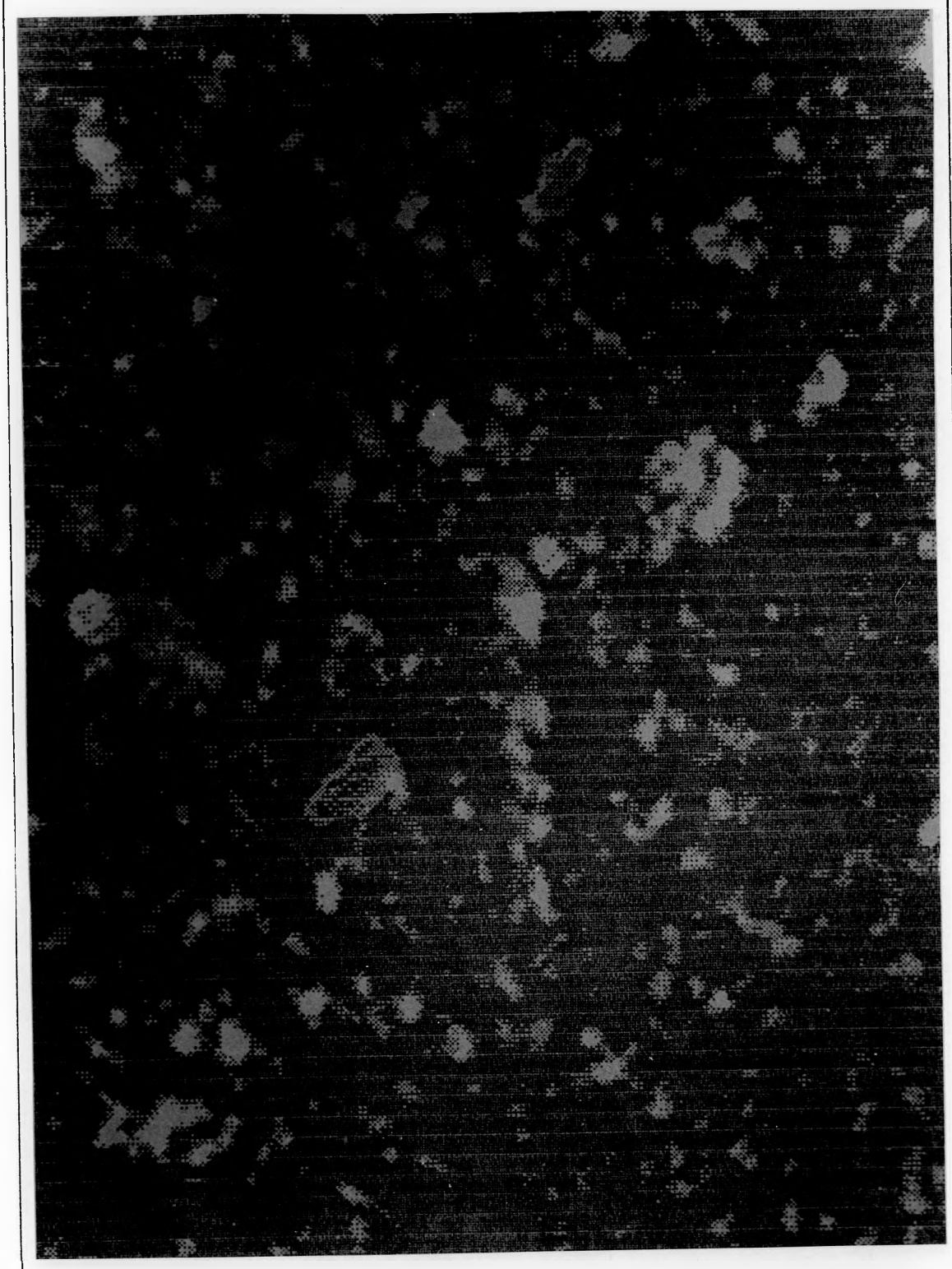

Figure 7.25. Magnification of the bright areas (iron crystallites) representing the most reactive section of the catalyst bed, taken from Figure 7.19. (MAG = x 7000)

Figure 7.26. Magnification of the bright areas (iron crystallites) representing the middle section of the catalyst bed, taken from Figure 7.20. (MAG = x 7000)

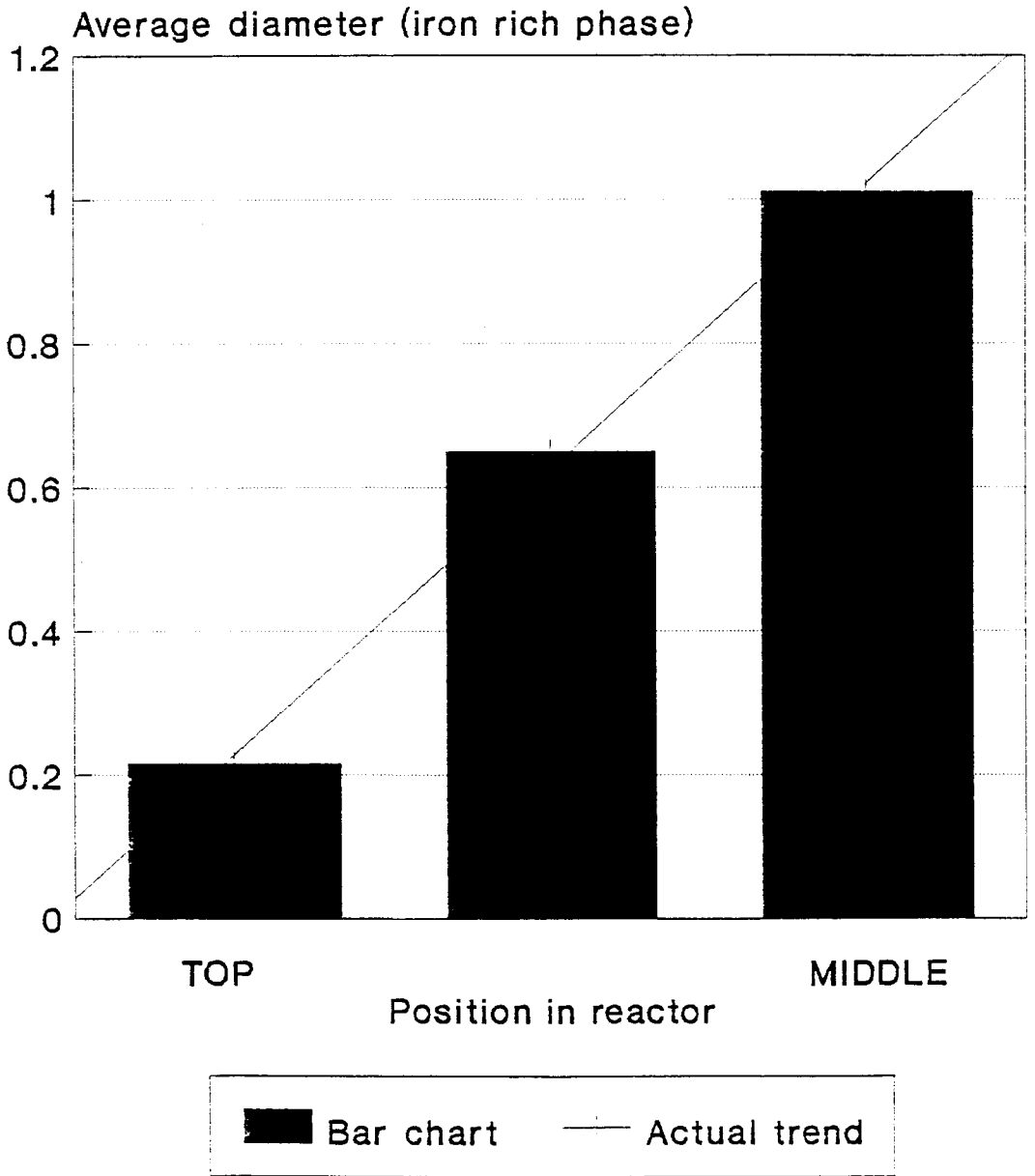

Figure 7.27. Increase in average particle diameter as a function of position in the reactor

Surface mappings of the interior of a catalyst pellet from the top section of the catalyst bed (Figure 7.28.) revealed large quantities of iron oxide (see Figure 7.29.) and sulphur (see Figure 7.30.) to be present on the analyzed surface. It was also found that iron carbide (Fe_2C^*) was present throughout the catalyst pellet (see Figure 7.31.). Unfortunately, due to poor contrast, these prints are not very clear.

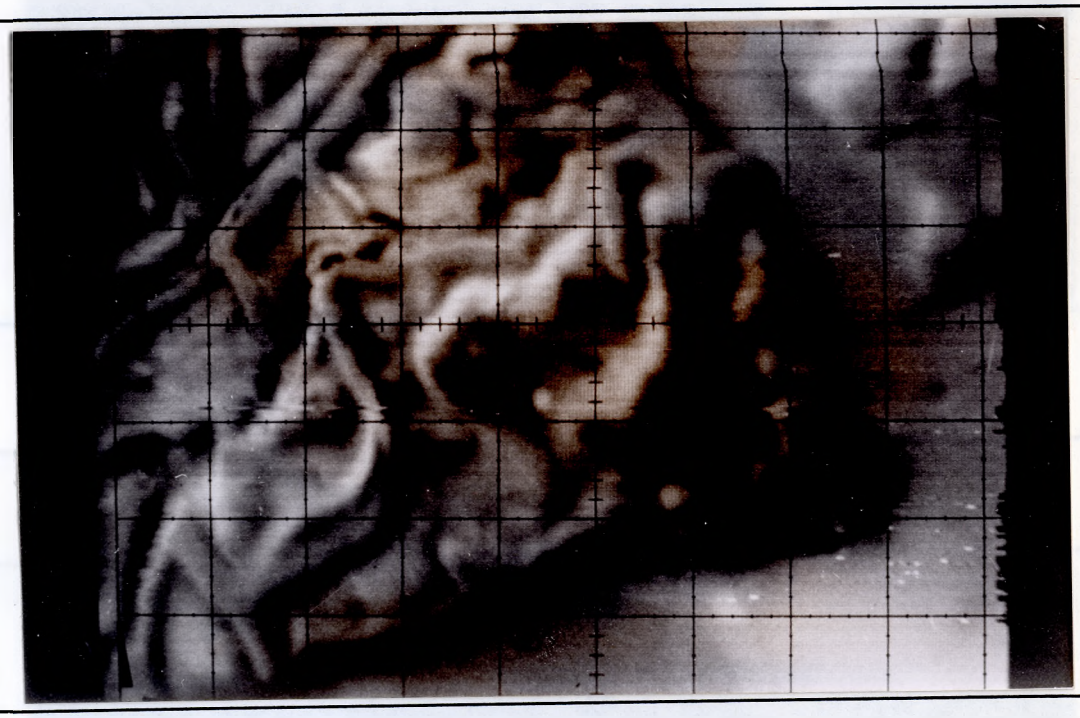

Figure 7.28. SIMS photo of the surface of a catalyst pellet representing the top section of the catalyst bed (MAG = x 100)

Ion mass spectral spot analysis of a catalyst pellet showed the expected result for the distribution of sulphur compounds throughout the catalyst pellet. A catalyst pellet shown in Figure 7.2. (discussed in Section 7.2., SEM analysis) clearly displayed higher sulphur concentrations to be present in the outer rim of the catalyst than in the interior of the catalyst pellet. It was also observed that the grey areas surrounding the cracks leading to the interior of the catalyst pellet also contained sulphur. This finding provides evidence for our speculation earlier in this

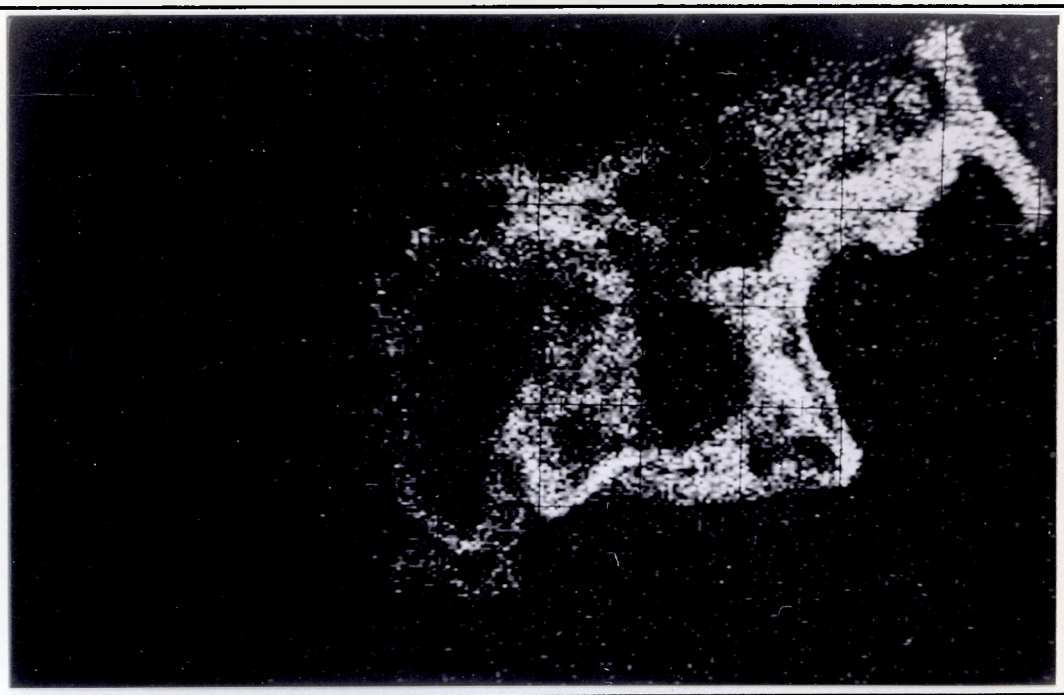

Figure 7.29. SIMS SURFACE MAP of iron oxide present on the surface of a catalyst representing the top section of the catalyst bed

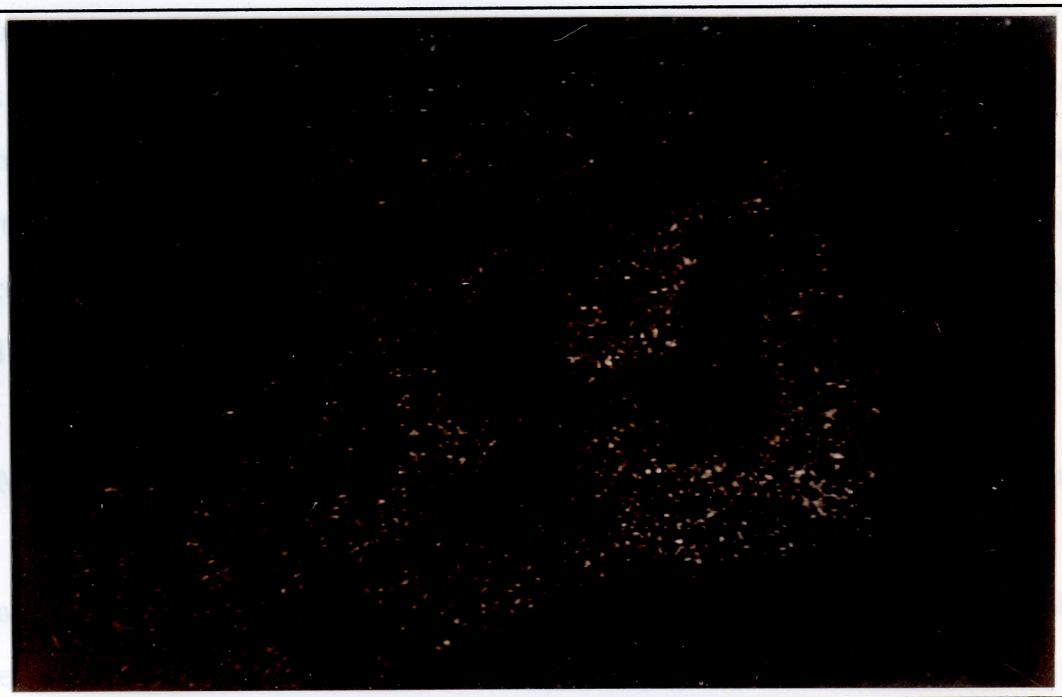

Figure 7.30. SIMS SURFACE MAP of sulphur present on the surface of a catalyst representing the top section of the catalyst bed

Figure 7.31. SIMS SURFACE MAP of iron carbide (Fe_2C^+) present on the surface of a catalyst representing the top section of the catalyst bed

chapter that sulphur compounds may not only be found on the outer surface of the catalyst pellet, but may also diffuse into the catalyst pellet along the cracks connecting the outer surface to the interior of the catalyst pellet. Ion mass spectra of the outer rim (area marked "B" in Figure 7.2.), the grey areas next to the cracks (area marked "C" in Figure 7.2.) and the bright areas in the interior of the catalyst pellet (area marked "D" in Figure 7.2.) are displayed in Figure 7.32..

SIMS analysis of the catalyst pellet therefore showed the sulphur concentration to be high on the outer surface and not detectable in the interior of the catalyst, and that sulphur, in concentrations similar to that of the outer surface, is found along the cracks leading to the interior of the catalyst pellet. These high sulphur concentrations found along the cracks in fact suggest that the areas along the cracks can also be regarded as part of the outer surface of the catalyst.

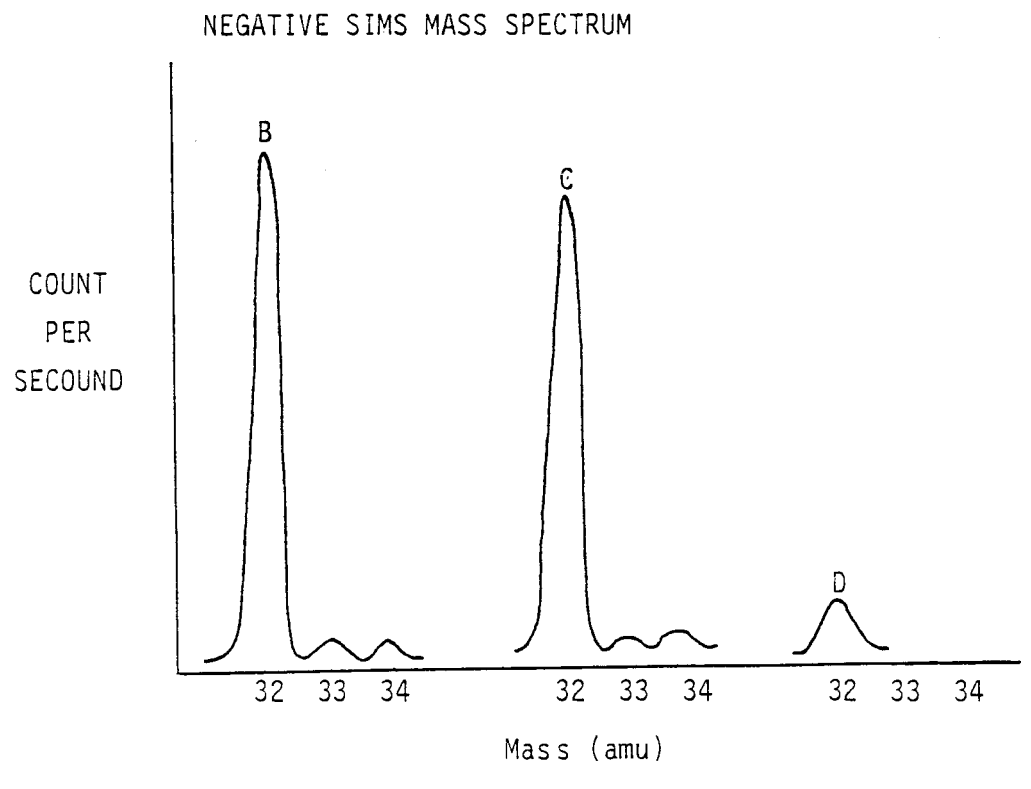

Figure 7.32. Ion Mass Spectra spot analysis within the black rim, within the grey area and within the bright area (marked B, C and D in Figure 7.2.) of a catalyst representing the top section of the catalyst bed

It is also believed that these results show that the loss of catalytic activity due to poisoning is only a result of the poisoning of the catalyst surface (as the poisoned areas around the cracks are equivalent to outer surfaces) and is not a consequence of bulk catalyst poisoning. This result is similar to that obtained by most other researchers[3,5,11,12] in the field of catalyst poisoning.

Finally, the negative (–) (Figure 7.33.) ion mass spectra analysis of the bright area in the middle of the catalyst pellet displayed in Figure 7.2. revealed the presence of large quantities of oxides, carbon chains (believed to be from hydrocarbons products not completely extracted) and impurities like chloride and fluoride

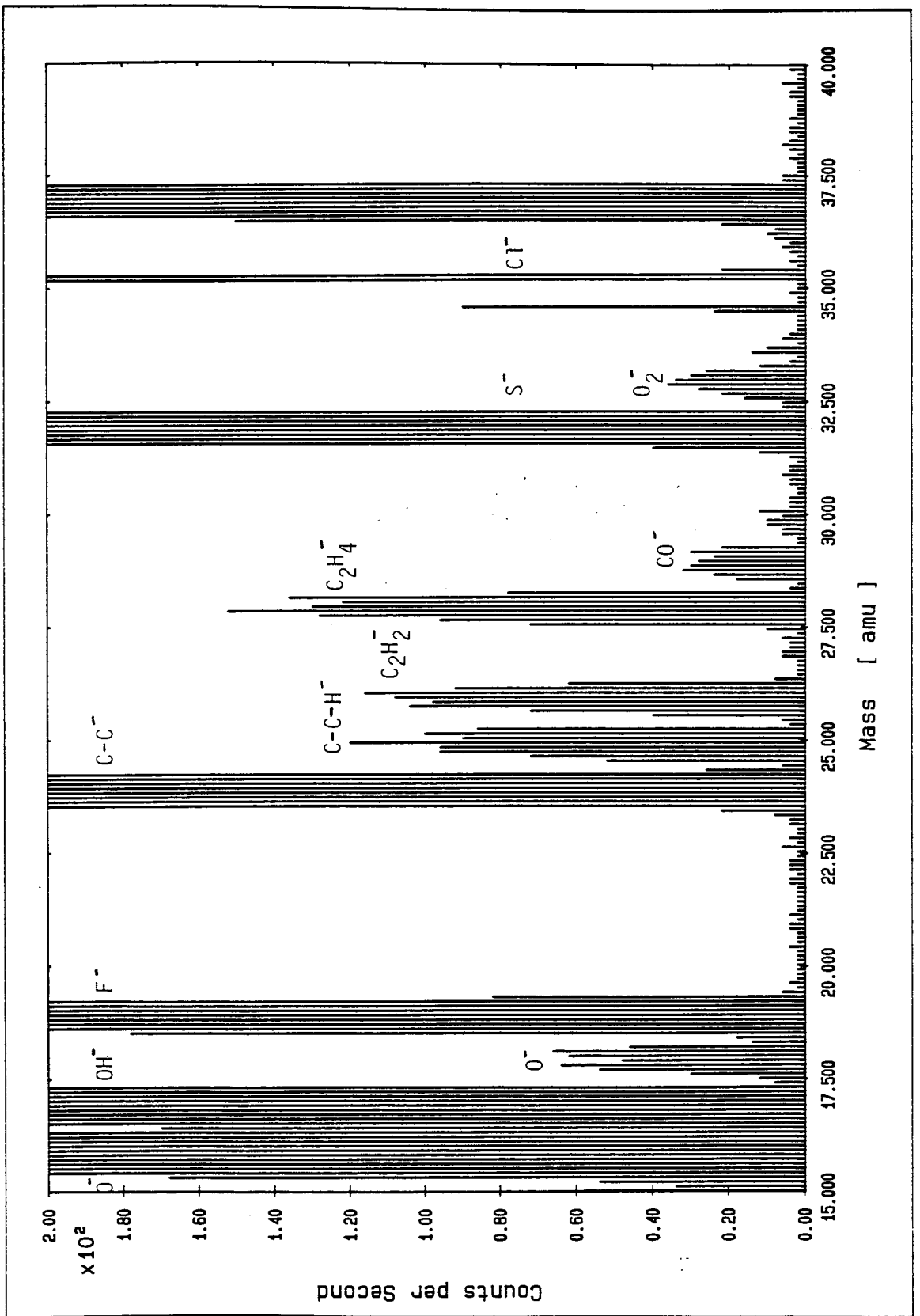

Figure 7.33. Negative ion mass spectra of the bright area, marked D in Figure 7.2.

(believed to be a result of contamination). Little or no sulphur is observed in this area.

These results also show the suitability of the SIMS technique for the study of the surface of used Fischer–Tropsch catalysts; particularly when used in conjunction with SEM–EDAX.

7.5. References

1. M.E. Dry, *Catalysis – Science and Technology, Vol. 1*, (J.R. Anderson and M. Boudard, eds.), Springer–Verlag, Berlin, 1981
2. G.W. Ewing, *Instrumental Methods of Chemical Analysis*, 5th Edition, McGraw–Hill Book Company, New York, 1985, 199, 401
3. A.L. Chaffee, I. Campbell and N. Valentine, *Appl. Catal., 47*, 1989, 253
4. R.J. Madon and H. Shaw, *Catal. Rev. – Sci. Eng., 15, 1*, 1977, 70
5. P.K. Agrawal, W.D. Fitzharris and J.R. Katzer, *Catalyst Deactivation 1980*, (B. Delmon and G.F. Froment, eds.), Elsevier Science Publishers B.V., Amsterdam, 1980, 179
6. E. Ruckenstein, *Metal–support interactions in Catalysis, Sintering and Redispersion*, Van Nostrand Reinhold Company, New York, 1987, 230 – 236, 239 – 241, 271, 287, 291 – 294, 296
7. Von H. Kölbel and F. Engelhard, *Erdol und Kohle, 3, 11*, 1950, 529
8. E. Ruckenstein and D.B. Dadyburjor, *J. Catal., 48*, 1977, 73
9. E. Ruckenstein and B. Pulvermacher, *J. Catal., 29*, 1973, 224
10. D.B. Dadyburjor, *Catalyst Deactivation 1987*, (B. Delmon and G.F. Froment, eds.), Elsevier Science Publishers B.V., Amsterdam, 1987, 21

11. S. Berkman, J.C. Morrell and G. Egloff, *Catalysis, Inorganic and Organic*, Reinhold Publishing Corporation, New York, 1940, 372

12. J.F. Shultz, F.S. Karn and R.B. Anderson, *U.S. Bur. Mines, Rep. Invest., 6974*, 1967 (as reported by R.J. Madon and H. Shaw, *Catal. Rev. – Sci. Eng., 15, 1*, 1977)

CHAPTER 8

CONCLUSIONS

The deactivation of an iron Fischer–Tropsch catalyst is not due to a single cause, but to a combination of factors. The most important causes are :

1. Sulphur

   The catalyst is mainly deactivated by sulphur in the top section of the catalyst bed. The source of sulphur are impurities in the feed gas.

2. Water

   A second problem is the water produced as a product in the Fischer–Tropsch reaction. The production of water during the Fischer–Tropsch reaction plays two main roles in the deactivation process of the low temperature precipitated iron catalyst.

   (i) The active metal phase is oxidized to the unreactive iron oxide phases; mostly magnetite (Fe_3O_4). This catalyst oxidation process mainly takes place in the bottom section of the fixed bed reactor.

   (ii) Furthermore, the presence of water vapour enhances the growth of crystallites (hydrothermal sintering).

3. Fouling

   Finally, but to a much lesser extent, fouling of the catalyst through carbon deposition is expected. However, the amount of carbon observed in the catalyst is low and so fouling is not considered to be a major reason for deactivation.

Surface studies making use of SEM and SIMS techniques, proved to be a great help in identifying the different deactivation phenomena. Poisoning (in this case by sulphur) and sintering were successfully identified by employing these techniques.

—— OOO ——